12-2016

Targeted Synthesis and Characterization of Novel Nanostructured Titanosilicates for Epoxidation and Hydrogen Storage

Austin Alan Albert
University of Tennessee, Knoxville, aalbert@vols.utk.edu

To the Graduate Council:

I am submitting herewith a dissertation written by Austin Alan Albert entitled "Targeted Synthesis and Characterization of Novel Nanostructured Titanosilicates for Epoxidation and Hydrogen Storage." I have examined the final electronic copy of this dissertation for form and content and recommend that it be accepted in partial fulfillment of the requirements for the degree of Doctor of Philosophy, with a major in Chemistry.

Craig Barnes, Major Professor

We have read this dissertation and recommend its acceptance:

Brian Long, David Jenkins, Paul Frymier

Accepted for the Council:

Carolyn R. Hodges

Vice Provost and Dean of the Graduate School

(Original signatures are on file with official student records.)

Targeted Synthesis and Characterization of Novel Nanostructured Titanosilicates for Epoxidation and Hydrogen Storage

A Dissertation Presented for the

Doctor of Philosophy

Degree

The University of Tennessee, Knoxville

Austin Alan Albert
December 2016

DEDICATION

This dissertation is dedicated

to everyone who has supported me over the years

especially my parents

Luanne and Randy Albert

luctor et emergo

ACKNOWLEDGEMENTS

This dissertation would not have been possible without the assistance of many individuals. I truly feel that words cannot describe how much I appreciate everyone who has supported me over the years.

First, I would like to thank my research adviser, Dr. Craig Barnes, for supporting and encouraging me over the years. I am cannot begin to repay him for his limitless patience and unwavering encouragement during the difficult trials that I faced during my graduate studies. He helped make me the chemist I am today and I absolutely feel the best decision I made in graduate school was to join his research lab. I would also like to thank my committee members, Dr. David Jenkins, Dr. Brian Long, and Dr. Paul Frymier for agreeing to commit time, effort, and constructive criticism to serve on my committee.

I would also like to thank the entire Chemistry Department staff, especially members of the Glassblowing Shop (Art Pratt and Bo Bishop), the Electronics Shop (Bill Gurley, Johnny Jones, Jim Murphy, Gary Wynn), the Machine Shop (Tim Free, Gene French) and the Business Office (Beverly Adams, Gail Cox, Darrell Lay, Sharon Marshall). These individuals provide vital support for the Chemistry Department and each of them deserves acknowledgment and thanks for all of the work that they do. I would not have been able to complete this dissertation without the assistance of each of the individuals mentioned above.

I gratefully acknowledge the motivation and support of current and former group members: Dr. Josh Abbott, Dr. Nan Chen, Dr. Michael Peretich, James Humble, Dan Taylor, Lena Elenchin, Matt Dembo, Desta Doro Bume, Pavlo Kravchenko, Michael Kandziolka, Michael Orick, Dr. Jiri Pinkas, Ales Styskalik, and Martin Sojka. I appreciate the helpful discussions about research, the long days and nights at Brookhaven, and generally making the research lab a fun place. I was excited to go to work each day knowing that I would spend my time with Josh, James, Micheal P., Micheal K., Micheal O., Matt, and Lena.

I would also like to thank Dr. David Keffer and the STAIR/IGERT fellowship. The funding that you have provided has allowed me the chance to extend my learning far past the standard chemistry curriculum.

I would also like to thank the chemistry faculty of UNCO. The education I received while at UNCO was a foundation that has laid the groundwork for my success. These faculty members started my development as a professional chemist and opened my eyes to the amazing world that surrounds us. I would like to thank Dr. David Pringle, Dr. Richard Schwenz, Dr. Richard Hyslop, Dr. Kimberly Pacheco, Dr. James Schreck and Dr. Robin Macaluso. You taught me how to learn.

I would also like to thank Laura Casto. She has suffered through the difficult times of my graduate studies and pursue of my Ph.D. She has been and will always be there for me, through good times and bad. She lent an ear allowing me to boast and complain about the everyday trials of graduate studies.

Last, but certainly not least, I would like to acknowledge my family for their love and support. My family, especially my parents (Luanne and Randy Albert), has been tremendously supportive and loving. I know I would not have finished this dissertation without their love and support.

ABSTRACT

The Barnes' research group has developed a general synthetic methodology for creating nanostructured silicate with targeted single sites. This methodology provides researchers with the ability to control the dispersion of surface functionality and metal centers, the number of linkages from metal center to the support, the surface area and the porosity of the support. This dissertation describes work aimed at synthesizing and characterizing nanostructured titanosilicates for hydrogen storage applications and as heterogeneous catalysts. Furthermore, none of the materials prepared in our investigations exhibited significant hydrogen bind beyond physisorption

Isolated surface titanium species were synthesized by reacting a nanostructured silicate support with titanium tetrachloride. These isolated titanium(IV) sites serve as a well-defined starting point for a "complex" reduction, resulting in reduced titanium centers that may be capable of Kubas' binding of hydrogen. These sites were exposed to a variety of reductants: lithium aluminum hydride, sodium borohydride, cobaltocene, hydrogen, and UV radiation with hydrogen. The majority of the work with these systems focused on characterizing the titanium species after reduction to understand their composition. Due to the amorphous nature and instability of the reduced titanium species, we were unable to develop a clear understand of their composition.

Nanostructured heterogeneous catalysts with isolated titanium(IV) centers were synthesized by reacting a limiting amount of metal chloride with octatrimethyltin spherosilicate, followed by dimethyldichlorosilane. Three catalyst ensembles were synthesized: 2-, 3-, and 4-connected titanium. The catalytic activity of each catalyst was examined in the epoxidation of cyclohexene with cumene hydroperoxide. Under identical conditions, high activities were observed in a sequence 2-connected > 3-connected > 4-connected titanium catalysts. Furthermore, these single site catalysts were compared to two commercially used catalysts (Grafted Titanium Mobil Composition of Matter-41 and Titanium Silicalite -1) and found to be superior in both activity and selectivity. A structure-function relationship was therefore developed through targeted synthesis of novel single sites titanosilicates.

TABLE OF CONTENTS

CHAPTER 1: ENGINEERED MATERIALS 1
AREAS OF FOCUS 3
GAS SEPARATION AND STORAGE 3
CATALYSIS 3
DEFINING A CATALYST 5
HOMOGENEOUS VERSUS HETEROGENEOUS CATALYSTS 5
ACTIVE SITE ANATOMY 7
CATALYSIS CHARACTERISTICS OF IMPORTANCE 10
(1) SELECTIVITY 10
(2) ACTIVITY 10
(3) STABILITY 10
TRADITIONAL SYNTHESES FOR TARGETED ACTIVE SITES 11
TRADITIONAL SYNTHESES FOR CREATING EMBEDDED SITES 11
SOL-GEL PROCESS 11
TEMPLATING PROCESS 13
NONHYDROLYTIC SOL-GEL 16
HYDROTHERMALLY PROCESS 16
SUMMARY OF EMBEDDED SITES 18
TRADITIONAL SYNTHESES FOR CREATING SURFACE SITES 18
INCIPIENT WETNESS 18
GRAFTING 18
TETHERING 20
SUMMARY OF SURFACE SITES 23
SUMMARY OF TRADITIONAL SYNTHESES 23
A NOVEL SYNTHETIC METHODOLOGY 23
THE MOLECULAR BUILDING BLOCK 23
THE LINKING AGENTS 25
THE CROSS-LINKING REACTION 25
THE SEQUENTIAL ADDITION STRATEGY 27
SUMMERY OF OUR NOVEL SYNTHETIC STRATEGY 27
CHARACTERIZATION METHODS 30

GRAVIMETRIC ANALYSIS 30
POROSITY MEASUREMENTS 31
ADSORPTION/DESORPTION ISOTHERMS AND HYSTERESIS LOOPS 31
BRUNAUER-EMMETT-TELLER (BET) SURFACE AREA 33
TOTAL PORE VOLUME 38
INFRARED SPECTROSCOPY 38
CONCENTRATION DETERMINATION USING PROBE MOLECULES 38
X-RAY ADSORPTION SPECTROSCOPY 41
THE FUNDAMENTALS OF X-RAY ABSORPTION SPECTROSCOPY 41
COLLECTION OF XAS DATA 51
ANALYSIS OF XAS DATA 56
DISSERTATION OVERVIEW 56
CHAPTER 2: INVESTIGATION OF SINGLE SITE TITANOSILICATE MATERIALS FOR HYDROGEN STORAGE 58
INTRODUCTION 58
CURRENT STRATEGIES FOR HYDROGEN STORAGE 60
INSTRUMENTATION 66
INFRARED SPECTROSCOPY 66
X-RAY ABSORPTION SPECTROSCOPY 68
POROSITY ANALYSIS 69
HYDROGEN ADSORPTION-DESORPTION ANALYSIS 69
EXPERIMENTAL AND RESULTS 69
REDUCTION WITH HYDRIDE REDUCING AGENTS 75
PROCEDURES 78
LITHIUM ALUMINUM HYDRIDE 78
SODIUM BOROHYDRIDE 78
RESULTS AND DISCUSSION 78
REDUCTION WITH HYDROGEN 82
PROCEDURES 82
PRESSURE VESSEL 82
t FLOW CELL PROCEDURE 88
RESULTS AND DISCUSSION 88

species is the addition of a hydrogen-activating agent that acts as a transfer agent creating an alternate mechanism to produce reduced titanium species. 92
REDUCTION WITH HYDROGEN WITH PLATINUM PROMOTER 92
PROCEDURE 92
RESULTS AND DISCUSSION 92
REDUCTION WITH COBALTOCENE 95
PROCEDURE 99
RESULTS AND DISCUSSION 99
REDUCTION WITH UV LIGHT AND HYDROGEN 99
PROCEDURE 99
RESULTS AND DISCUSSION 103
TITANIUM TRICHLORIDE 103
ACTIVATION PROCEDURE 103
RESULTS AND DISCUSSION 107
SUMMARY 107
THE LOSS OF X-RAY ABSORPTION SPECTROSCOPY 110
CHAPTER 3: INVESTIGATION OF SINGLE SITE TITANOSILICATE MATERIALS FOR EPOXIDATION 113
INSTRUMENTATION 115
GRAVIMETRIC ANALYSIS 117
INFRARED SPECTROSCOPY 117
POROSITY ANALYSIS 117
NUCLEAR MAGNETIC RESONANCE (NMR) 117
ELEMENTAL ANALYSIS 118
EXPERIMENTAL 118
CHARACTERIZATION OF SINGLE SITE CATALYSTS 120
CATALYTIC TEST REACTIONS 121
CATALYTIC PROTOCOL 123
CHARACTERIZATION OF ALIQUOTS 126
RESULTS & DISCUSSION: 126
STABILITY 131
PROTOCOL: 131
RESULTS & DISCUSSION: 132

SUMMARY: 132
CHAPTER 4: CONCLUSION AND FUTURE WORK 136
APPLICATIONS IN HYDROGEN STORAGE: 136
APPLICATIONS IN HETEROGENEOUS CATALYSIS: 136
FUTURE WORK 137
INCORPORATION OF METAL CLUSTERS 137
HETEROGENEOUS CATALYSTS WITH NON-EQUILIBRIUM GEOMETRIES VIA IMPRINTING 139
DEVELOPMENT OF METHODS TO REMOVE RESIDUAL TRIMETHYLTIN GROUPS 139
DEVELOPMENT OF NEW BUILDING BLOCK APPROACH 139
REFERENCES 141
VITA 148

LIST OF TABLES

Table 1: List of inert and catalytically active linking agents. 26
Table 2: Summary of the key characteristics of each type of adsorption/desorption isotherm. 35
Table 3: Summary of the nomenclature for specific X-ray absorption transitions (X-ray absorption edges)..... 43
Table 4: Department of Energy goals for hydrogen storage in the near future. [61] 59
Table 5: The approximate ratios and concentrations within trimethyltin cube based silicate platform... 72
Table 6: Results of catalytic properties in the epoxidation of cyclohexene to cyclohexene oxide. 129
Table 7: Results of the leaching study in the epoxidation of cyclohexene to cyclohexene oxide..... 133

LIST OF FIGURES

Figure 1: A plot demonstrating the contrast in understand of heterogeneous catalysis and practical catalysis. The red arrow indicates the difference in knowledge. 2
Figure 2: a diagram showing the reactants (unburned fuel, carbon monoxide, oxygen, nitrogen oxide) and products (nitrogen, oxygen, carbon dioxide, and water) of a catalytic converter (Figure was reproduced from [5]). 4
Figure 3: Illustration of the energy diagram of an uncatalyzed (blue) and catalyzed (red) reaction showing that a catalyzed reaction has a lower activation energy (E_a) than the same reaction when not catalyzed (Figure was reproduced from [7]). 6
Figure 4: Illustration of metallocene complexes with different Cp ligands.[9] 8
Figure 5: Illustration of an active site showing the terminating ligands (L, Red), metal-to-surface binding interactions (M-O-Si, Blue), and the support (SiO_2). 9
Figure 6: Illustration of a templating process using a soft template.[22] 14
Figure 7: Illustration of the pore structure of three MCM materials (left- MCM-41, center- MCM-48, and right-MCM-50).[18] 15
Figure 8: Illustration of two types of zeolite structures (left-BEA and right- MFI) (Figure was reproduced from [24]). 17
Figure 9: Generic illustration of the grafting of a catalytically active metal center (ML_6, L = hydride, alkyl, amide, halide) onto the surface of a silica support (Figure was reproduced from[28]). 19
Figure 10: Illustration of the grafting of a titanium amide species(Figure was reproduced from [28]) 21
Figure 11: Generic illustration of the tethering of a catalytically active metal center onto the surface of a silica support (Figure was reproduced from [28].) 22
Figure 12: a) Illustration of the structure of the building block $Si_8O_{12}(OSnMe_3)_8$. Silicon atoms are purple, oxygen atoms are red, tin atoms are green, and methyl groups are gray. b) Illustration of the core structure of the building block $Si_8O_{12}(OSnMe_3)_8$.[31] Silicon atoms are light blue and oxygen atoms are red. 24
Figure 13: Illustration of the method of sequential additions synthetic strategy. (Figure was reproduced from [28]). 28
Figure 14: a cross-linking reaction with a limiting amount $TiCl_4$ and Trimethyltin cube, producing small oligomers of embedded titanium sites. 29
Figure 15: IUPAC adsorption/desorption isotherm classifications (Figure was reproduced from [34]). 32
Figure 16: IUPAC hysteresis loop classifications (Figure was reproduced from [34]). 34
Figure 17: Nitrogen adsorption/desorption isotherm for Davisil® silica gel (the blue diamonds correspond to adsorption branch and the pink squares correspond to the desorption branch). 36
Figure 18: IR spectrum (400-2000 cm^{-1}) of the silicate building block $Si_8O_{12}(OSnMe_3)_8$ with the vibrational frequencies and modes labeled. The inset contains the entire IR spectrum (400-3400 cm^{-1}). 39
Figure 19: Illustration of the types of pyridine interactions with acidic sites found in heterogeneous catalysts.[x] 40
Figure 20: Illustration of X-ray absorption and fluorescence. 42
Figure 21: Plot of X-ray absorption energies as a function of atomic number. 44
Figure 22: Representative XAS spectrum (Ti K-edge) divided into two distinct areas: XANES and EXAFS. 45

Figure 23: Representative XANES spectrum (Ti K- edge) for a tetrahedral Ti(IV) center in a silicate matrix. 46
Figure 24: Plot illustrating how the coordination geometry of the titanium atom influences the Ti (K-edge) pre-edge feature intensity and the position of the pre-edge feature. (Figure was reproduced from [38]). 48
Figure 25: XAS spectrum (Ti K-edge) of titanium metal with E_0 marked at 4966 eV. 49
Figure 26: XANES spectra (K-edge) comparing the edge position of titanium(VI) oxide, titanium(III) nitride, titanium(II) oxide and titanium(0) foil. 50
Figure 27: a) XAS spectrum (Zr K-edge) showing the absorption edge background (smooth "bare atom" background) and b) XAS spectrum (Zr K-edge) showing fine structure superimposed on the absorption edge 52
Figure 28: Illustration of constructive (right side) and destructive (left side) interference, absorbing atom is blue and the backscattering atoms are red and green. 53
Figure 29: Illustration of the scattering spheres. 54
Figure 30: Illustration of a typical XAS setup. 55
Figure 31: An illustration showing the relationship between hydrogen accessibility and hydrogen density of current methods for hydrogen storage. 61
Figure 32: A plot of the storage density (volumetric H_2 density vs. gravimetric H_2 density) for various hydrogen storage forms currently being investigated. [44] 62
Figure 33: Components of Kubas binding between a metal atom and molecular hydrogen. 65
Figure 34: A sample FT-IR spectrum showing the main areas of interest. 67
Figure 35: A schematic illustration chemisorption found from the difference in adsorption and desorption curve. 70
Figure 36: series of surface titanium species synthesized from a trimethyltin silicate platform. 73
Figure 37: The IR spectrum of titanated silicate platform. 74
Figure 38: Titanium XANES data (K-edge) of titanated silicate platform. 76
Figure 39: The EXAFS data (K space and R space) of titanated silicate platform. 77
Figure 40: illustrates schematically a possible sequences of steps in the reaction of a hydride base reducing reagent with our trichloro-titanium species. 79
Figure 41: The IR spectrum of titanated silicate platform exposed to sodium borohydride. 80
Figure 42: Titanium XANES data (K-edge) of titanated silicate platform exposed to sodium borohydride. 81
Figure 43: Titanium XANES data (K-edge)of titanated silicate platform exposed to sodium borohydride as it compares to known standards and titanated silicate platform. 83
Figure 44: The EXAFS data (K-space and R-space) of titanated silicate platform exposed to sodium borohydride. 84
Figure 45: illustrations a theorized reaction of a hydrogen with our trichloro-titanium species. 85
Figure 46: A picture of the pressure vessel used for the reduction with hydrogen. 86
Figure 47: A picture of the flow cell used for the reduction with hydrogen 87
Figure 48: An IR of both the pressure vessel and flow cell samples exposed to hydrogen at 350°C 89
Figure 49: Titanium XANES data (K-edge) from both the pressure vessel and flow cell samples exposed to hydrogen at 350°C 90

Figure 50: The EXAFS data (K-space and R-space) from both the pressure vessel and flow cell samples exposed to hydrogen at 350°C..... 91
Figure 51: schematically illustrates a generalized hydrogen spillover mechanism..... 93
Figure 52: Titanium XANES data (K0edge) from a sample exposed to hydrogen with high loading platinum promoter. 94
Figure 53: The EXAFS data (K-space and R-space) from a sample exposed to hydrogen with high loading platinum promoter. 96
Figure 54: Platinum XANES (LIII-edge) spectra from a high Pt loaded sample before and after exposure to hydrogen. 97
Figure 55: A general reaction of cobaltocene with a trichloro-titanium surface species 98
Figure 56: an IR spectrum of titanated silicate platform exposed to cobaltocene. 100
Figure 57: The hydrogen adsorption-desorption isotherm of titanated silicate platform exposed to cobaltocene..... 101
Figure 58: An IR spectrum of titanated silicate platform exposed to UV light and hydrogen..... 102
Figure 59: The IR spectrum of titanated(III) silicate platform. 104
Figure 60: The IR spectrum of titanated(III) silicate platform exposed to hydrogen. 105
Figure 61: Titanium XANES data (K-edge) from titanium(III) silicate platform before and after exposure to hydrogen for activation. 106
Figure 62: The EXAFS data (K-space and R-space) from titanium(III) silicate platform before and after exposure to hydrogen for activation. 108
Figure 63: Generalized Epoxidation Reaction..... 114
Figure 64: Titanium centers with different connectivity on silica matrices 116
Figure 65: IR spectrum for the 4-connected embedded titanium centers..... 122
Figure 66: Generalized epoxidation of cyclohexene with cumene hydroperoxide catalyzed by titanium. 124
Figure 67: Image of catalytic test reaction set-up..... 125
Figure 68: An example NMR spectrum from an aliquot of the catalytic test reaction..... 127
Figure 69: An example mole fraction plot generated from the quantitative NMR data collected from the catalytic test reaction..... 128
Figure 70: A 4-connected tetrahedral embedded titanium site reacting with a peroxide..... 130
Figure 71: Titanium metal clusters capable of reacting with trimethyltin cube. 138
Figure 72: Titanium tetrachloride bispyridine reacting with trimethyltin cube, followed by dimethyldichlorosilane to produce a square planar titanium site. 140

CHAPTER 1: ENGINEERED MATERIALS

Modern society depends on the use and application of engineered materials which may be defined as materials designed and employed for specific applications. These engineered materials are used in a plethora of applications including catalysis, semi-conductors, porous solids for gas storage and separation, fuel cells, and high-K dielectrics materials. Many of these engineered materials go unnoticed by the majority of the populous, but without them, contemporary day-to-day life would quickly come to a standstill.

For more than a century, many engineered materials have been created using more empirically based procedures. The field of heterogeneous catalysis is a prime example of this. Figure 1 indicates the understanding of heterogeneous catalysis vs time. This limited understanding of heterogeneous catalysis can be attributed the inability to target and characterize sites of interest. Early heterogeneous catalysts were mineral supports (silicates and aluminates) with trace transition metals. Through a series of trial and error experiments "special ones" were identified that have superior catalytic activities. At the turn of the century, the field of catalysis and its application to the emerging chemical industries developed rapidly. However, a fundamental understanding of what the actual active sites were remained mostly absent (as seen in Figure 1). This is partially due to most heterogeneous catalysts having multiple types of active sites, leading to uncertainty within the importance of sites and difficulty in characterization. These factors hampered the development of catalysis. One challenge that has slowed development is the lack of techniques that are sensitive enough and selective enough to allow scientists to "see" and characterize potential active sites that exist only on the surface of support materials.

In the last 30 years or so this situation has changed. The study of single crystal surfaces has begun to shed light on the properties of well-defined surfaces sites. Atomic-force microscopy (AFM), scanning tunneling microscope (STM) and X-ray absorption spectroscopy (XAS) have given scientists the ability to better characterize catalytic materials. Density functional theory (DFT) and other computational methods have allowed scientists to model and study individual sites and their activity. However, one area for which much work is still needed is synthetic strategies that are capable of targeting active single sites that can then be called single-site heterogeneous catalysts.

In ordered to keep up with ever-increasing needs for more engineered materials new synthetic strategies are needed. The syntheses of new engineered materials need to be more targeted and directed. These advanced engineered materials need their composition and structure controlled at many different length scales, allowing for the targeted synthesis of materials with specific, desired characteristics. An approach in which the targeted site is identified initially and then built into the matrix as it is being created is one approach to this idea. This sort of targeted synthesis is still quite difficult and there are relatively few synthetic strategies that can offer this control.

A significant scientific and technological step forward in this area would be the development of new, general, rationally based synthetic strategies for the preparation of advanced engineered materials that have homogenously dispersed, metal atom sites on the surface of metal oxide supports. Furthermore, these synthetic strategies should produce high densities of sites on a porous, high surfaces areas support.

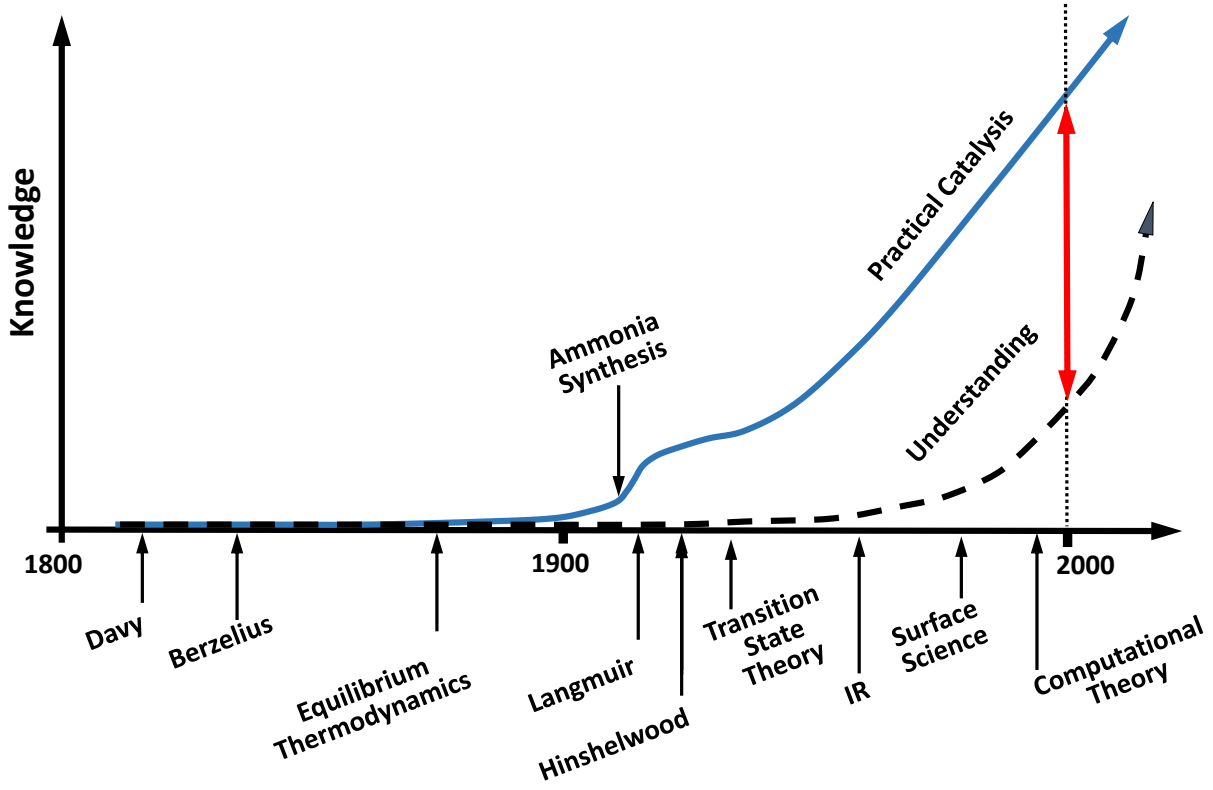

***Figure 1**: A plot demonstrating the contrast in understand of heterogeneous catalysis and practical catalysis. The red arrow indicates the difference in knowledge.*

Additionally, these synthetics strategies would be tailored at several different length scales, and would be applicable for multiple active sites. Ideally, these strategies should also be appropriate to a broad range of applications including catalysis, semi-conductors, porous solids for gas storage and separation, fuel cells, and high-K dielectrics materials. The types of sites needed for the variety of applications listed can be quite similar. The key is to be able to target and prepare sites that have specific characteristics that are believed to be critical for their desired reactivity. This will be a major theme of this dissertation. This dissertation will focus on a novel synthetic approach that achieves these goals and how it can be applied to catalysis and hydrogen storage.

AREAS OF FOCUS

GAS SEPARATION AND STORAGE

Porous solids like those found in gas separation and gas storage media are ideal candidates for advanced engineering. The ability to prepare porous materials while targeting a single site that is capable of only binding a substance of interest would for allow storage media to be more selective and efficient. With the supply of fossil fuels being exhausted in the future, the storage of hydrogen in onboard systems is of great importance. Finding a storage medium that combines a hydrogen density greater than that of the liquid with fast kinetics allowing rapid charging and discharging has been challenging in the area of utilizing hydrogen as an energy source. The targeted synthesis of advanced engineered materials designed to do just that may lead to advancements in alternative energy sources and help minimize the dependence on foreign sources.

CATALYSIS

Almost every facet of our daily lives depends on catalysis and its contributions to present day society cannot be overstated. The production of fuels, plastics, chemicals, and pharmaceuticals all rely on catalysis on an industrial scale.[1] Catalysis also plays a vital role in almost every biological reaction in the form of enzymes.[2] Finally, catalysis plays a major role in the reduction of harmful pollutants that are present in automobile emissions and the waste streams from fossil fuel power plants. [3]

An example of a familiar application of catalysis in everyday life is the catalytic converter found in modern automobiles. Catalytic converters transform unburned fuel, carbon monoxide, and nitrogen oxides to less harmful emissions, such as carbon dioxide, nitrogen, and water (equations 1- 3, Figure 2). All these reactions are accomplished by platinum and rhodium active sites on a ceria support.[4] Ideally, the catalytic converter on an automobile should never need to be replaced because a catalyst is not consumed as it performs its function even though the amount of exhaust that is treated is many times the weight of the catalyst.

$$2CO + O_2 \rightarrow 2CO_2 \qquad \text{Eq. 1}$$

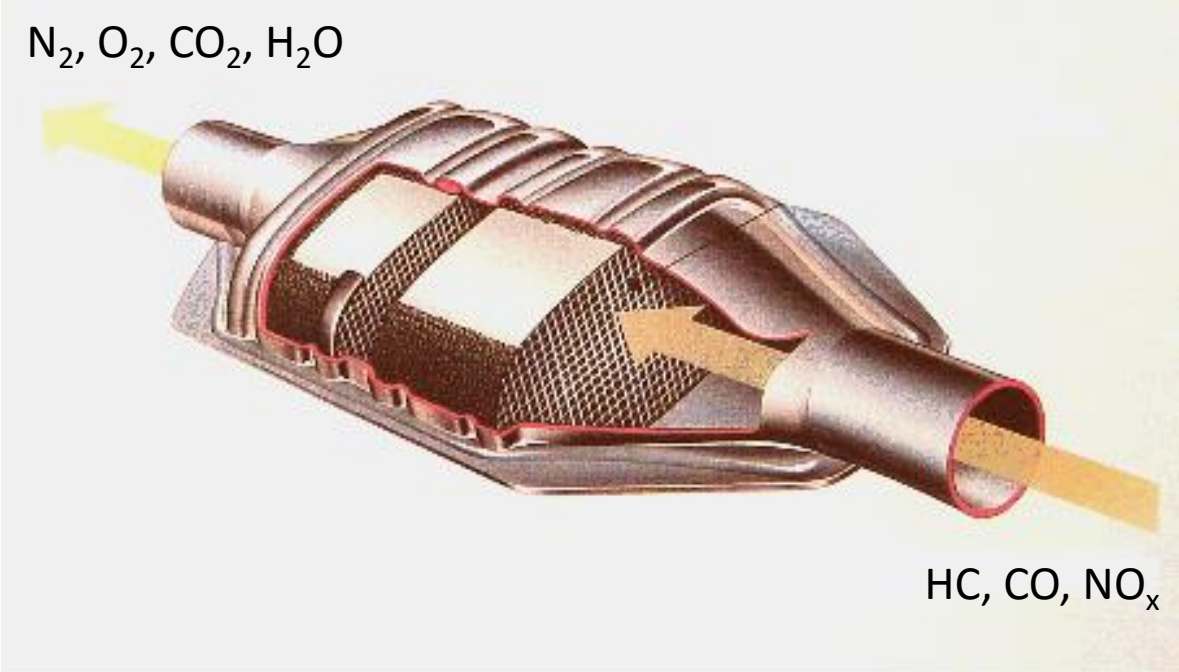

***Figure 2**: a diagram showing the reactants (unburned fuel, carbon monoxide, oxygen, nitrogen oxide) and products (nitrogen, oxygen, carbon dioxide, and water) of a catalytic converter (Figure was reproduced from [5]).*

$$2NO_x \rightarrow 2N_2 + XO_2 \quad \text{Eq. 2}$$

$$C_xH_{2x+2} + \left(\frac{3x+1}{2}\right)O_2 \rightarrow XCO_2 + (x+1)H_2O \quad \text{Eq. 3}$$

DEFINING A CATALYST

A catalyst is an ensemble of atoms that increases the rate of a reaction without being consumed during the reaction. A catalyst increases the reaction rate by lowering the activation energy (E_a) of a chemical reaction (Figure 3). A catalyzed reaction has a lower energy barrier than the same reaction when not-catalyzed (Figure 3). Therefore, catalyzed reactions proceed through an alternative mechanism than that of a non-catalyzed reaction.

The functioning of a catalyst during a catalytic cycle can be divided into three distinctive steps. (1) Binding: Assuming mass transport of reagents to and from an active site are fast, a catalytic reaction begins when the catalyst chemically binds a substrate. (2) Transformation: The catalyst then transforms the bound substrate through a series of intermediates to the final product. (3) Release: The last step of the catalytic cycle involves release of the product from the catalyst, thus returning the site to its initial active state. Once the catalyst has returned to its initial active state it can combine with another substrate and go through the cycle again. Satisfactory catalysts can proceed through a catalytic cycle repeatedly. Ideally, a catalytic cycle continues without limit, but in reality, undesired changes can render the catalyst less active with continued use. For this reason, many catalysts must be periodically regenerated or replaced.

HOMOGENEOUS VERSUS HETEROGENEOUS CATALYSTS

Catalysts can be classified by their phase compared to their substrate. Homogeneous catalysts are catalysts that are in the same phase as the substrate. In contrast to this, heterogeneous catalysts reside in a phase that is different from that of the substrate. There are five main fundamental differences between homogeneous and heterogeneous catalysts.

First, homogeneous catalysts are in general easier to characterize than heterogeneous analogs. Homogeneous catalysts benefited greatly from the development of several molecular characterization tools, such as X-ray diffraction and NMR spectroscopy, allowing precise characterization of the stable precursors or even active species. In contrast to this, the spectroscopic approaches used for characterizing and identifying heterogeneous catalysts generally do not give as clear a picture of the active site. In fact, heterogeneous catalysts generally require the use of several characterization tools to construct a model of the active species.

Second, heterogeneous catalysts frequently exhibit greater thermal stability than homogeneous analogs. Therefore, heterogeneous catalysts are better suited than homogeneous catalysts for use in reactions requiring higher temperatures. Heterogeneous catalysts frequently involve reactions that occur over a broad range of temperatures (up to 1000°C) while most homogeneous catalysts are stable only below 200°C.[6] This thermal stability allows heterogeneous catalysts to be used in reactions that are not suitable for homogeneous catalysts e.g. cracking of crude oil. The use of catalysts at high reaction

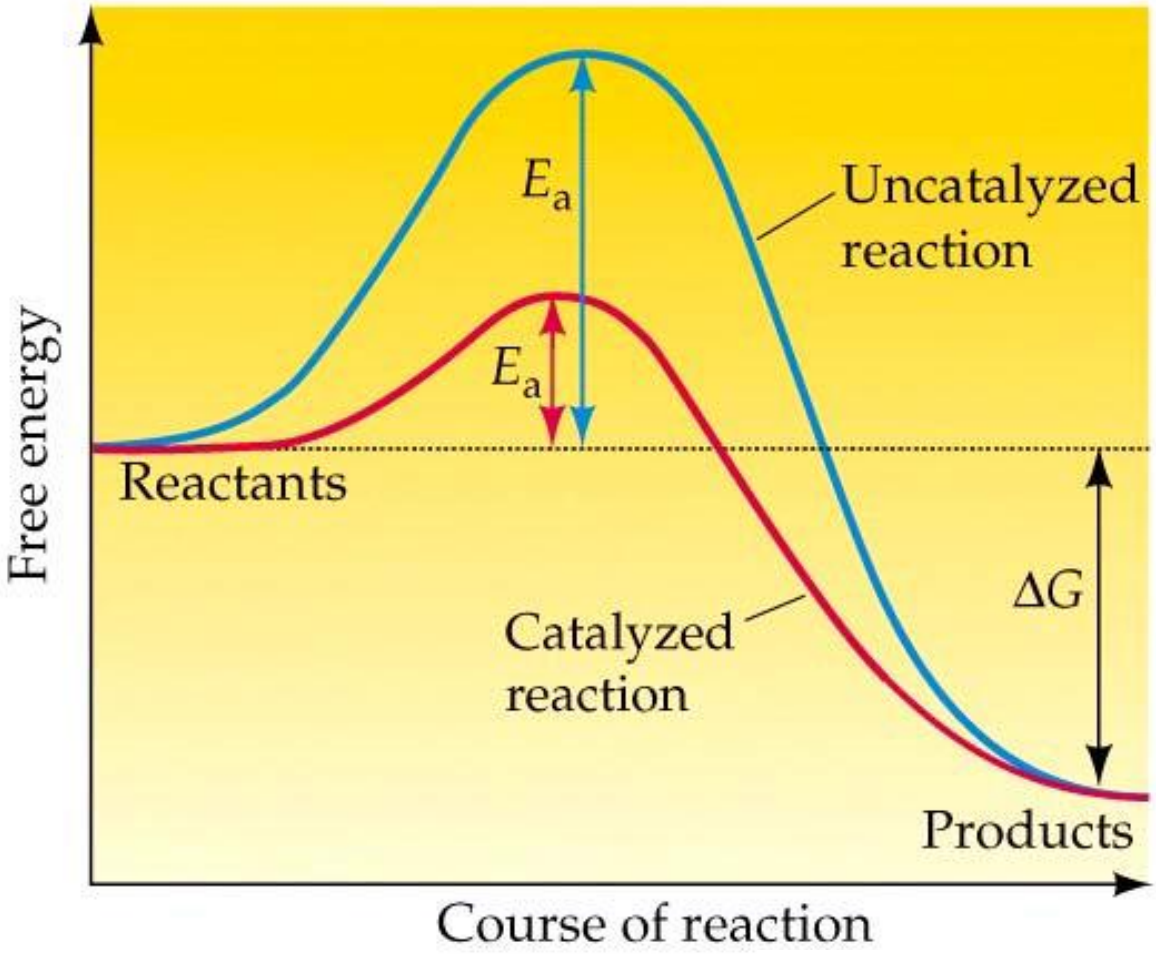

***Figure 3**: Illustration of the energy diagram of an uncatalyzed (blue) and catalyzed (red) reaction showing that a catalyzed reaction has a lower activation energy (E_a) than the same reaction when not catalyzed (Figure was reproduced from [7]).*

temperatures frequently lead to high rates of reaction which mean increased catalytic activity which allows a heterogeneous catalyst to be as active as or more active than its homogeneous counterparts.

Third, heterogeneous catalysts are easier to recycle and separate from the products than their homogeneous counterparts. This results from the catalyst and products being in separate phases, while the separation of homogeneous catalysts from the products tends to be a more complicated procedure since the catalysts are in the same phase as the products. The ease of separation from reaction products that is associated with heterogeneous catalysts results in lower processing costs. Additionally, heterogeneous catalysts are readily applied to both continuous flow and batch reaction systems, whereas homogeneous catalysts are predominantly only appropriate to batch reaction systems. As a result, the chemical industry tends to favor heterogeneous catalysts when the expense of separating the catalyst and the products is a large portion of the overall cost of the process.

Fourth, the ligands found in homogeneous catalysts can be tailored to a much higher degree than is typically possible in the case of heterogeneous catalysts. Thus, it is possible to vary the steric and electronic features of homogeneous catalysts much easier and to a greater extent than heterogeneous catalysts.[8] An example of this can be seen in metallocene catalysts. Metallocene complexes are commonly used as homogeneous catalysts and the sterics and electronics of the cylcopentadienyl (Cp) ligands can easily be altered. As shown in Figure 4, Pentamethylcyclopentadienyl (Cp*) ligands are sterically larger and donate more electron density to the metal center than standard Cp ligands. Linking two Cp ligands together producing *ansa*-Cp ligands, allows one to open up access to the metal center and control both the sterics and electronics of the active site. The ability to control the sterics and electronics of ligands, as in the case of Cp ligands for homogeneous metallocene catalysts, is a component of heterogeneous catalyst synthesis that is largely absent. As a result, heterogeneous catalysts cannot be modified as easily as their homogeneous counterparts. Within this context, new synthetic methodologies that can be used to prepare tailored heterogeneous catalysts have been a longstanding challenge for the heterogeneous catalysis community.

Finally, homogeneous catalysts are frequently single site while heterogenous catalysts are rarely single site. Reasons for this are discussed in detail below.

ACTIVE SITE ANATOMY

Understanding the active site is a key factor for synthesizing tailored heterogeneous catalysts. The active site of a heterogeneous catalyst is more than the catalytically active metal site in/on the support. It is generally thought that the immediate environment of the metal cations also influences the observed catalytic behavior. Typically, a metal site will be bound to a support, frequently a metal oxide such as silica, alumina, or titania (SiO_2, Al_2O_3, or TiO_2) via terminating oxygen atoms existing on the surface of the support Figure 5. These bonds to the surface serve to hold the metal cation in place as well as contribute to the overall charge on the metal site. Additionally, the arrangement of the bonds between the metal and support will influence the electronics of the metal site and thereby its reactivity. Finally, to fill out the coordination sphere of the metal site, a number of terminating ligands may be present. Usually these

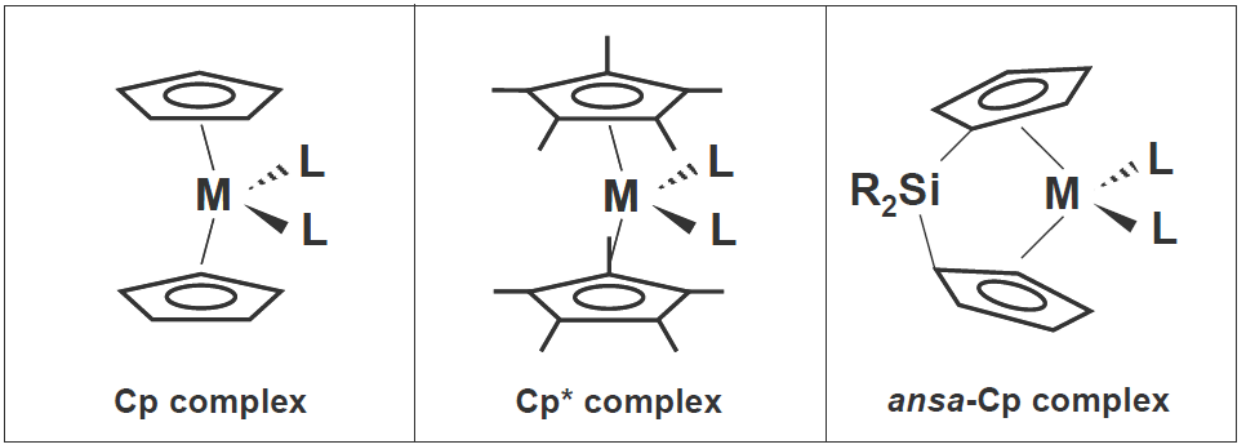

***Figure 4**: Illustration of metallocene complexes with different Cp ligands.[9]*

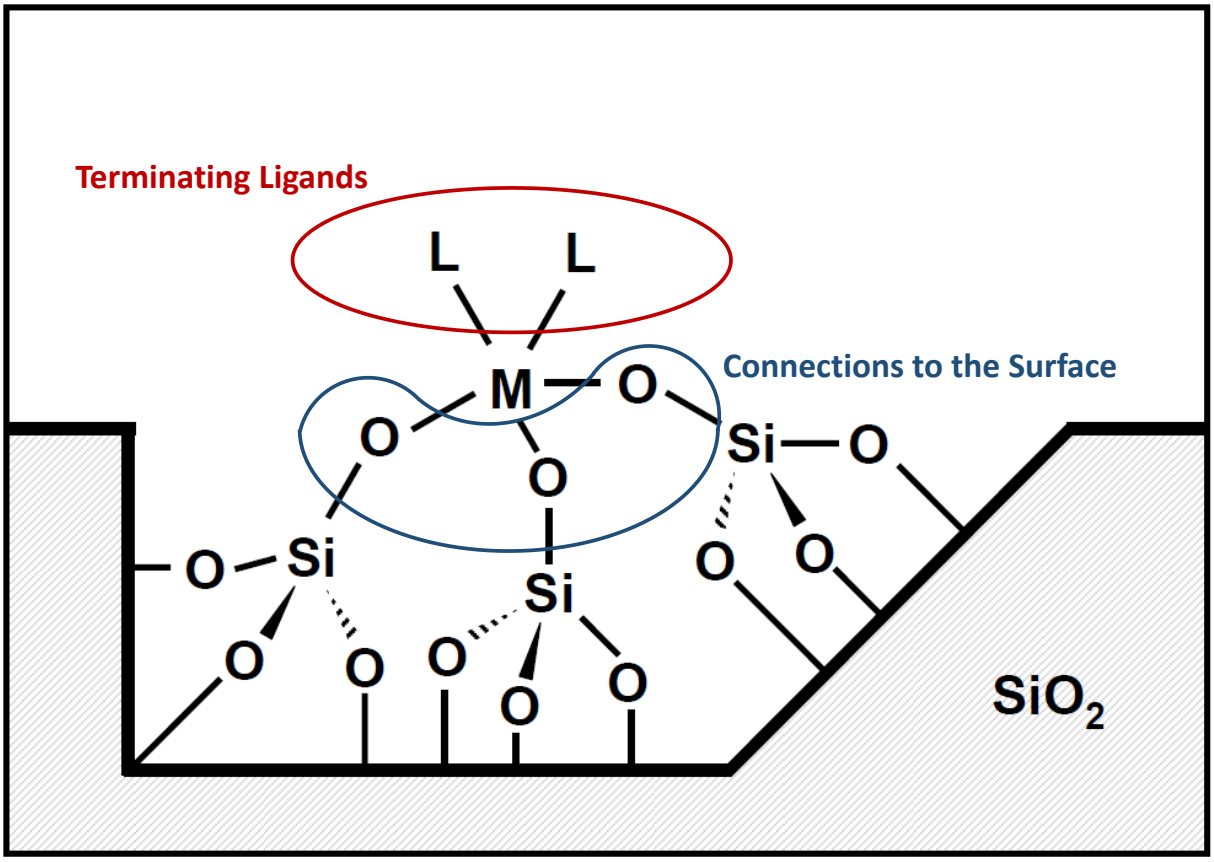

***Figure 5**: Illustration of an active site showing the terminating ligands (L, Red), metal-to-surface binding interactions (M-O-Si, Blue), and the support (SiO_2).*

additional ligands exchange with reactants to initiate catalysis. The metal sites, terminating ligands, and bonds between the metal and support that are directly associated with the binding and transformation of a substrate into a product are referred to as the catalyst ensemble.

CATALYSIS CHARACTERISTICS OF IMPORTANCE

As important as the characterization of a catalyst's physical properties is, it is meaningless if the material is incapable of acting as a catalyst. For this reason, every research program focused on catalyst development conducts catalytic test reactions in parallel with more classic characterization methods. These test reactions attempt to define three important quantities that can be used to determine the effectiveness of a catalyst.

(1) SELECTIVITY

Selectivity is a measure of a specific product relative to all of the products of a reaction. Selectivity is generally represented as the percent yield of a specific product relative to the stoichiometric yield from the substrate. Selectivity is a property of great importance in industry because high selectivity means the yield of a desired product will be high and there will be less cost associated with the separation from unwanted byproducts. Single site catalysts are widely considered to have higher selectivity than their multi-site counterparts. This is justified by the concept that each individual type of site is predicted to accomplish specific reactions. Therefore, fewer types of sites should give rise to higher selectivity by a catalytic material. Selectivity is easy to determine as long as researchers can detect and quantify the products of a reaction.

(2) ACTIVITY

Activity is a measure of the amount of substrate that is converted during the reaction over a specified time interval. Percent conversion is sometimes considered an appropriate measure of activity. However, percent conversion data generally does not take into account the number of active sites present in the catalyst. As a result, these numbers can be easily manipulated by simply adding more catalyst, decreasing the concentration of substrate, or changing the temperature and time. Consequently, the observation of increased conversion does not necessarily mean a catalyst is more active. More accurate measures of activity are turnover number and turnover frequency. Turnover number, TON, measures the number of substrate molecules converted per active site. Turnover frequency, TOF, quantifies the activity of a catalytic site occurring at the site per unit time. In addition to determining conversion, researchers must be able to quantify the number of active sites in a sample of the material in order to determine turnover numbers and turnover frequency. Counting the number of active sites in a catalyst can present a number of challenges, which is the reason that many catalysis studies still only report percent conversions.

(3) STABILITY

A component of catalytic test reactions involving heterogeneous catalysts that are less frequently studied is stability. The apparent reactivity of a catalyst frequently can decline over the course of a run due to several factors. The most important pathways by which catalyst deactivate are leaching, active site

decomposition, or blocking access to the active site. Leaching studies arguably provide information that is more critical in the determination of the effectiveness and longevity of a heterogeneous catalyst than activity and selectivity. The ideal case is that the active sites do not leave the support surface to become potentially soluble homogeneous active sites. If leaching does not occur, then the observed catalysis is truly heterogeneous in nature. However, if the components of the active sites of a heterogeneous catalyst leach during reaction one can envisage three different consequences: (1) the leached species is not an active homogeneous catalyst and the apparent activity of the catalyst system is not an accurate measure of the sites initially present. (2) The leached species is an active homogeneous catalyst and the apparent activity of the catalyst system decrease. (3) The leached species produces undesired byproducts, reducing the selectivity of the overall reaction.

TRADITIONAL SYNTHESES FOR TARGETED ACTIVE SITES

Traditionally, heterogeneous active sites are prepared using a variety of synthetic procedures. In general, these procedures can be divided into two groups. (1) Procedures in which the deposition of the active metal site occurs during the synthesis of the material. These sites are generally referred to as framework or embedded sites. (2) Procedures in which the active metal sites are deposited onto a pre-synthesized support. These sites are generally referred to as surface sites. Generally speaking, embedded sites have multiple links to the support, while surface sites have fewer links to the support, and in the extreme cases may only have only one link to the support. By and large, none of these procedures are capable of producing single sites, but rather a mixture of sites. These mixtures of sites are often overlooked within the literature as they present a limitation found for all conventional synthesis methods.

TRADITIONAL SYNTHESES FOR CREATING EMBEDDED SITES

Traditional methods from the literature for preparing embedded active sites include sol-gel, templating, nonhydrolytic sol-gel, and hydrothermal processes which are discussed in more detail in the following sections.

SOL-GEL PROCESS

The sol-gel process is a common procedure used to prepare supports and heterogeneous catalysts because the chemicals and apparatus are relatively inexpensive, the reactions are simple, and the required reaction conditions are mild. The sol-gel process is divided into six steps: preparation of a sol, hydrolysis, condensation, formation of a gel, aging, and drying.[10,11] A typical sol-gel process begins with the active site precursor being dissolved in an aqueous solution. Metal alkoxides are usually used as metal precursors in the sol-gel processes because they react readily with water and are relatively inexpensive which helps minimize the cost of the process. In the presence of water, metal alkoxides hydrolyze to form metal hydroxides (Equation 4).

$$M(OR)_4 + X\ H_2O \ \rightarrow \ M(OR)_{4-x}(OH)_x + X\ ROH \qquad \text{Eq. 4}$$

A condensation reaction that produces water or an alcohol can then link two metal alkoxides complexes or metal hydroxides together. Two complexes containing hydroxide ligands can be seen in equation 5.

Equation 6 shows the condensation reaction between a hydrolyzed molecule and a molecule containing an alkoxide ligand. Hydrolysis and condensation represent a very complicated series of coupled reactions which are difficult to control. Therefore, it is almost impossible to tailor the catalyst ensemble using the sol-gel process.

$$(RO)_3M - OH + HO - M(OR)_3 \rightarrow (RO)_3M - O - M(OR)_3 + H_2O \quad \text{Eq. 5}$$

$$(RO)_3M - OR + HO - M(OR)_3 \rightarrow (RO)_3M - O - M(OR)_3 + ROH \quad \text{Eq. 6}$$

The combination of hydrolysis and condensation reactions will continue to build larger and larger molecules until a gel is formed. Gel formation occurs when a molecule reaches macroscopic dimensions so that it extends throughout the solution.[10,11] Once a gel forms, it can be aged before drying. Aging is the further cross-linking of unreacted sites after gelation occurs. Aging can result in a significant increase in the surface area and porosity of the final material.

The final step of the sol-gel process is drying of the gel. Drying is the process by which the solvent is removed from the pores of the sol-gel product. If the drying occurs via evaporation under normal conditions the resulting material is classified as a xerogel. This drying process gives rise to capillary pressure that can cause the pore structure to collapse. An aerogel is produced when a wet gel is placed in an autoclave and dried under supercritical conditions. This drying process does not produce capillary pressure and therefore there is relatively little collapse of the pore structure.[11]

Even though the sol-gel process is one of the most common synthetic techniques for making metal oxides there are several disadvantages associated with the process. A drawback is that the condensation step can be reversible which means that even if the desired pattern of linkages to an active metal site is formed initially, it can still be lost as the system anneals itself (Equation 7).

$$M - O - M' + H_2O \leftrightarrow M - OH + HO - M' \quad \text{Eq. 7}$$

Another shortcoming arises when using the sol-gel process to prepare mixed metal oxides. In the case of mixed metal oxides, the dispersion of a metal in the final product is influenced by the relative rates of homocondensation (formation of M-O-M or Si-O-Si) versus heterocondensation (formation M-O-Si) for the reactants involved. Controlling the hydrolysis and condensation rates can be rather difficult in the sol-gel process. The degree of homogeneity of the final material will depend on the ability to favor heater condensation. Several partially successful strategies have been reported in the literature to compensate for the differences in condensation rates form mixed metal oxides.[12-14]

Although it is one of the most common procedures used to prepare supports and heterogeneous catalysts, the sol-gel process suffers from a lack of synthetic control with respect to the active site. This lack of control often leads to materials with multiple sites. The number of linkages that a metal cation forms to a support as well as the dispersion of the surface functionality on the support and metal cations throughout the support are not easily controlled using the sol-gel process. Additionally, simple first order

sol-gel processes offer little control of the surface area and porosity of the final material. This lack of control often leads to catalysts with multiple sites. The sol-gel process can be used to prepare amorphous porous materials but it is not ideal for the preparation of tailored supports and heterogeneous catalysts.

TEMPLATING PROCESS

Templated mesoporous materials represent a subcategory of the materials produced using the sol-gel process. Templated mesoporous materials typically are high surface area amorphous materials with ordered pore structures.

The templates used to produce these materials can be divided into two groups: soft and hard. Soft templates usually consist of organic surfactants, polymers, and even biological viruses, which are relatively flexible in shape. Whereas hard templates normally possess well-defined shapes and voids which can be in the form of channels, pores, or connected hollow space. Anodic aluminum oxide membranes and porous silica are typical examples of hard templates.[15] Figure 6 illustrates the general process that is used to synthesize templated mesoporous silica, typically a soft template approach. Initially, a surfactant is added to an aqueous solution where it forms micelles. The micelles then self-assemble into a specific arrangement. Once the self-assembly process is complete, the silica precursor then undergoes the sol-gel process, forming a silica matrix around the template micelle assemblies. Finally, the template is removed either by calcination at high temperature or repeated washing resulting in a high surface area mesoporous silica with ordered porosity.

The two most common examples of templated mesoporous supports are MCM-41 (MCM = Mobil Crystalline Material)[16] and SBA-15 (SBA = Santa Barbara Amorphous).[17] Both supports are synthesized using soft templates. SBA-15 is synthesized using nonionic surfactants, specifically amphiphilic triblock copolymers, while MCM-41 is synthesized using cationic surfactants, specifically quaternary ammonium salts.

By varying the ratio of surfactant to silicon precursor, the structure of the resulting material can be influenced. MCM-41 has an ordered hexagonal structure and is produced when the ratio is less than 1, MCM-48 is produced when the ratio is greater than 1 and has an ordered cubic structure, and MCM-50 is produced at ratios much greater than 1 and has an ordered lamellar structure. These three different structures of MCM materials are shown in Figure 7.[18]

Similar to MCM materials, several different structures of SBA materials have been identified. SBA-15 has an ordered 2-dimensional hexagonal structure, SBA-2 and SBA-12 have ordered 3-dimensional hexagonal structures, SBA-1, SBA-16 and SBA-11 all have ordered 3-D cubic structures.[19]

Metal cations can be incorporated into the framework of templated mesoporous silicas such as SBA-15[20] and MCM-41[21] during synthesis, which is known to result in the production of high surface area heterogeneous catalysts. Similar to basic sol-gel process, there is little if any control of the dispersion of the metal cations in these materials.

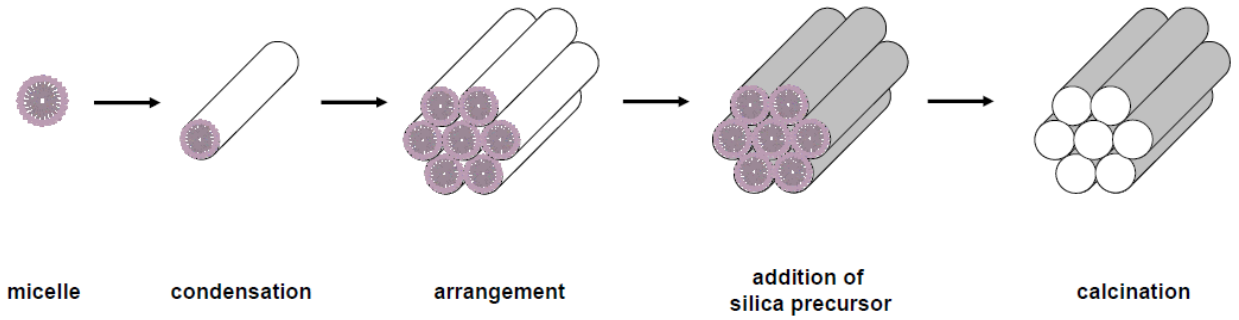

***Figure 6**: Illustration of a templating process using a soft template.[22]*

.

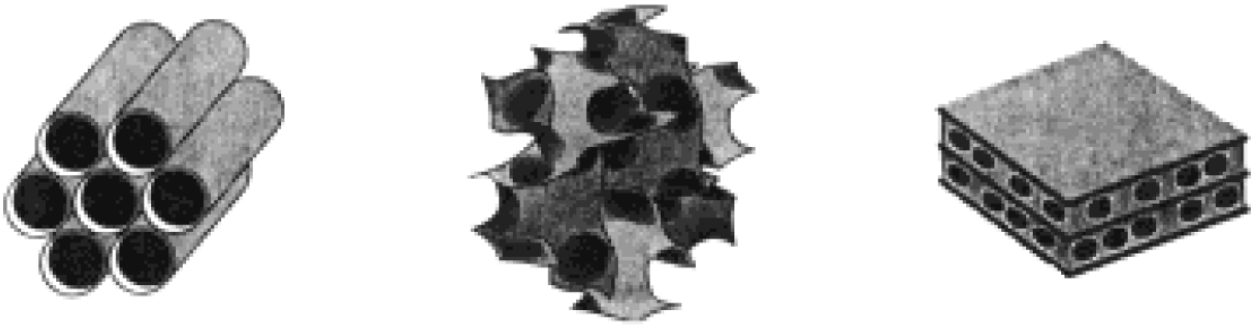

***Figure 7**: Illustration of the pore structure of three MCM materials (left- MCM-41, center- MCM-48, and right- MCM-50).[18]*

NONHYDROLYTIC SOL-GEL

A nonhydrolytic sol-gel process occurs when the oxygen donor is not water and more specifically water is not present at any point during the process. Similar to hydrolytic sol-gel processes both metal oxides and mixed metal oxides can be synthesized using nonhydrolytic sol-gel processes. Metal precursors are typically linked together via a condensation reaction between two different metal precursors bearing two different functional groups by eliminating a small organic molecule. A nonspecific reaction can be seen in equation 8.

$$M - OR + X - M \quad \leftrightarrow \quad M - O - M + RX \qquad \text{Eq. 8}$$

M-OR is a metal alkoxide and M-X can be a metal alkoxide, metal halide or a metal carboxylate. Nonhydrolytic sol-gel process may be classified according to the nature of the metal precursor (halide, alkoxide, etc.), the nature of the oxygen donor (alkoxide, alcohol, ether, etc.) or the nature of the predominant molecule eliminated (alkyl halide, ether, ester, etc.). One of the key advantages of nonhydrolytic sol-gel processes is that the condensation reactions are usually irreversible. One shortcoming is the necessity for the complete exclusion of water, which means moisture-sensitive techniques are required for these syntheses. Nonhydrolytic sol-gel processes provide a variety of condensation reactions that can be used to synthesize porous metal oxides and mixed metal oxides. However, nonhydrolytic sol-gel processes suffer from the same problems as sol-gel processes. The number of linkages that a metal cation forms to a support as well as the dispersion of the surface functionality on the support and the metal cations throughout the support are not easily controlled using nonhydrolytic sol-gel processes. Also, the nonhydrolytic sol-gel process offers little control of the surface area and porosity of the final material. Nonhydrolytic sol-gel processes can be used to prepare amorphous porous materials but they are not ideal for the preparation of tailored heterogeneous catalysts.

HYDROTHERMALLY PROCESS

Hydrothermal synthesis refers to high-temperature reactions involving water in sealed reaction vessels above ambient temperature and pressure. Zeolites are examples of the materials prepared using hydrothermal processes. Zeolites are among the most important materials in the chemical industry with a multitude of technical applications which includes heterogeneous catalysis. Zeolites are crystalline silicates built from SiO_4 tetrahedral that are arranged in such a manner that the pores present in these materials are of molecular dimensions. Typically, the pores found in zeolites have diameters in the range of 4-12 Å. Each zeolite structure type features a unique micropore system with the sizes and shapes of the micropores being defined exclusively by the crystal structure of the matrix. Currently, more than 170 different zeolite structure types are known. Figure 8 illustrates the pores and molecular scaffolding in two common zeolite structure types, BEA and MFI. Zeolites can be used as either supports or heterogeneous catalysts. One major drawback of zeolites is that they are microporous materials, which limits the range of substrates and reactions that are possible.[23] For example, titanium silicalite-1, TS-1, (Ti in MFI type zeolite, pore diameter = 5.5 Å) readily catalyzes the epoxidation of 1-hexene in aqueous H_2O_2 but does not catalyze the epoxidation of cyclohexene. Cyclohexene is too large to fit into the pores of TS-1 and consequently, cannot be epoxidized using TS-1.

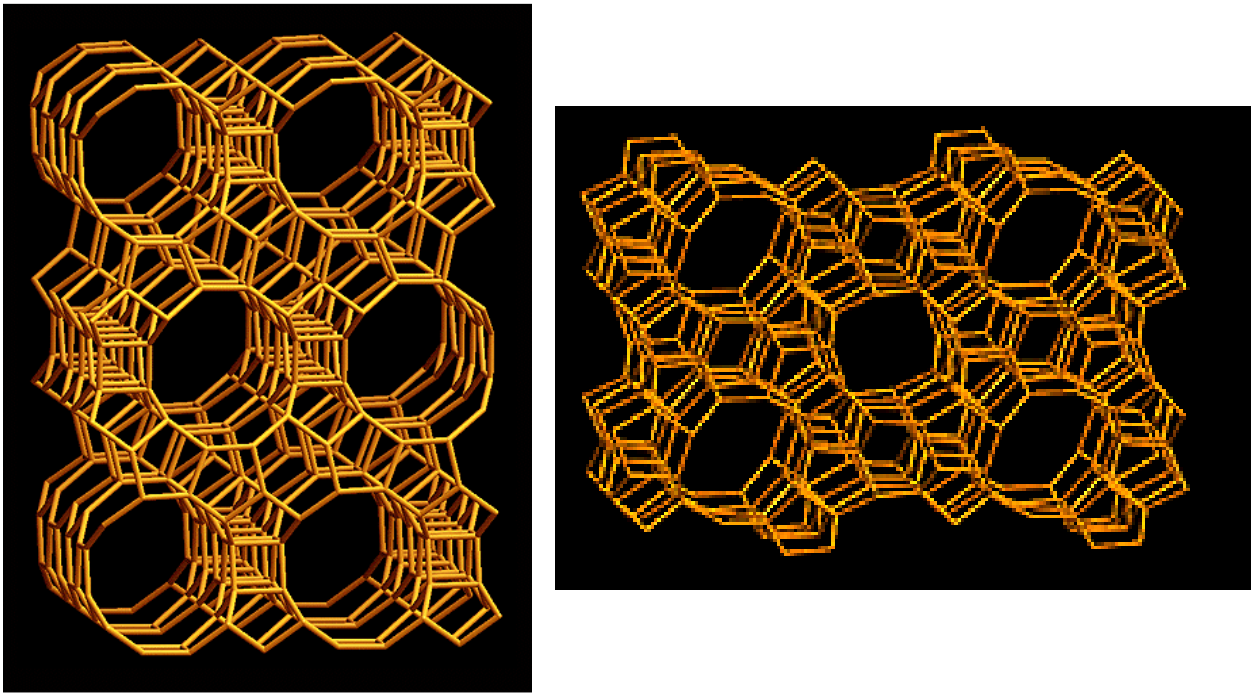

***Figure 8**: Illustration of two types of zeolite structures (left-BEA and right- MFI) (Figure was reproduced from [24]).*

Although zeolites can suffer from mass transport problems due to their microporosity, zeolites are widely used in the chemical industry. The hydrothermal processes used to produce zeolites require harsh temperatures and pressures, which provide little synthetic control. Additionally, the number of linkages that a metal cation forms to a support, as well as the dispersion of the surface functionality on the support, and the metal cations throughout the support are not easily controlled using hydrothermal processes.

Finally, the hydrothermal processes offer little control with which to target specific surface areas and porosities in the final materials. Therefore, hydrothermal processes are not broadly applicable to the preparation of many desirable advanced engineered solid materials.

SUMMARY OF EMBEDDED SITES

In order to prepare advanced engineered materials with embedded active sites, one must be able to prepare identical active sites throughout the matrix. These active sites must have the same number of linkages to the support. Furthermore, the surface area of the support and the dispersion of the surface functionality must be controlled during synthesis. None of the traditional syntheses for preparing embedded active sites provide the necessary synthetic control for creating single site engineered materials in a targeted manner.

TRADITIONAL SYNTHESES FOR CREATING SURFACE SITES

Traditional methods used to prepare surface active sites via incipient wetness, grafting and tethering will be discussed in the following sections. Generally, as with embedded site syntheses, these procedures are not capable of producing single sites, but rather a mixture of surface sites.

INCIPIENT WETNESS

Incipient wetness is both simple and probably the oldest method of putting surface active site on supports. A typical incipient wetness procedure can be accomplished in three general steps. (1) The active site precursor is dissolved in an aqueous solution. (2) This solution is then put in contact with a porous support. Capillary action draws the solution into the pores and distributes the active site precursor throughout the pores. Ideally, only enough solution is used to fill the pores of the support resulting in the precursor being evenly distributed in the pores of the support.[25] (3) The solvent is then allowed to evaporate leaving the active site precursor within the pores of the support. The exact interactions between the active site precursor and the support depend on the metal complex or complexes that are formed in the solution.[26] Incipient wetness has two key limitations: (1) it is only applicable to water-soluble and water stable active sites and (2) incipient wetness produces a wide variety of sites from atomically dispersed to macroscopic crystalline species.

GRAFTING

Grafting of metal complexes onto the surface of supports is a re-embodiment of incipient wetness where organometallic precursors are used in which ligands are chosen specifically to react with functionality found on the surface of the support material. For example, metal alkyls will react with surface hydroxyl groups to form alkanes and Si-O-M bonds that are the attachment points of the metal to the support (Figure 9). Several examples of grafted metal cations can be found in the literature.[27] An example of a

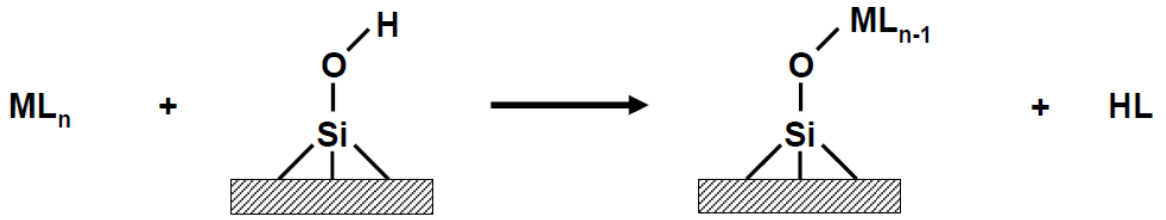

***Figure 9**: Generic illustration of the grafting of a catalytically active metal center (ML_6, L = hydride, alkyl, amide, halide) onto the surface of a silica support (Figure was reproduced from[28]).*

grafting procedure is when titanium(IV) diethylamide ($Ti(NEt_2)_4$) reacts with an isolated silanol to produce the grafted titanium species shown in Figure 10.

The immediate environment around the active site changes in incipient wetness and grafting procedures since at least one ligand on the active site precursor reacts with the surface functionality of the support. In many cases, after the active metal site is deposited on the surface, the material is calcined. In addition to generating more direct linkages to the support, calcination can change the immediate environment around the active site by destroying unreacted ligands on the active site. In most cases, the grafted active site (post and prior calcination) will exhibit different reactivity than is observed by the active site precursor.[8]

Incipient wetness and grafting procedures are similar in that both procedures deposit metal cations onto the surface of a pre-existing support. As a general rule, grafting procedures produces more uniform dispersion of active sites, but are dependent on the distribution of surface functional groups, which can vary across a support.[29] Conversely, incipient wetness has very little control of "anything" and therefore produces a wide variety of active sites. A drawback of incipient wetness and grafting procedures (both before and after calcination) is the generation of multiple types of active sites is possible and generally occurs in most cases. Those active sites will be randomly spread across the surface of the support with little control of dispersion. Therefore, incipient wetness and grafting are not ideal for the preparation of advanced engineered solid materials.

TETHERING

Tethering is similar to incipient wetness and grafting except for one major difference. What separates tethering from incipient wetness and grafting is that the active site is not directly bound to the support in tethering whereas the active site directly binds to the support in incipient wetness and grafting. In tethering procedures, the active site is connected to the support via an additional ligand, i.e. the tether (Figure 11). There are two parts to a tether: the linking group, often a hydrocarbon chain, and a functional group designed to react with surface functionality. The end of the tether that is directly attached to the active site will remain unchanged during the tethering process while the opposite end of the tether will react with the surface functionality. In general, this method is looked at as heterogenizing a homogeneous catalyst and therefore the tethered active site should exhibit similar reactivity to its precursor in addition to having all of the benefits of heterogeneous catalysts.[26]

There are several disadvantages to tethering. First, the tether-to-support linkages, typically Si-C bond, and tether-to-metal, typically metal-main group bonds, tend to be weak. Second, the tether, most often a hydrocarbon chain is vulnerable to attack and decomposition at high temperature. Finally, it is difficult to keep active sites isolated from one another because the tether is generally flexible enough that the active sites can come in contact with each other if the metal loadings are not kept quite low.

Tethering provides researchers a way to secure catalyst ensembles to supports and is often used as an approach to heterogenize a homogeneous catalyst. Although the immediate environment around the active site does not change during a tethering procedure, tethering suffers from a lack synthetic control with respect to the active site. The heterogeneity of the surface functionalities found on the support

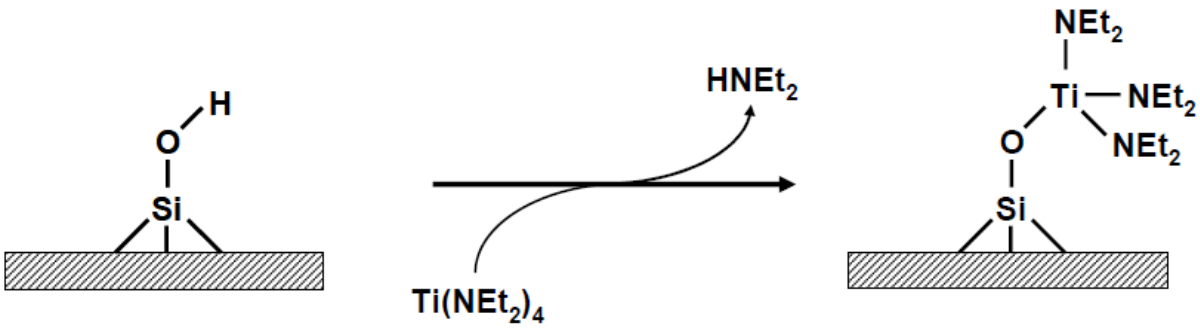

***Figure 10**: Illustration of the grafting of a titanium amide species(Figure was reproduced from [28]).*

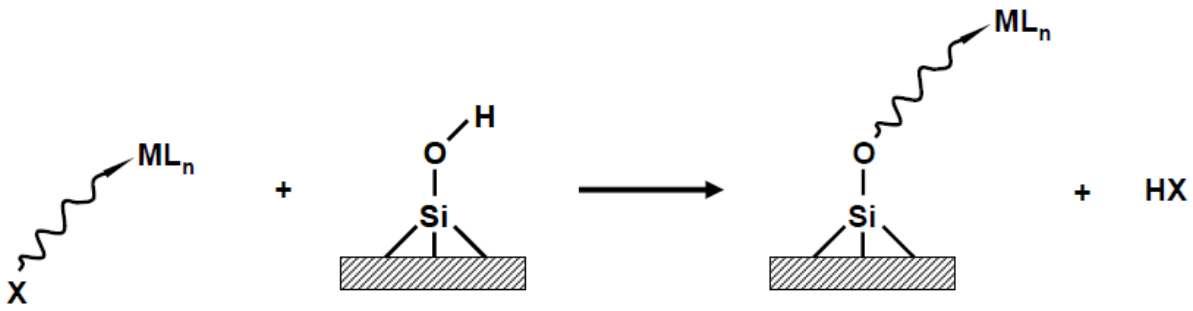

***Figure 11**: Generic illustration of the tethering of a catalytically active metal center onto the surface of a silica support (Figure was reproduced from [28].)*

leads to no control of the number of linkages that a metal cation forms to a support as well as the dispersion of the metal cations on the support.

SUMMARY OF SURFACE SITES

In order to prepare advanced engineered solid materials with surface active sites, one must be able to control the dispersion of the active sites and the number of linkages from the active site to the support. The heterogeneity of real world supports makes controlling the dispersion of the actives sites and the number of linkages from the active site to the support difficult. Therefore, none of the traditional syntheses for preparing surface sites described above provides the necessary synthetic control to reliably and generally achieve the goal of advanced engineered solid materials.

SUMMARY OF TRADITIONAL SYNTHESES

The traditional synthetic methods mentioned in the above sections have all been used to prepare a variety of metal sites within or on supports. However, each of these methods illustrates some of the challenges facing the scientific community. These challenges include the lack of synthetic control with respect to the active site ensemble, the surface functionalities present on a support, the surface area of the support, and the porosity of the support. Therefore, a new synthetic methodology is required to produce a new generation of advanced engineered solid materials. The dispersion of surface functionalities, the dispersion of the active sites, the number of linkages from the active sites to the support, the surface area, and the porosity must be controlled in the new methodology.

A NOVEL SYNTHETIC METHODOLOGY

Over the past decade, the Barnes group has developed a methodology that focusses on for the synthesis of defined geometry, single-site metal centers that are atomically dispersed within porous support matrices such as amorphous silicates. The methodology involves a synthetic strategy referred to as sequential additions with nanometer-sized building blocks. In this approach, rigid, well defined, chemically robust, molecular building blocks are used to build the support matrix in a controlled fashion rather than using a preexisting support or building the support atom-by-atom. This approach allows for the synthesis of a variety of materials with single-site metal centers that have targeted connectivities to the matrix. Generally speaking, this synthetic approach requires three components: a molecular building block, linking agents, and a cross-linking reaction.

THE MOLECULAR BUILDING BLOCK

Building blocks form the majority of the matrix. When cross-linked together, they create a rigid, and chemically robust matrix that allows for the creation of isolated, single-site metal centers. Building blocks that are nanometer-sized or greater will make it easier to ensure that catalytic centers remain chemically isolated from one another and non-interacting. Linking points on the building block that are fixed in space and that are well separated from one another will also help ensure site isolation. In the work described here, each building block contains a silicate cubic core with the molecular formula of Si_8O_{20} (Figure 12). This silsesquioxane core is then functionalized on each corner allowing the building blocks to be linked together to construct the desired matrix vide infra. Although it is possible to functionalize these building blocks in a variety of ways,[30] the synthetic methodology required for the group's synthetic strategy involves the use of a trimethyltin group bound to the terminal oxygen off each silicon corner of the cube.

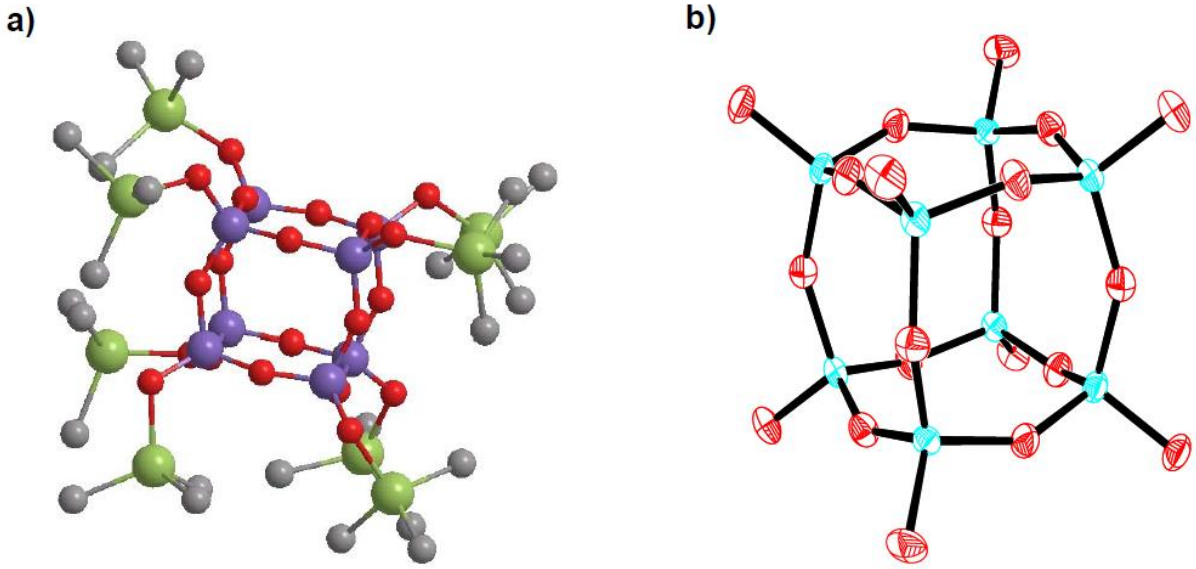

***Figure 12**: a) Illustration of the structure of the building block $Si_8O_{12}(OSnMe_3)_8$. Silicon atoms are purple, oxygen atoms are red, tin atoms are green, and methyl groups are gray. b) Illustration of the core structure of the building block $Si_8O_{12}(OSnMe_3)_8$.[31] Silicon atoms are light blue and oxygen atoms are red.*

Previous work in the Barnes group has found that oxo trimethyltin groups have several advantages as a functionalization of the building block. First, oxo trimethyltin group reacts cleanly and irreversible with high valent metal and main group chloride complexes to produce the volatile compound trimethyltin chloride with the concomitant formation of desired M-O-Si_{cube} link. Additionally, trimethyltin chloride can be quantitatively removed by mild heating under vacuum allowing for a gravimetric analysis of the reaction. The complete structure of the building block can be seen in (Figure 12). This structure will be henceforth referred to as trimethyltin cube and has a chemical formula of $Si_8O_{12}(OSnMe_3)_8$.

THE LINKING AGENTS

As mentioned above, trimethyltin groups rapidly react with a variety of high valent metal and main group halides, which as you would expect are selected as the linking agents. This reaction is favored due to the oxophilic nature of high valent metal and main group halides. Equation 9 illustrates a general linking reaction. Metal and main group chlorides are convenient linking agents because acceptable quantities of high purity material are commercially available and are generally inexpensive. Care must be taken when handling and storing these materials because of their hydrolytic sensitivity. Standard air sensitive (inert atmosphere glovebox and Schlenk line) techniques are required. The linking agents can be divided into two types: those that insert the catalytic active centers into the material and those that insert more silicon into the material, referred to as inert linking agents. Table 1 shows linking agents that have been studied with $Si_8O_{12}(OSnMe_3)_8$ by the Barnes group to date.

$$\equiv Si - O - SnMe_3 + M - Cl \rightarrow \equiv Si - O - M + Cl - SnMe_3 \qquad \text{Eq. 9}$$

THE CROSS-LINKING REACTION

A simple nonhydrolytic sol-gel linking reaction between the “tin cube” and PCl_5 was first reported by Feher.[32] This linking reaction is run in anhydrous organic solvents at temperatures ranging between 20°C and 80°C for less than 24 hours. In each linking reaction, a linking agent (discussed above), and the trimethyltin cube reacts to produce a new siloxane linkage (M-O-Si (M = metal or Si)) and trimethyltin chloride. This process will continue until all the chloride ligands on linking agent are consumed or a chloride ligand becomes unreactive as more M-O-Si bonds are formed to the metal center. The first chloride ligand on the linking agent is thought to react upon contact with solutions of the trimethyltin cube. The rate of reaction of each subsequent chloride ligand decreases as more chloride ligands react.[33] Generally, it has been found that all of the chloride ligands will react with any accessible trimethyl tin group within 24 hours. Preliminary results also indicate that upon phase separation of the growing cross-linked product the reaction is complete. However, more studies are needed to confirm and quantify this statement. Under non-aqueous conditions, trimethyltin chloride is only produced when a building block reacts with a linking agent. The linkages that formed are irreversible, which means that the Si-O-M linkages are stable under the reaction conditions employed. This results in the formation of porous amorphous silicate materials.

In each cross-linking reaction, a linking agent, and the trimethyltin cube react together to produce M-O-Si (M = metal or Si) links and trimethyltin chloride (Fig). After all the cross-linking reagent is consumed, the solid residue is isolated by removing the solvent and volatile byproduct, trimethyltin chloride, under

Table 1: *List of inert and catalytically active linking agents.*

Inert linking agents	**Catalytically active linking agents**	
$SiCl_4$	W^{6+}---	WCl_6, $WOCl_4$, WO_2Cl_2
$SiCl_4py_2$	V^{5+}---	$VOCl_3$
$HSiCl_3$	Zr^{4+}---	$ZrCl_4$
$MeSiCl_3$	Ti^{4+}---	$TiCl_4$, $Ti(OiPr)Cl_3$, $Ti(OiPr)_2Cl_2$ $Ti(OiPr)_3Cl$, $[(Et)_2N]_4Ti$, $TiCl_4py_2$
Me_2SiCl_2	V^{4+}---	VCl_4
Me_3SiCl	Sn^{4+}---	$SnCl_4$, $BuSnCl_3$, Bu_2SnCl_2
	B^{3+}---	BBr_3
	Al^{3+}---	$AlCl_3$
	Ga^{3+}---	$GaCl_3$
	P^{3+}---	PCl_3
	Au^{3+}---	$AuCl_3py$

vacuum. If the linking reaction occurs as expected and no side reactions occur, then the measured weight loss is directly related the amount of trimethyltin chloride produced. The amount of trimethyltin chloride produced during each cross-linking reaction is related to the connectivity (number of linkages to the support) achieved by the metal or silicon center.

THE SEQUENTIAL ADDITION STRATEGY

A synthetic strategy of sequential additions was developed to target and achieve specific connectivities from metals in these building block matrixes. The method of sequential additions relies on both the sequence and the size of doses of different linking agents in the above synthetic approach. Two major types of assemblies can be synthesized using this method: embedded and surface sites. Figure 13 illustrates the dosing strategies used to synthesize the two types of assemblies.

Embedded assemblies within a silicate building block support are obtained when a *limiting* amount of linking agent is initially reacted with the trimethyltin cube. All of the chloride ligands on the linking agent should react forming the maximum number of linkages to the building block support. Following this first cross-linking reaction, the structure will consist of small oligomeric species and possibly unreacted building blocks (Figure 14). These small oligomers will contain the linking centers with the maximum number of linkages to the support and the immediate environment and connectivity around every linker should be identical. These small oligomeric species and trimethyltin cubes are subsequently be exposed a second dose of an inert linking agent such as which will link the oligomers and building blocks together to produces a rigid polymeric structure with porosity. This porosity, created during the second cross-linking reaction, can be tailored by simply adjusting the ratio of inert linking agent to trimethyltin cube. Following the second cross-linking reaction, the final matrix contains metal centers dispersed throughout the silicate support and in which immediate environment around every metal center should be identical and remain unchanged from the first cross-linking reaction.

Surface assemblies on a silicate building block support may be obtained by reversing the sequence of linking reactions. First, an initial silicate support is synthesized using trimethyltin cube and an inert linking agent such as a silyl chloride in limiting amount. The porous silicate support that is formed will have some unreacted trimethyltin groups still present due to the use of limiting amounts of inert linking agent. The number of trimethyltin groups that remain and the porosity generated during the first cross-linking reaction can be tailored by simply adjusting the ratio of the inert linking agent to building block. If a large enough dose is used, the matrix should be rigid and the remaining trimethyltin groups will be well separated on the support diminishing the probability of multi-linked species being formed when a second linking agent is delivered, regardless of the size of the dose. Thus, when a second metal-based linking agent is introduced the subsequent reaction with trimethyltin groups then leads to isolated, “one-connected” surface assemblies.

SUMMERY OF OUR NOVEL SYNTHETIC STRATEGY

The above synthetic strategy applies a building block methodology to a sequential addition strategy. As a result, it is capable of produce both embedded and surface single site species and can be applied to a variety of advanced engineered materials. This work will focus on its application to heterogeneous catalysis

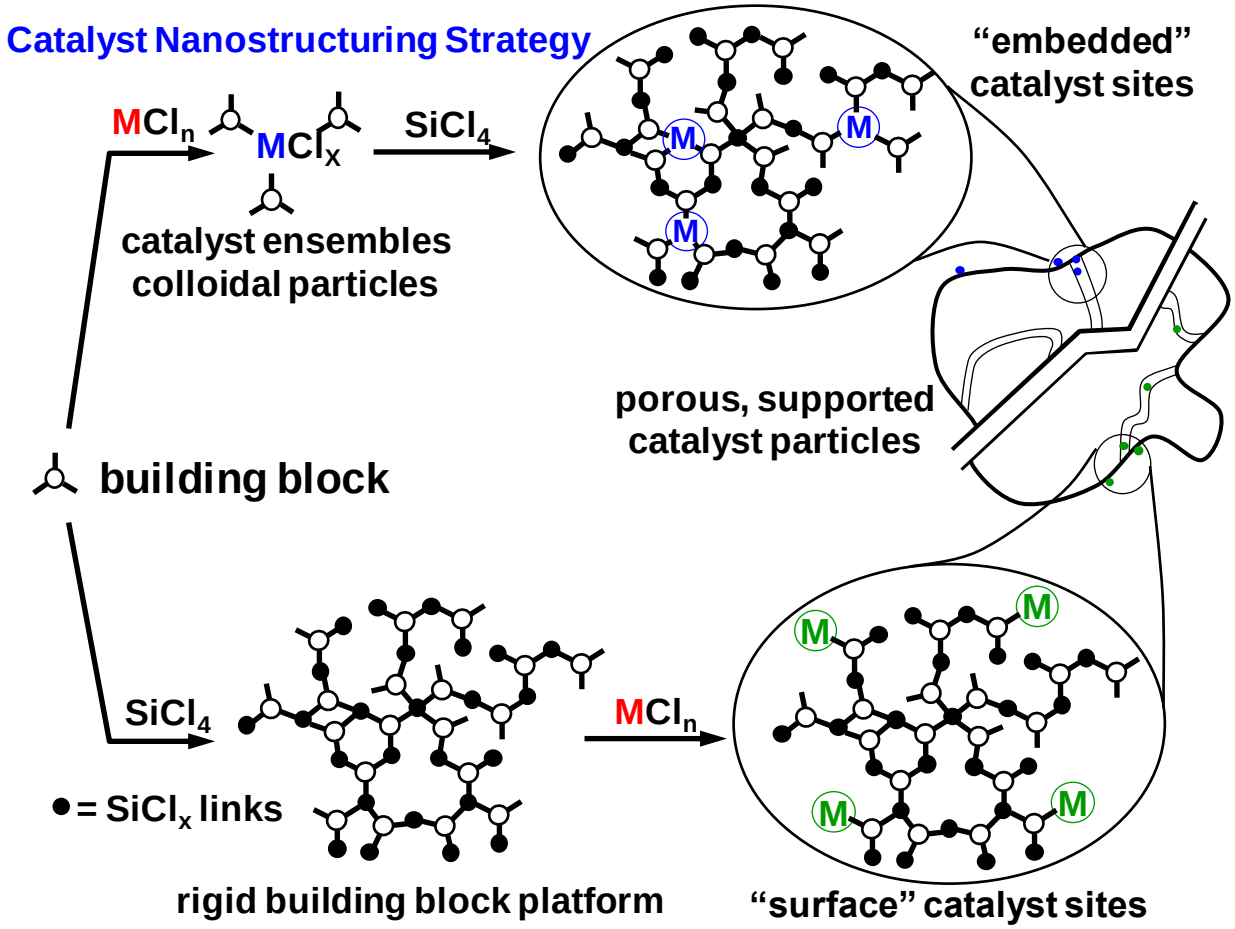

***Figure 13**: Illustration of the method of sequential additions synthetic strategy. (Figure was reproduced from [28]).*

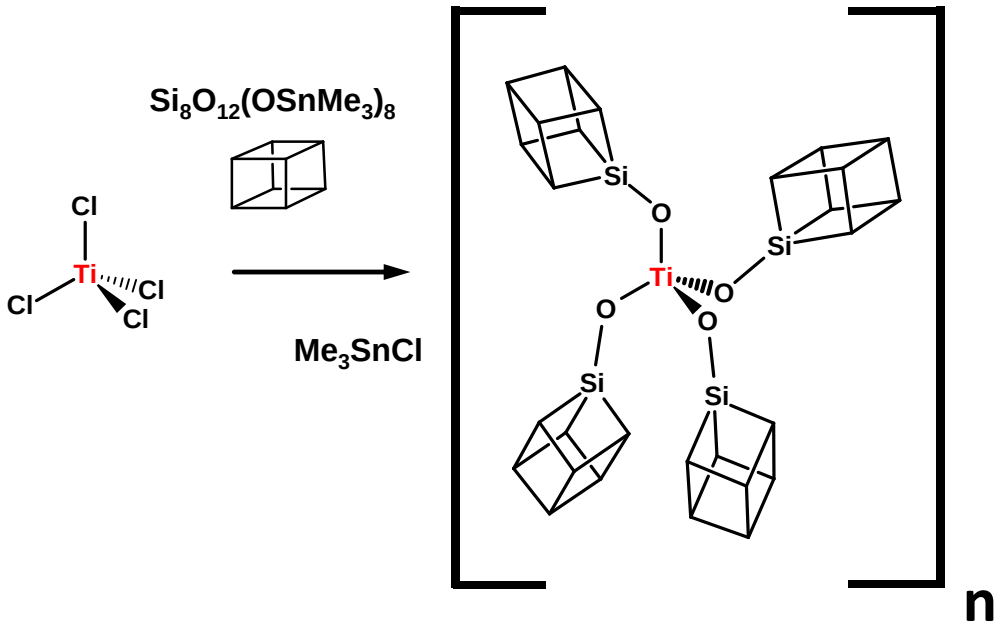

***Figure 14**: a cross-linking reaction with a limiting amount $TiCl_4$ and Trimethyltin cube, producing small oligomers of embedded titanium sites.*

and the synthesis gas storage media. From the perspective of heterogeneous catalysis, higher connectivities around the metal sites are generally favored over that of lower connectivities, as these sites are considered to be more stable towards leaching. In gas storage and separation applications, however, low connectivities are favored, creating more open sites for the binding of gas molecules.

CHARACTERIZATION METHODS

Amorphous systems like the ones described in this dissertation can be quite difficult to characterize due to lack of long range order. The two most commonly used techniques for analyzing solid crystalline materials with metal centers, x-ray crystallography, and solution state NMR techniques, are not available. Despite these challenges, there are several methodologies which can be used to probe the properties of the titanosilicates described here. Gravimetric analysis, Fourier Transform Infrared spectroscopy (FTIR), BET surface area analysis, and X-Ray Adsorption spectroscopy (XAS), X-Ray Photoelectron Spectrometry (XPS), Atomic Absorption (ICP), Diffuse Reflectance Infrared Fourier Transform Spectrometry (DRIFTS), and Raman Spectrometry each contribute pieces of information which help determine the properties of a sample. By selecting a number of these techniques and combining the information gained from each a picture of the local environment surrounding an active site may be pieced together. Furthermore, the characteristics of the macrostructure in which the titanium sites are located are also needed. It is important to use as many complementary lines of evidence as possible when characterizing amorphous materials, as no one technique gives all information needed to obtain a clear understanding of the material and specifically the active sites that are present. The following section discusses characterization techniques use in this dissertation.

GRAVIMETRIC ANALYSIS

Measuring the weight change that occurs following the linking reaction given by equation 10 gives gravimetric data that provides two types of information about the reaction and resulting material. (1) It directly defines the overall reaction stoichiometry. (2) It indirectly defines the local environment around the metal or silicon center. The exact connectivity for a site is obtained in cases when either only one or all of the chloride ligands on the linking agent react with trimethyltin groups. When gravimetric data indicate that the connectivity achieved by the linking agent is intermediate, between one and the maximum, then the gravimetric connectivity number represents the average for the distribution of centers present in the material.

$$\frac{mols\ of\ Me_3SnCl\ produced}{mols\ of\ linking\ precursor} = Connectivity \qquad \text{Eq. 10}$$

The following example illustrates a typical gravimetric analysis for a cross-linking reaction between $SiCl_4$ and $Si_8O_{12}(OSnMe_3)_8$ (2.5 $SiCl_4$: 1.0 $Si_8O_{12}(OSnMe_3)_8$).

The mass of $Si_8O_{12}(OSnMe_3)_8$ used (1.000 g ± 0.01 g) is determined by the weight difference between the reaction vessel with $Si_8O_{12}(OSnMe_3)_8$ under vacuum and the empty reaction vessel under vacuum. The mass of $SiCl_4$ used (0.229 g ± 0.01 g) is determined by the weight difference between the $SiCl_4$ capillary tube source before and after vapor transfer. $SiCl_4$ and $Si_8O_{12}(OSnMe_3)_8$ react to form one equivalent of Me_3SnCl for every new siloxane bond formed. The volatile byproduct trimethyltin chloride, Me_3SnCl is

completely removed from the reaction vessel under dynamic vacuum and cryogenically trapped at 100°C for 18 hours. Proton NMR showed evidence of only solvent and trimethyltin chloride (0.68 ppm, $CDCl_3$), indicating the reaction proceeded as expected. The mass of the solid residue (0.536 g) is determined by the weight difference between the reaction vessel after the volatiles are removed under vacuum and the empty reaction vessel under vacuum. The weight difference between the reactants (1.000 g $Si_8O_{12}(OSnMe_3)_8$ and 0.229 g $SiCl_4$) and products (0.536 g solid residue) equals the amount of Me_3SnCl produced (0.693 g). If all of the chlorides of $SiCl_4$ react then 1.074 g of Me_3SnCl would be produced. The connectivity (i.e. the number of chloride ligands that reacted or the number of new siloxane bonds formed) is determined from the equation below.

$$\frac{\text{mols of } Me_3SnCl}{\text{mols of } SiCl_4} = Connectivity$$

$$\frac{3.478 \text{ mmol of } Me_3SnCl}{1.348 \text{ mmol of } SiCl_4} = 2.6 \pm 0.1 \; Connectivity$$

POROSITY MEASUREMENTS

Gas adsorption and desorption methods are often used to assess the surface area, total pore volume, and pore size distribution of porous materials. The following provides a brief introduction to adsorption/desorption isotherms and hysteresis loops, Brunauer-Emmett- Teller (BET) surface area, and total pore volume determination. Nitrogen adsorption/desorption data for Davisil® silica gel is presented to illustrate the concepts and calculations that are discussed in this section

ADSORPTION/DESORPTION ISOTHERMS AND HYSTERESIS LOOPS

The absorption/desorption measurement involves dosing a known amount of sample with a known amount of nitrogen. During the measurement, the instrument doses a known amount of nitrogen into a known volume with a sample. The instrument then allows equilibrium to be reached and measure relative pressures, P/P_0. The data collected by the instrument are the volume of nitrogen adsorbed, V_{ads}, at varying relative pressures, P/P_0 which, when graphically represented, are referred to as an adsorption/desorption isotherm. There are six different isotherms types or categories, which are presented in Figure 15. Type I isotherms are concave to the x-axis exhibiting prominent adsorption at low relative pressures with the amount adsorbed, V_{ads}, leveling off as P/P_0 approaches 1. Type I isotherms are observed for microporous materials. Type II isotherms are concave to the x-axis at low relative pressures then increase linearly and are convex to the x-axis at high relative pressures. Type II isotherms are given by non-porous or macroporous adsorbents. Type II isotherms represent unrestricted monolayer-multilayer adsorption. Type III isotherms are convex to the x-axis over the entire P/P_0 range. Type IV isotherms are concave to the x-axis at low relative pressure, exhibiting prominent adsorption, followed by leveling off at high relative pressures. A characteristic of Type IV isotherms is the presence of a hysteresis loop, which is associated with capillary condensation taking place in mesopores. Type V isotherms visually appear to be similar to Type III isotherms at low P/P_0 and Type IV at high P/P_0. Type VI isotherms are characterized by a series of adsorption "steps" over the relative pressure range. Type VI

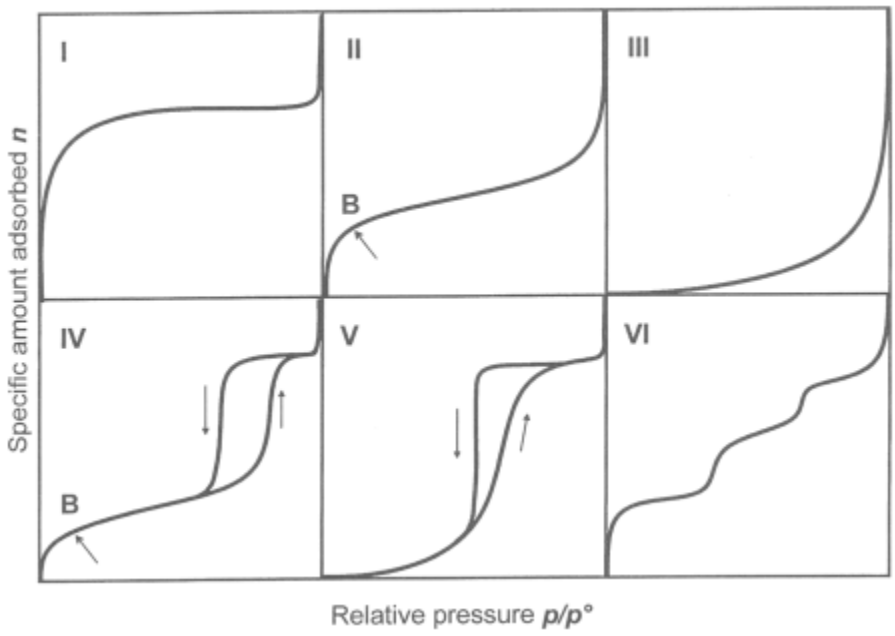

Figure 15*: IUPAC adsorption/desorption isotherm classifications (Figure was reproduced from [34]).*

isotherms are observed for samples that exhibit stepwise multilayer adsorption on a uniform nonporous surface. The height of each step represents the monolayer capacity for each adsorbed layer.

Table 2 below summarizes the key characteristics of each type of IUPAC adsorption/desorption isotherm. The hysteresis loops appearing between 0.4 – 0.8 P/P_0 of many isotherms are associated with capillary condensation in mesopores. The IUPAC classifies hysteresis loops into one of four types, which can be seen in Figure 16. H1 hysteresis loops are characterized by parallel and nearly vertical adsorption and desorption branches. H1 hysteresis loops are often associated with porous materials known to exhibit relatively high pore size uniformity. H2 hysteresis loops have a triangular shape with a steep desorption branch. Many porous adsorbents such as inorganic oxide gels and porous glasses tend to exhibit H2 hysteresis loops. In these systems, the distribution of pore size and shape is broad and not well-defined. H3 hysteresis loops do not exhibit any limiting adsorption at high P/P_0 and are observed with slit-shaped porous materials, such as aggregates of plate-like particles. H4 hysteresis loops exhibit parallel and almost horizontal adsorption and desorption branches. H4 hysteresis loops have been associated with narrow slit-like pores and the presence of large mesopores embedded in a matrix with pores of much smaller size. [35]. Table 2 summarizes the key characteristics of each type of hysteresis loop.

Figure 17 displays the nitrogen adsorption/desorption isotherm for Davisil® silica gel. At low P/P_0, the isotherm is concave to the x-axis, has gradually increasing uptake over a range of high P/P_0, and has a hysteresis loop. The isotherm is classified as Type IV. The hysteresis loop is classified as Type H1 even though the branches are not absolutely parallel or vertical. Davisil® silica gel is known to be a mesoporous silica gel and the information obtained from the nitrogen adsorption/desorption isotherm is consistent with that classification.

BRUNAUER-EMMETT-TELLER (BET) SURFACE AREA

The Brunauer-Emmett-Teller (BET) method is generally considered the standard procedure for the determination of the surface area of porous materials. The BET method is based on the five following assumptions: (1) the surface is flat, (2) all adsorption sites exhibit the same adsorption energy, (3) there are no lateral interactions between adsorbed molecules, (4) the heat of adsorption for all molecules except for the first layer is equal to the heat of condensation, and (5) an infinite number of layers can form.[36] The BET equation is seen in equation 11.

$$\frac{1}{w[(P_0/P)-1]} = \left(\frac{c-1}{W_m c}\right)\left(\frac{P}{P_0}\right) + \frac{1}{W_m c} \qquad \text{Eq. 11}$$

In equation 11, P/P_0 is the reduced pressure. c is the BET constant, and is related to the energy of desorption in the first adsorbed layer and indicates the magnitude of the adsorbent/adsorbate interactions, w is the total adsorbed quantity of gas at the given reduced pressure, and W_m is the monolayer adsorbed gas quantity (extracted from the isotherm plot). As previously mentioned the raw experimental data obtained is V_{ads} vs P/P_0 so some calculations are required to obtain the weight of gas adsorbed at a given relative pressure. The ideal gas equation is used to determine w.

A linear plot is obtained when the BET transform is plotted versus p/p_0. Most instruments will automatically calculate the BET transform, but it is important to understand how it is determined.

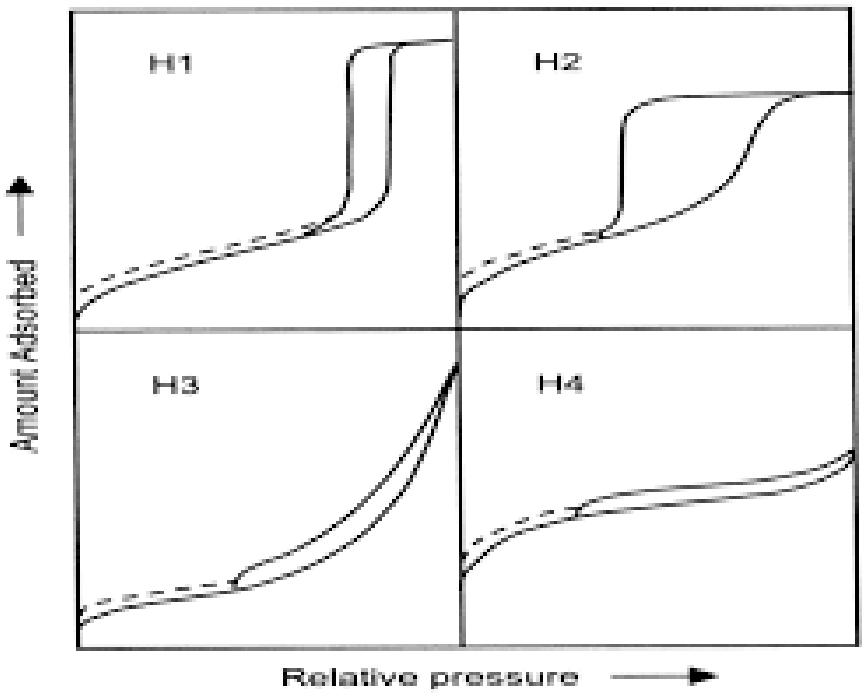

***Figure 16**: IUPAC hysteresis loop classifications (Figure was reproduced from [34]).*

Table 2: *Summary of the key characteristics of each type of adsorption/desorption isotherm.*

Isotherm Type	Key Characteristics	Comments
Type I	Prominent adsorption at low P/P_0, levels off at high P/P_0	Microporous material
Type II	Concave at low P/P_0, Linear in the middle of the P/P_0 range, Convex at high P/P_0	Macroporous material
Type III	Convex over the entire P/P_0 range	Uncommon
Type IV	Concave at low P/P_0, Hysteresis loop, Levels off at high P/P_0	Mesoporous material
Type V	Similar to Type III at low P/P_0, Similar to Type IV at high P/P_0	Uncommon
Type VI	steps	

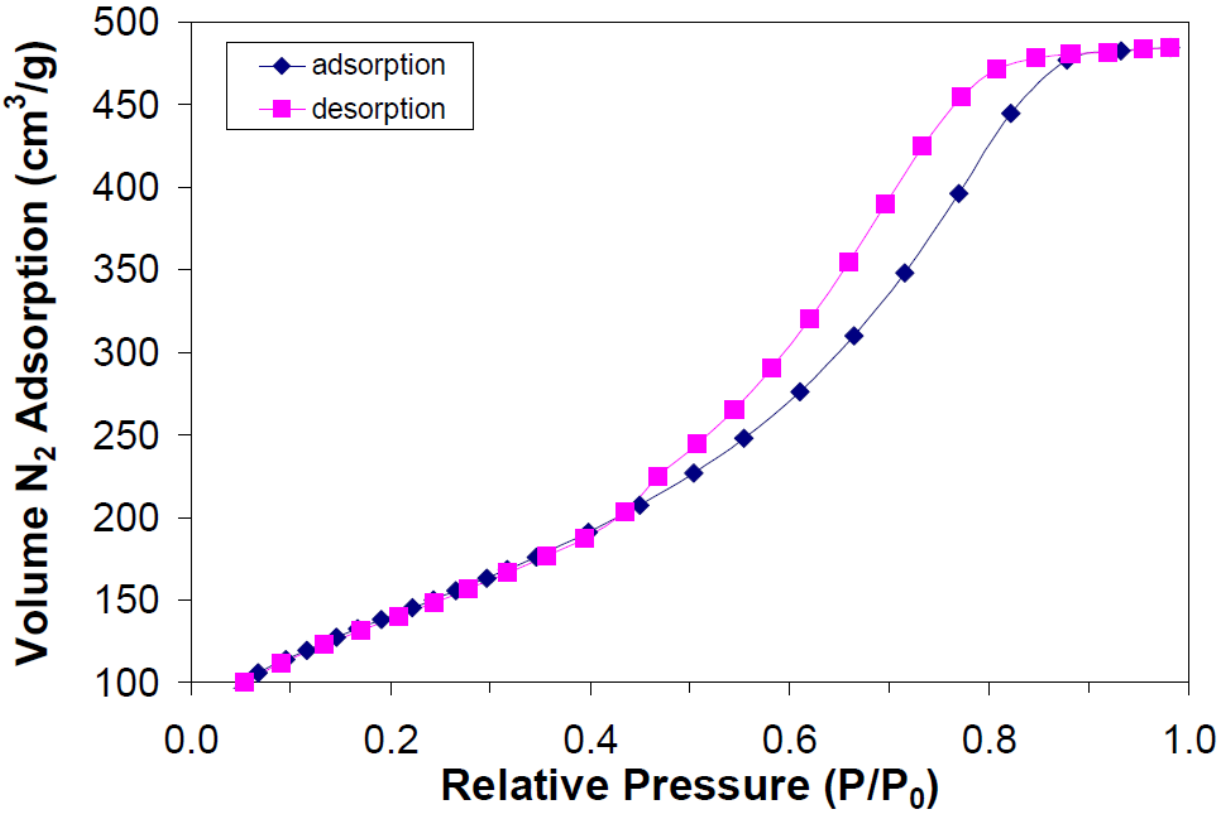

***Figure 17**: Nitrogen adsorption/desorption isotherm for Davisil® silica gel (the blue diamonds correspond to adsorption branch and the pink squares correspond to the desorption branch).*

$$\text{BET transform} = \frac{1}{w[(P_0/P)-1]} \quad \text{Eq. 12}$$

$$\text{slope} = \frac{c-1}{W_m c} \quad \text{Eq. 13}$$

$$\text{Intercept} = \frac{1}{W_m c} \quad \text{Eq. 14}$$

This plot typically deviates from linearity outside of the P/P_0 range of 0.05 to 0.35.[36] This linear region is shifted to lower relative pressures for microporous materials.

The weight of adsorbate constituting a monolayer of surface coverage (W_m) and the BET c constant can be determined from the slope and intercept of the BET plot (BET Transform vs P/P_0).

$$W_m = \frac{1}{\text{slope}+\text{intercept}} \quad \text{Eq. 15}$$

$$c = 1 + \frac{\text{slope}}{\text{intercept}} \quad \text{Eq. 16}$$

Once W_m has been determined, the BET surface area can be determined using the following equation:

$$\text{BET surface area} = S_{BET} = \frac{W_m N A_{cs}}{M} \quad \text{Eq. 17}$$

In equation 17, N is Avogadro's number (6.023×10^{23} molecules/mol), M is the molecular weight of adsorbate, A_{cs} is the cross-sectional area of the adsorbate, typically nitrogen is used with a A_{cs} value of 16.2 $Å^2$ for a monolayer at 77K.

The following section is an example calculation for Davisil® silica gel presented in Figure 17. This section will be used to illustrate how the BET surface area is determined from a BET plot. The slope and intercept of the linear regression are 6.64 $g_{material}/g_{nitrogen}$ and 0.0988 $g_{material}/g_{nitrogen}$ respectively. These values are used to determine W_m and the BET c constant for Davisil® silica gel. W_m is then used to determine the BET surface area for Davisil® silica gel which is consistent with the value given by the manufacturer (Sigma-Aldrich, 480 m^2/g).

$$W_m = \frac{1}{\text{slope} + \text{intercept}} = \frac{1}{6.64\,\frac{g_{material}}{g_{nitrogen}} + 0.0988\,\frac{g_{material}}{g_{nitrogen}}} = 0.148\,\frac{g_{nitrogen}}{g_{material}}$$

$$c = 1 + \frac{\text{slope}}{\text{intercept}} = 1 + \frac{6.64\,\frac{g_{material}}{g_{nitrogen}}}{0.0988\,\frac{g_{material}}{g_{nitrogen}}} = 68.2$$

$$S_{BET} = \frac{\left(0.148\,\frac{g_{nitrogen}}{g_{material}}\right)(6.023 \times 10^{23}\,\frac{molecules}{mole})(16.2 \times 10^{-20}\,\frac{m^2}{molecules})}{28.01\,\frac{g_{nitrogen}}{mole}} = 516\,\frac{m^2}{g}$$

TOTAL PORE VOLUME

The total pore volume calculates the total volume of porosity in a material. The total pore volume of a given adsorbent can be calculated from the amount adsorbed at a relative pressure close to the saturation vapor pressure simply by converting the amount adsorbed to the corresponding volume of liquid adsorbate at the temperature of the adsorption measurement. The volume of liquid adsorbate at the temperature of the adsorption measurement is determined using the following equation:

$$\text{Total pore volume} = V_{liq} = \frac{P_a V_{abs} V_m}{RT} \qquad \text{Eq. 18}$$

In equation 18, P_a is ambient pressure (atms), T is temperature (Kelvin), V_m is the molar volume of liquid adsorbate (34.7 cm^3/mol for N_2), and V_{ads} is the amount adsorbed at a relative pressure close to the saturation vapor pressure (P/P_0 =0.99) for Davisil® silica gel is 484 cm^3/g (Vads). Substituting these values into the above equation gives the total pore volume for Davisil® silica gel, which is consistent with that given by the manufacturer (Sigma-Aldrich, 0.750 cm^3/g).

$$V_{liq} = \frac{(0.998\ atm)(484\frac{cm^3}{g})(34.7\frac{cm^3}{mole})}{(82.057\frac{cm^3 atm}{mole\ K})(273\ K)} = 0.748\ \frac{cm^3}{g}$$

INFRARED SPECTROSCOPY

Infrared (IR) spectroscopy is a spectroscopic technique used to study the vibrational and rotational modes of a sample. IR is commonly used to characterize amorphous systems like the ones discussed here. Assigning IR features are fairly straightforward as references spectra are abundant in the literature. Some of the common vibrational modes of metal oxides and mixed metal oxides that are identified using IR spectroscopy include ν_{sym}(Si-OSi), ν(Si-OH), and ν(M-O-Si) where M = Ti, V, Mo, Sn, Zr, W, etc. The IR spectrum of the trimethyltin functionalized building block $Si_8O_{12}(OSnMe_3)_8$, is shown in Figure 18 with the main IR features labeled as an example.

CONCENTRATION DETERMINATION USING PROBE MOLECULES

The use of probe molecules to investigate the concentration, strength, and accessibility of particular sites on materials has become common practice in the characterization of the surfaces of materials. Identifying the concentration, strength, and accessibility of the acid sites in heterogeneous catalysts is of great importance.[37,38] All three of these properties influence the catalytic activity of the heterogeneous catalysts. The IR spectrum of pyridine absorbed on acidic heterogeneous catalysts can be used to identify the types of acid sites present in the material. Pyridine is an excellent probe molecule which allows one to distinguish between Brønsted and Lewis acidic sites. Metal cations in heterogeneous catalysts act as Lewis acidic sites while surface metal hydroxyl groups are sometimes able to protonate probe molecules, thus acting as Brønsted sites.[37] As seen in Figure 19, pyridine coordinately binds to Lewis acidic sites,

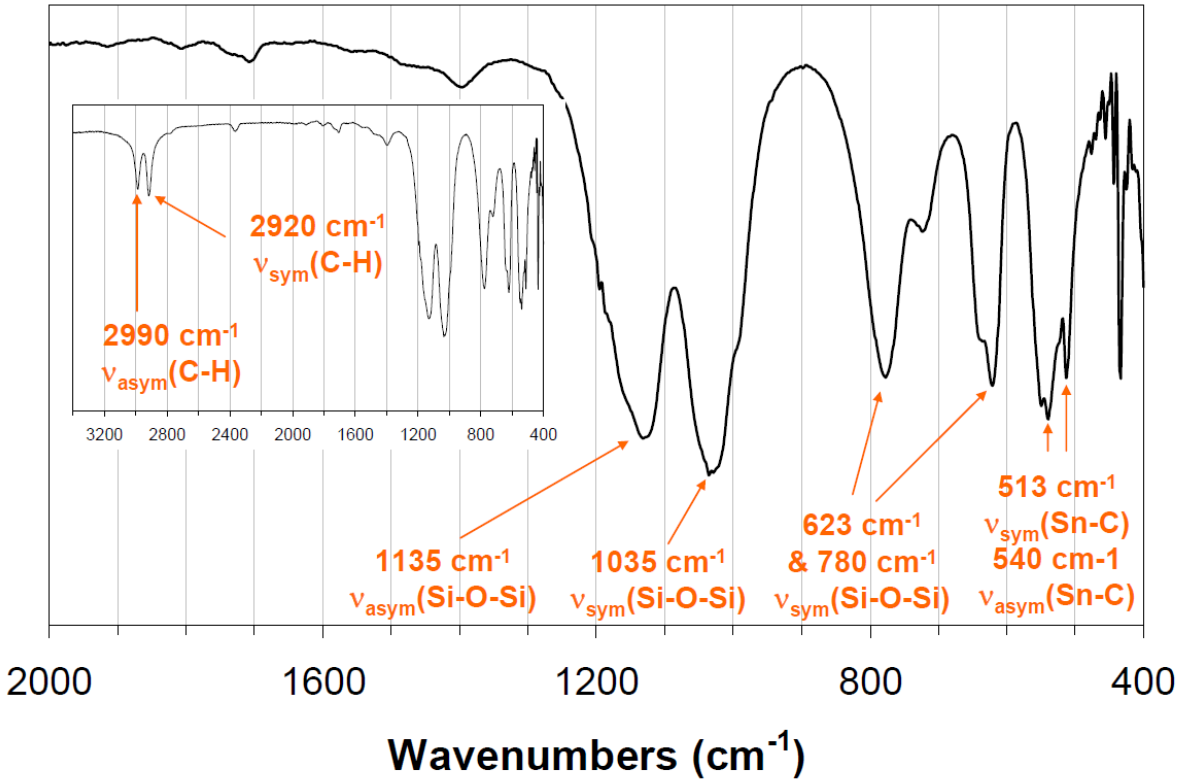

***Figure 18**: IR spectrum (400-2000 cm^{-1}) of the silicate building block $Si_8O_{12}(OSnMe_3)_8$ with the vibrational frequencies and modes labeled. The inset contains the entire IR spectrum (400-3400 cm^{-1}).*

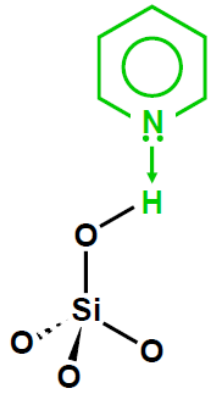	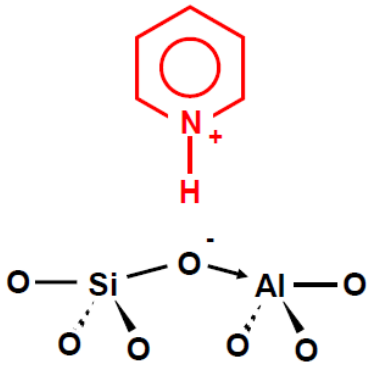	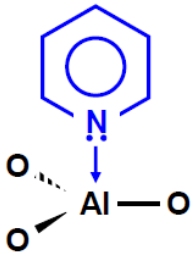
Silanol **Hydrogen bonded py**	**Bronsted Acid** **Pyridinium ion**	**Lewis Acid** **Coordinately bonded py**
~1445 cm^{-1} **~1485 cm^{-1}** **~1590 cm^{-1}**	**~1490 cm^{-1}** **~1540 cm^{-1}** **~1620 cm^{-1}** **~1640 cm^{-1}**	**~1450 cm^{-1}** **~1490 cm^{-1}** **~1580 cm^{-1}** **~1615 cm^{-1}**

***Figure 19**: Illustration of the types of pyridine interactions with acidic sites found in heterogeneous catalysts.[x]*

forms hydrogen bonds to silanols, and is protonated by Brønsted sites forming the pyridinium ion. The ring vibrations of pyridine produce characteristic patterns in the IR spectrum between 1400 and 1700 cm^{-1} depending on the type of pyridine interactions present. An IR feature at ~1450 cm^{-1} is characteristic of Lewis acidic sites, one at ~1540 cm^{-1} is characteristic of Brønsted acidic sites, and one at ~1590 cm^{-1} is characteristic of silanols.[38]

Sterically hindered alkyl substituted pyridines such as 2, 6-di-tertbutyl-pyridine can also be used as probe molecules to study the accessibility of acidic sites within heterogeneous catalysts.[39] The use of probe molecules of different base strengths allows for the investigation of the strength of the acid sites via desorption studies. In general, stronger acid sites will bind weaker basic probe molecules than weaker acid sites. Additionally, stronger acid sites desorb basic probe molecules at higher temperatures than weaker acid sites. Other IR probe molecules include ammonia, aliphatic amines, nitriles, benzene, substituted benzenes, and carbon monoxide.

X-RAY ADSORPTION SPECTROSCOPY

X-ray Absorption Spectroscopy, XAS, is an element specific averaging spectroscopic technique that probes the immediate environment (~6 Å) around the absorbing element and provides both structural and electronic information about the element. XAS can be used to characterize a variety of materials, both crystalline and amorphous. XAS has proven to be an especially powerful characterization tool in several areas of chemistry, biology, and material science where crystalline materials are impossible to obtain or samples are inherently amorphous, such as those found in this dissertation. XAS has been used extensively to characterize heterogeneous catalysts.[40,41] The following will provide a brief introduction to XAS, the collection of XAS data, and the analysis of XAS data. A more in-depth discussion of XAS can be found in XAFS for Everyone.[42]

THE FUNDAMENTALS OF X-RAY ABSORPTION SPECTROSCOPY

X-ray absorption occurs when an atom absorbs a photon of the appropriate energy which results in the excitation of core electrons into the continuum where the electron is no longer associated with the atom (Figure 20). The resulting core-hole is then filled by an electron from a higher energy orbital which produces fluorescence radiation. Table 3 summarizes the nomenclature for specific X-ray absorption edges and Figure 21 shows energies of edges for the elements according to their atomic number (Z).

XAS may be divided into two distinct areas: X-ray absorption near edge structure (XANES) and extended X-ray absorption fine structure (EXAFS) (Figure 22). The XANES portion (approximately -50 to +100 eV relative to the absorption edge energy) of an X-ray absorption spectrum includes any pre-edge features, the absorption edge itself, and other features on or just above the absorption edge (Figure 23).

Pre-edge features refer to features below the absorption edge that are the result of transitions between two bound states (generally s to d transitions) of the atom. These bound transitions must adhere to the selection rules for electric dipole transitions. The presence and intensities of pre-edge features are sensitive to the symmetry around a metal site. For example, the ground states of a Ti(IV) d^0 center in octahedral or tetrahedral environments are A_{1g} and A_1 respectively.[43] The pre-edge feature observed

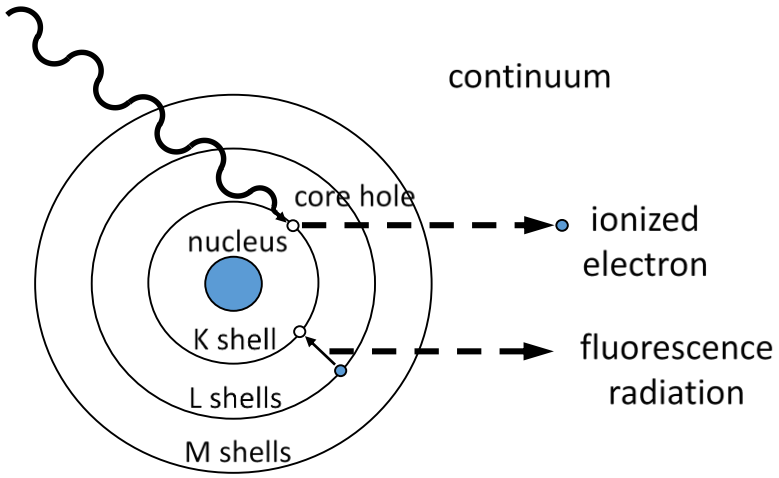

***Figure 20**: Illustration of X-ray absorption and fluorescence.*

Table 3: *Summary of the nomenclature for specific X-ray absorption transitions (X-ray absorption edges).*

Edge	Excited Core Electron
K	1s
L_I	2s
L_{II}	$2p_{1/2}$
L_{III}	$2p_{3/2}$

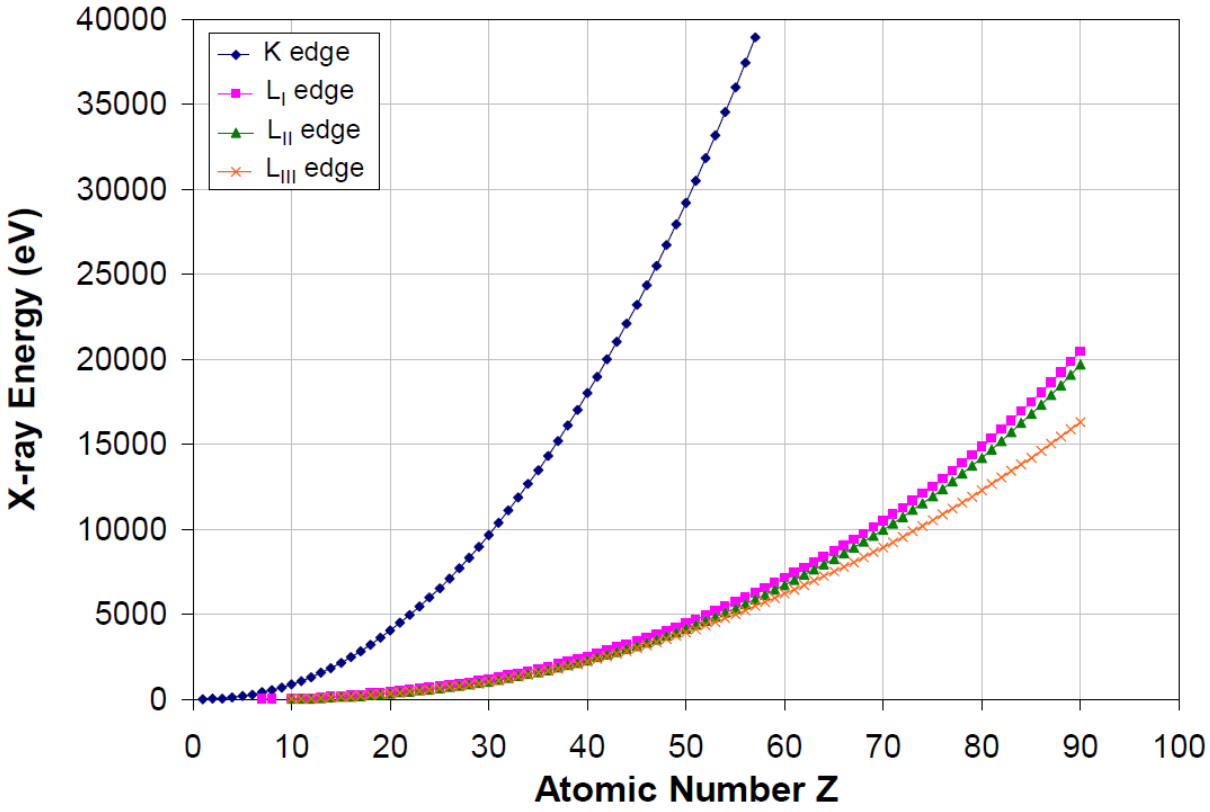

***Figure 21**: Plot of X-ray absorption energies as a function of atomic number.*

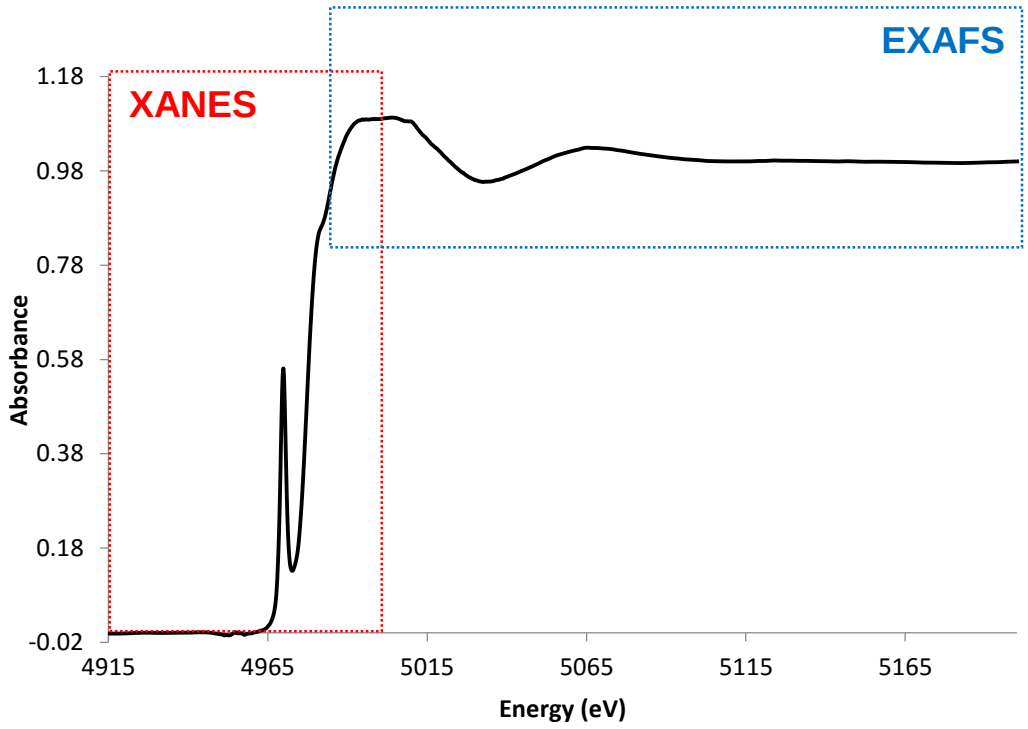

***Figure 22**: Representative XAS spectrum (Ti K-edge) divided into two distinct areas: XANES and EXAFS.*

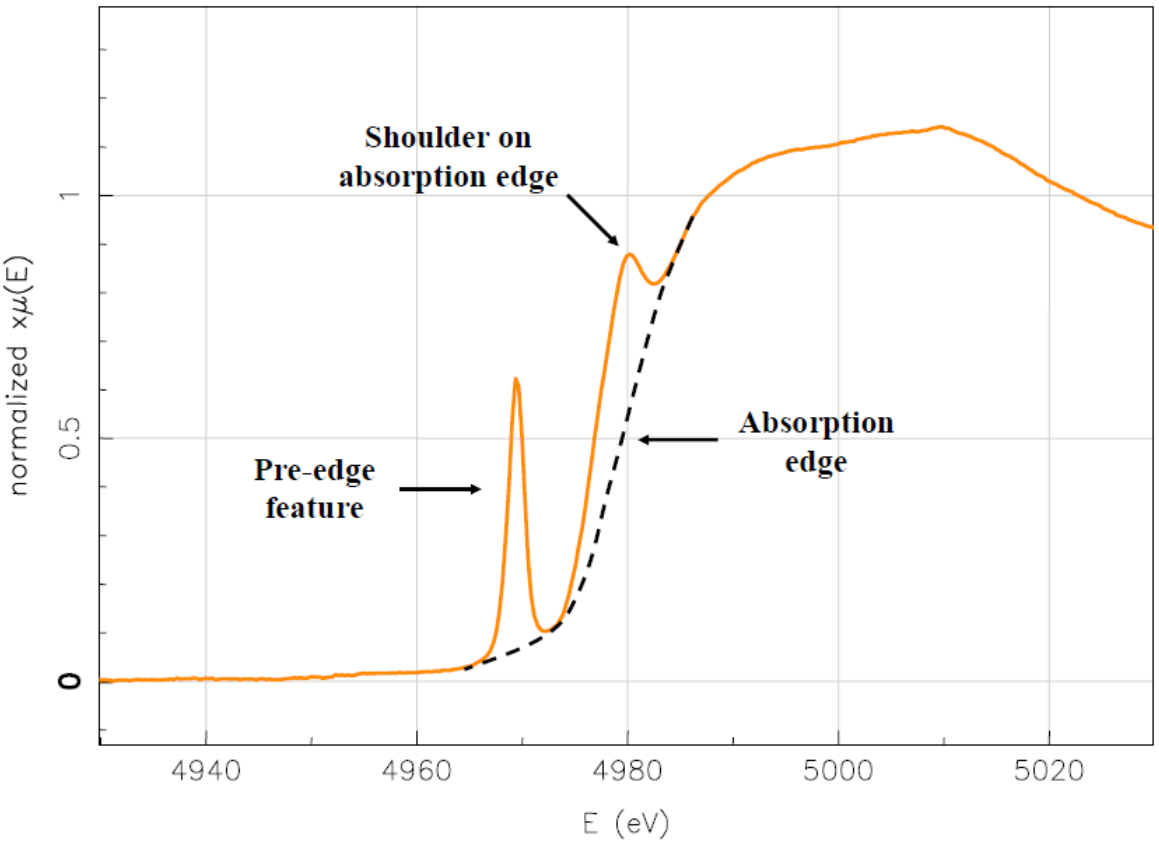

***Figure 23**: Representative XANES spectrum (Ti K- edge) for a tetrahedral Ti(IV) center in a silicate matrix.*

below the Ti edge in Figure 23 is assigned to the 1s to 3d transition. When the Ti(IV) site has octahedral (O_h) symmetry, the direct product for the electronic transitions does not contain A_{1g} so the electronic transitions are Laporte forbidden. As a result, the pre-edge feature is not observed or of very low relative intensity when the Ti(IV) sites have octahedral symmetry. When the Ti(IV) site have tetrahedral (T_d) symmetry, the direct product for the electronic transitions does contain A_1 so the electronic transitions are Laporte allowed. As a result, a strong pre-edge feature is usually observed when the Ti(IV) site have tetrahedral symmetry.

Pre-edge features are generally only observed at the K and LI edges of an absorbing atom with the appropriate symmetry and unoccupied valence orbitals. For example, XAS spectra collected at the tin K-edge does not exhibit pre-edge features because the Sn d-orbitals are occupied. At the same time, XAS spectra collected at the tungsten LIII edge do not exhibit pre-edge features because core s electrons are not being excited. The intensity, width, and position of the pre-edge feature can provide information about the coordination geometry and the oxidation state of the absorbing atom.[43] Figure 24 demonstrates an example of this relationship between the intensity of the pre-edge versus the position of the pre-edge feature for four-coordinated, five-coordinated, and six-coordinated Ti observed in a number of titanium oxides.[44] Additionally, examples illustrating the relationship between the pre-edge features and the coordination geometries and/or oxidation states of the absorbing atom can be found throughout the literature.[45,46]

The absorption edge, E_0 (generally defined as the point of inflection of the absorption edge) can provide information about the oxidation state of the absorbing atom. Figure 25 illustrates a typical XANES spectrum at the titanium K-edge with E_0 labeled. In an atom, the positively charged of the nucleus is shielded by the negative charge of the electrons. In an atom of higher oxidation state, the electrons are held tighter, which causes the ionization energy defined by absorption edge to increase. Thus, an X-ray with slightly greater energy is required to ionize a core electron. The position of the absorption edge for an atom in a higher oxidation state is usually shifted to a higher energy relative to the neutral atom (Figure 25). Several examples illustrating the relationship between the position of the absorption edge and the oxidation state of the absorbing atom are present in the literature.[45,47]

X-ray absorption threshold resonances, also known as white lines, generally refer to features on the absorption edge that are the result transitions between two bound states similar to those seen in pre-edge features. These transitions are typically p to d transitions and must adhere to the similar selection rules as pre-edge features, although those associated with L_{II} and L_{III} edges are not affected by the symmetry around the absorbing atom. The intensity of the white line observed at the L_{III} edge gives information on the occupancy of the d orbitals of the absorbing atom.[48]

The presence of other features on or above the absorption edge can provide information about certain ligands bound to the absorbing atom as well as the coordination geometry around the absorbing atom. For example, the presence of a shoulder on the K absorption edge of titanium, as seen in Figure 24, has been shown to qualitatively indicate whether a chloride ligand is bound to the absorbing atom.[46]

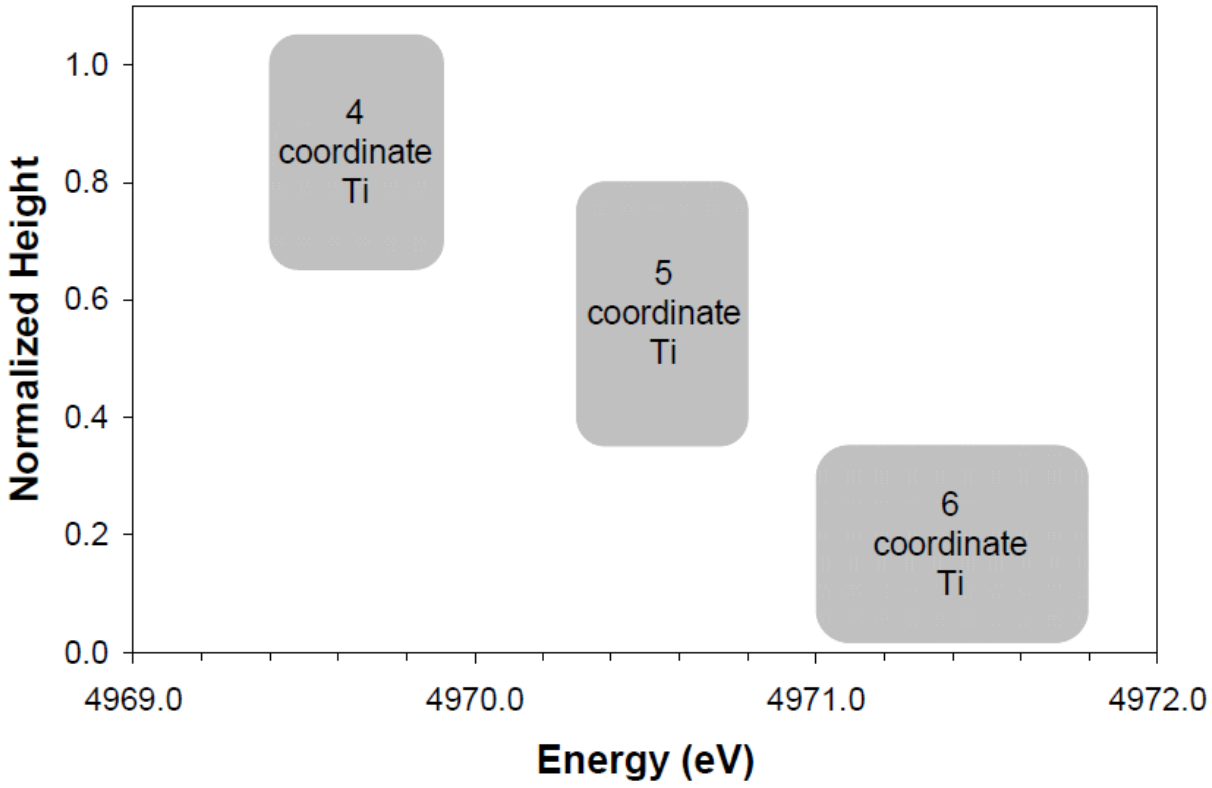

***Figure 24**: Plot illustrating how the coordination geometry of the titanium atom influences the Ti (K-edge) pre-edge feature intensity and the position of the pre-edge feature. (Figure was reproduced from [38]).*

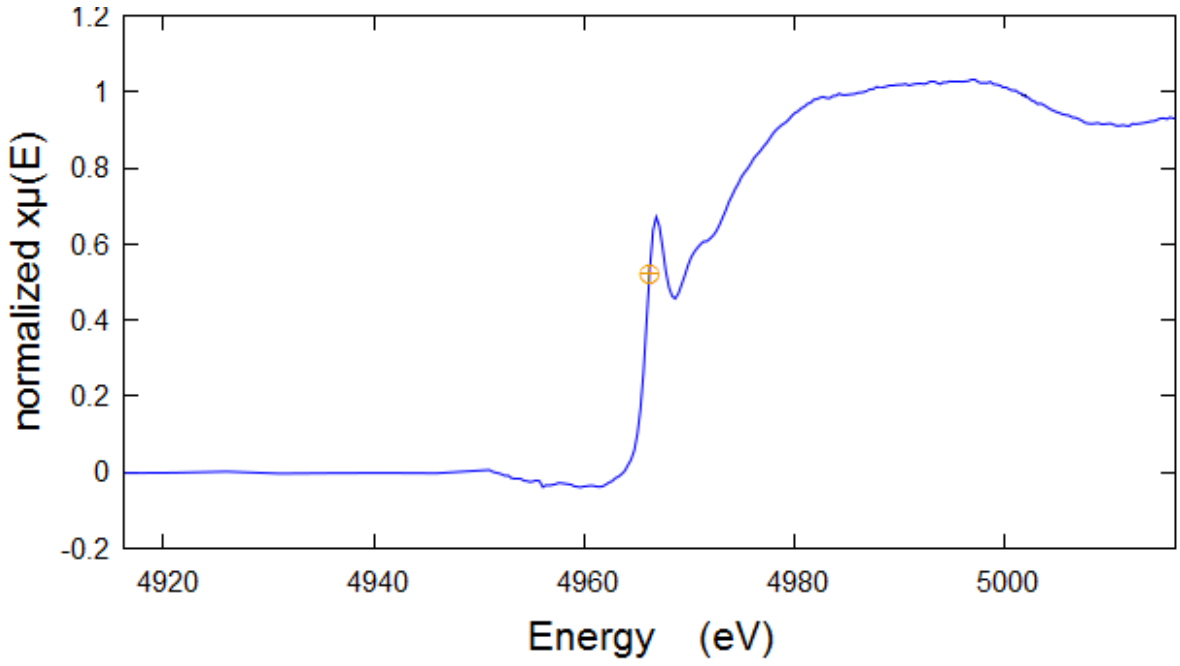

***Figure 25**: XAS spectrum (Ti K-edge) of titanium metal with E_0 marked at 4966 eV.*

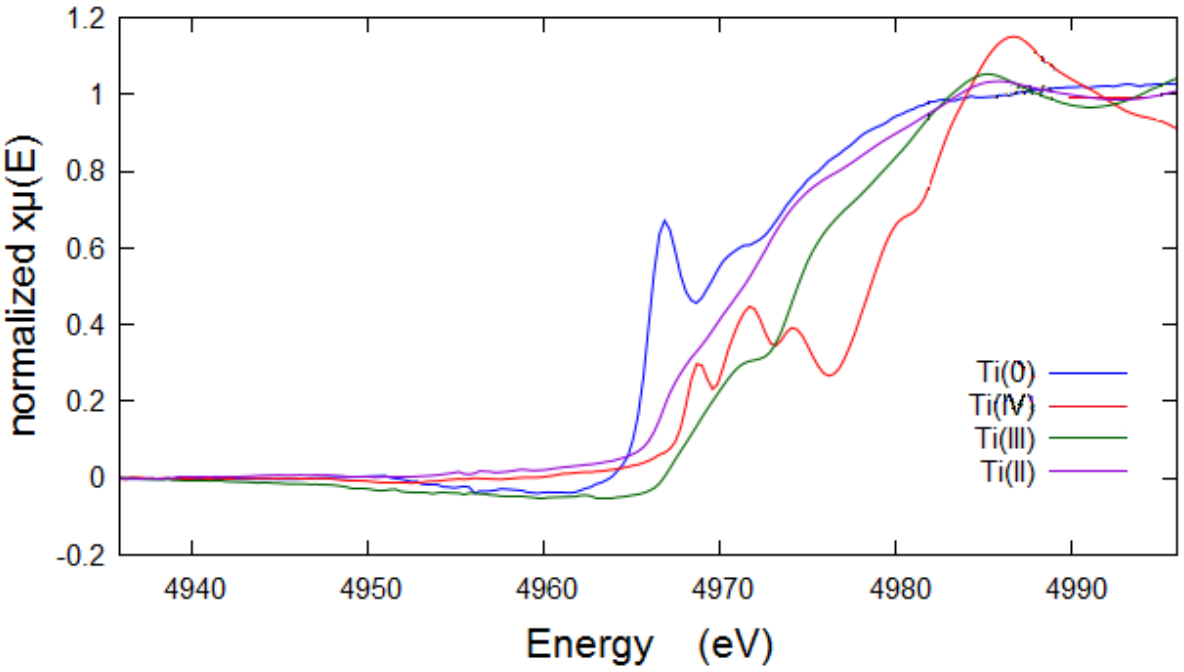

***Figure 26**: XANES spectra (K-edge) comparing the edge position of titanium(VI) oxide, titanium(III) nitride, titanium(II) oxide and titanium(0) foil.*

In summary, the XANES portion of an XAS spectrum is affected by the coordination geometry and oxidation state of the absorbing atom. In most cases, assignment of these features is based upon empirically based correlations with analogous features observed for reference compounds.

The EXAFS portion (roughly +20 to +1000 eV above to the edge energy) of an X-ray absorption spectrum contains fine structure superimposed on the absorption edge background (Figure 27). This fine structure is derived from backscattering of the outgoing photon by shells of neighboring nuclei around the absorbing atom (Figure 28). The EXAFS spectrum contains both qualitative and quantitative information about the coordination spheres around the absorbing atom in a sample. Typically the first sphere is defined as atoms directly bound to the absorbing atom while scattering from spheres beyond the first are defined as atoms bound to the first scattering sphere but not directly bound to the absorbing atom (Figure 28). Frequently an analytical theory is used to model the EXAFS fine structure. This theory may be used to develop a quantitative model for the immediate environment around the absorbing atom. An in-depth discussion on this theory and derivement can be found *XAFS for Everyone*.[42] The information derived from successful modeling of EXAFS data includes the identity of backscattering atoms around the absorbing atom, the bond/separation distance, the number of these bonds/interactions present in the shell (i.e. coordination number), and the amount of disorder in the backscatterer shell.

COLLECTION OF XAS DATA

Tunable monochromatic X-rays are required for XAS. Furthermore, due to the attenuation of the EXAFS signal, a high flux of these X-rays is needed to accurately measure EXAFS fine structure. For these reasons, XAS measurements are most commonly made at synchrotron radiation facilities. In the United States, there are three major synchrotron user facilities capable of making XAS measurements: the Advanced Photon Source (APS) at Argonne National Laboratory, the National Synchrotron Light Source (NSLS) at Brookhaven National Laboratory, and the Stanford Synchrotron Radiation Laboratory (SSRL) at Stanford Linear Accelerator Center. A fourth major synchrotron user facility, National Synchrotron Light Source II (NSLS-II), is currently being constructed at Brookhaven National Laboratory and is expected to be operational for users in 2016. NSLS-II will be a new state-of-the-art, medium-energy electron storage ring designed to deliver world-leading intensity and brightness, and will produce X-rays more than 10,000 times brighter than currently available at the NSLS.

Figure 30 presents a schematic illustration of the general experimental setup for making XAS measurements. In general, white light from a synchrotron X-ray source passes through a tunable monochromator producing a monochromatic X-ray beam. The beam then encounters vertical and horizontal slits which trim it to the desired size. The beam passes through an initial ion chamber detector I_o before impacting the sample which can be perpendicular or at a 45° angle to the incoming beam. The transmitted light passes through detector I_t while the fluorescence signal, I_{fluor}, is collected perpendicular to I_0.

XAS data collection is typically divided into four energy regions: pre-XANES (-150 to -15 eV relative to the absorption edge), XANES (-15 to +75 eV relative to the absorption edge), EXAFS near the absorption edge (+75 to +550 eV relative to the absorption edge), and EXAFS farther from the absorption edge (+550 to +1000 eV relative to the absorption edge). The monochromator step size and integration time are

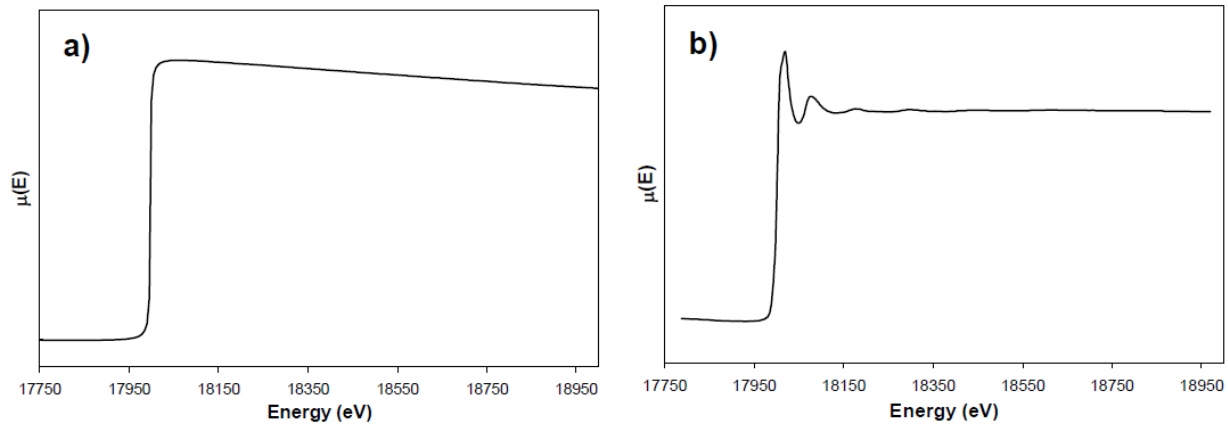

Figure 27: *a) XAS spectrum (Zr K-edge) showing the absorption edge background (smooth "bare atom" background) and b) XAS spectrum (Zr K-edge) showing fine structure superimposed on the absorption edge*

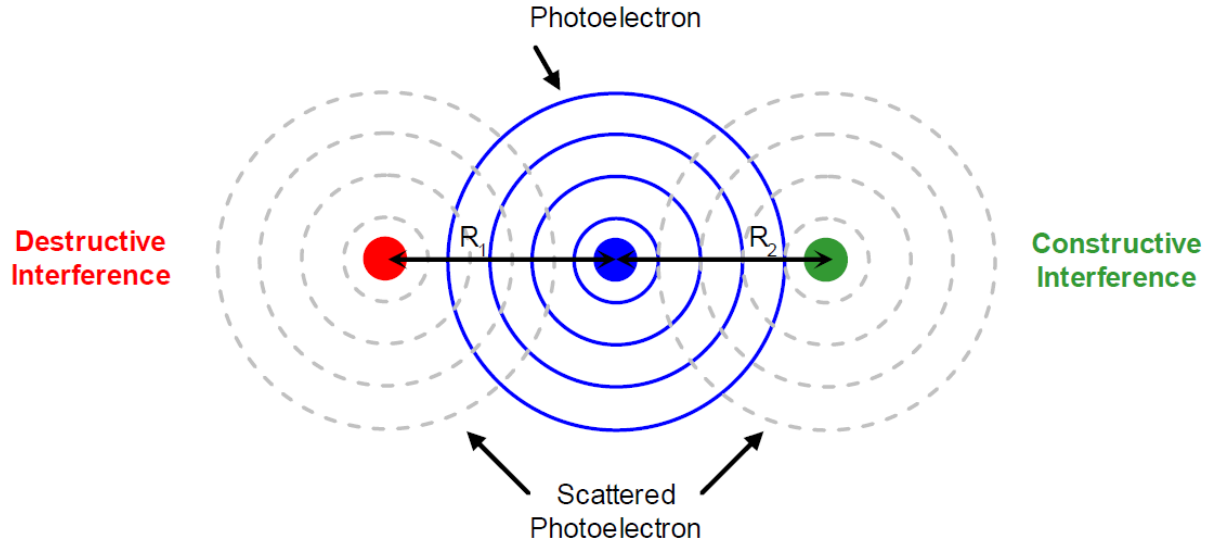

***Figure 28**: Illustration of constructive (right side) and destructive (left side) interference, absorbing atom is blue and the backscattering atoms are red and green.*

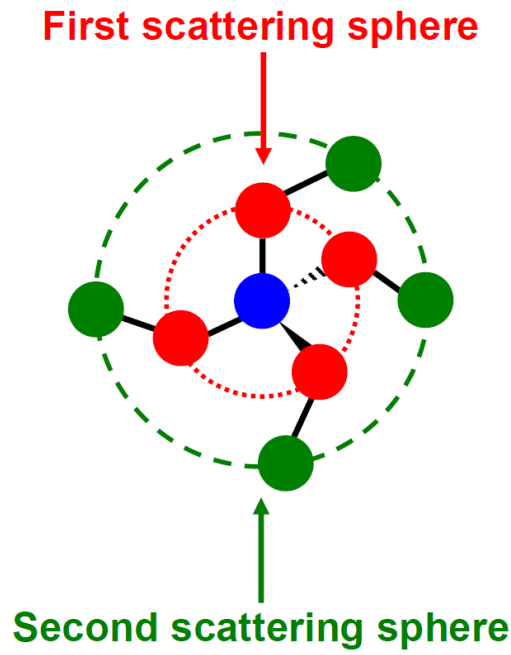

***Figure 29**: Illustration of the scattering spheres.*

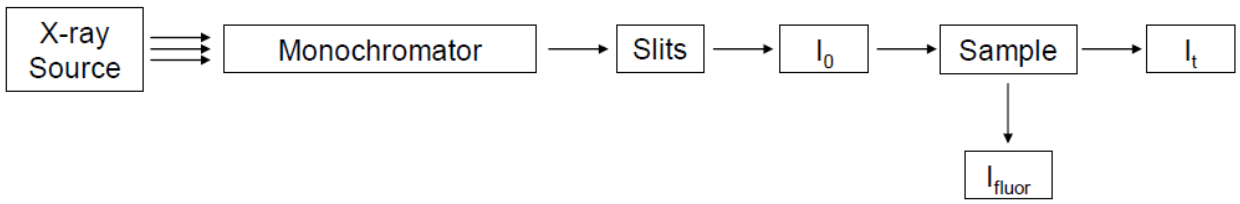

***Figure 30**: Illustration of a typical XAS setup.*

.

typically adjusted depending on the intensity of the EXAFS signal for each energy region mentioned above, which decreases as the energy of the X-ray beam increases above the absorption edge. The monochromator step size defines the spectral resolution for each energy region. The smallest possible step size should be used through the XANES region in order to observe narrow pre-edge features and edge structure present in this region accurately. The step size is defined by the monochromator stepper motor, which controls the angle of a matched pair of Si crystals. Typical step sizes for the different regions are: pre-XANES region is 5 eV, 0.3-1.5 eV for the XANES region, ~1.5-4.5 eV (0.05k) in the EXAFS near the absorption edge region, and ~4.5-6.1 eV (0.05k) in the EXAFS farther from the absorption edge region. The EXAFS signal decreases significantly at energies above the edge so the integration time is increased in order to increase the signal to noise ratio of the data. A typical integration time for the pre-XANES region is 1 s, followed by 2 s for the XANES region, 3 s in the EXAFS near the absorption edge region, and 4 s in the EXAFS farther from the absorption edge region. The specific data collection parameters used to collect the XAS data presented in this dissertation can be found in the experimental section of chapter 2.

ANALYSIS OF XAS DATA

In general, while XANES analysis relies comprehensively on comparisons with standards there are two methods of X-ray absorption analysis within the EXAFS region. The first method is based on comparing unknown spectra with those of well-characterized, physical standards. For EXAFS analysis, spectra for physical standards can be used to make comparisons, optimize the theoretical models, and assess the performance of the beamline. The second method involves modeling the experimental spectrum for an unknown sample with a theoretical spectrum generated using a structural model. The theoretical spectrum is then fit to the experimental spectrum via a non-linear least squares analysis to determine if the structural model is accurate. Usually, a combination of these two techniques is used for EXAFS analysis.

DISSERTATION OVERVIEW

This dissertation describes work performed over the past five years. It aims to demonstrate a novel synthetic approach, using building block and sequential additions, to construct advanced engineered solids applied to hydrogen storage materials and single-site heterogeneous catalysts. The materials that are described here can also be characterized as nanostructured materials in which their atomic scale (targeted active site) and bulk (porosity, surface area) structures are simultaneously controlled during synthesis.

Chapter 2 describes the synthesis and characterization of these advanced engineered materials for hydrogen storage applications. The work focuses around a series of surface titanium(IV) species constructed using the building block and sequential addition discussed above. A porous silicate support based on $(Si_8O_{12}(OSnMe_3)_8$ is constructed. These isolated titanium(IV) sites serve as a well-defined starting point for a “complex” reduction, resulting in reduced titanium centers potentially capable of binding H_2 reversibly. The reduction of these titanium sites should activate them for Kuba’s type interactions with molecular hydrogen. Multiple methods for reduction of the titanium(IV) sites were attempted. A discussion of these methods and their characteristics are presented this chapter.

Chapter 3 describes the synthesis and characterization of nanostructured heterogeneous catalysts that contain a single type of isolated titanium (VI) catalyst ensemble for epoxidation. The isolated titanium (VI) catalyst ensembles are synthesized via the reaction of the silicate building block $Si_8O_{12}(OSnMe_3)_8$with different titanium reagents ($TiCl_4$, $Ti(OiPr)Cl_3$, and $Ti(OiPr)_2Cl_2$). Completely embedded (4 bonds to the matrix) titanium catalyst ensembles are synthetically targeted by reacting the silicate building block with a limiting amount of a titanium tetrachloride. The material is further cross-linked with a dimethyldichlorosilane resulting in a high surface area silicate support that is generated around the embedded titanium (VI) catalyst ensembles. By altering the titanium(IV) precursors used in the first cross-linking, catalytic ensemble with different connectivities can be synthesized. This series of catalyst ensembles were thoroughly characterized which resulted in the development of reasonably clear pictures of the immediate environment around the titanium(VI) catalyst ensembles. Furthermore, the series of titanium (VI) catalyst ensembles were tested in the epoxidation of cyclohexene with cumyl hydroperoxide and found to be experimentally different from one another. This is consistent with the single site hypothesis that is central to our research program.

The final summary and conclusions, as well as potential future work, are described in Chapter 4. The synthetic methodology presented in this dissertation can be used to synthesize advanced engineered solids with targeted transition metal sites. Future work may focus on the incorporation of metal clusters into the silicate building block matrices, the investigation of a variety of catalytic reactions using nanostructured heterogeneous catalysts that contain different metal centers in silicate building block matrices, the development of a new building block approach, and the investigation of these materials for gas separation.

CHAPTER 2: INVESTIGATION OF SINGLE SITE TITANOSILICATE MATERIALS FOR HYDROGEN STORAGE

INTRODUCTION

Modern society depends on cheap and plentiful sources of energy. For more than a century, that source of energy has come in the form of fossil fuels.[49] However, we know that the supply of coal, natural gas, and crude oil will be exhausted in the future, and we have also learned that their use has caused and is still causing severe damage to the earth's atmosphere.[50,51] With these reasons in mind, new sources of inexpensive and abundant energy must be found which are renewable and environmentally sound. Currently, no one source can both achieve these goals and accommodate the world's population. At the same time, however, hydrogen, as an energy source, has great potential of contributing to the solution of this challenging problem.

Hydrogen in many ways is an ideal fuel because it has the highest energy density of any material currently known and only produces water as a combustion product thereby avoiding greenhouse gas emissions.[52] Achieving the promise of hydrogen as an efficient, sustainable, and environmentally friendly fuel requires widespread innovation and development of means of its production, storage, and use. Current models for a hydrogen economy are comprised of five key elements - production, delivery, storage, conversion, and application. Each is in a different stage of technological advancement. While hydrogen production and conversion are already technologically feasible, its delivery and storage face serious challenges. For example, due to possible hydrogen embrittlement of steel, existing natural gas transmission systems may be unsuitable for the transportation of pure hydrogen gas.

The challenge for the production of hydrogen is finding a source that can supply the needs of a full-fledged hydrogen economy that is not dependent on fossil fuels as a feedstock. Currently, a great deal of hydrogen is produced from natural gas by a process called natural gas reformation. Producing hydrogen from natural gas in sufficient quantities to power the world's transportation needs would strain the world's supply of conventional methane, making natural gas as geopolitically sensitive as crude oil. Furthermore, the production of hydrogen from natural gas also generates as much pollution and carbon dioxide per unit of energy output as burning the gas directly. Aside from fossil fuels, sources of hydrogen include splitting water molecules thermally[53], electrolytically[54-57], or photochemically[58,59] and reforming carbohydrates found in biomass.[60-62] Although these nonfossil fuel methods are attractive, they require breakthroughs in materials research to discover effective and robust catalysts that lower the energy barrier for potential routes of hydrogen production.

To facilitate the hydrogen economy, reduce greenhouse gas emissions, and our dependence on foreign oil, the Department of Energy (DOE) set targets for 2015 performance with regard to the storage of hydrogen.[63] These targets are purpose driven, based on achieving similar performance and cost as currently available for gasoline systems. Selected performance targets for 2015 and the corresponding ultimate goals are shown in Table 4. This chapter will focus on the synthesis and characterization of novel hydrogen storage materials.

Table 4: *Department of Energy goals for hydrogen storage in the near future. [61]*

Storage Parameter	2015	Ultimate Goal
System gravimetric capacity:		
usable, specific-energy from H_2	1.8 kWh/kg	2.5 kWh/kg
(weight percent)	(5.5 wt %)	(7.5 wt %)
System volumetric capacity:		
usable energy density from H_2	1.3 kWh/L	2.3 kWh/L
(net useful energy/max system volume)	(0.040kg H_2/L system)	(0.070kg H_2/L system)
Durability/operability		
Operating ambient temperature	−30/60 °C (sun)	−40/60 °C (sun)
Min/max delivery temperature	−40/85 °C	−40/85 °C
Cycle life (1/4 tank to full)	1500 Cycles	1500 Cycles
Minimum delivery pressure from tank: FC = fuel cell, ICE = Internal combustion engine	5 FC/35 ICE atm (abs)	3 FC/35 ICE atm (abs)
Charging/discharging rates		
System fill time (for 5 kg)	3.3 min	2.5 min
Minimum full flow rate	0.015 (g/s)/kW	0.02 (g/s)/kW
Transient response 10–90% and 90–0%	0.75 s	0.75 s

Hydrogen storage for transportation presents another major obstacle to the development of a hydrogen economy. Finding a storage medium that combines a hydrogen density greater than that of the liquid with fast kinetics allowing rapid charging and discharging is challenging. Many conventional routes and materials have been explored and rejected as storage media because they do not meet one or more of the criteria above. The challenge in hydrogen storage research is to find a material that satisfies three competing requirements: high hydrogen density, reversibility of release/charge cycling at moderate temperatures, and fast release /charge kinetics with minimum energy barriers to hydrogen release and charge. The first requires close atomic packing and strong chemical interactions, whereas the second requires weak interactions that are breakable at moderate temperatures, and the third requires loose atomic packing to facilitate fast diffusion of hydrogen between the bulk and surface. The ideal hydrogen storage material will achieve a balance between all three of these requirements. No material to date has found this "sweet spot". Figure 31 represents the relations between hydrogen accessibility and hydrogen density. An optimal system would replace the fuel tank on current automobile allowing for an easy transition from petroleum-based fuels. The material inside the system would have a strong enough affinity for hydrogen that it would absorb significant amounts with overpressures less than 100 bar, but would easily release the hydrogen on demand. Such materials would be driven by a pressure gradient produced as the hydrogen was consumed. Furthermore, the system would require minimal maintenance and would be possible to operate at filling stations similar to those used for petroleum products.

CURRENT STRATEGIES FOR HYDROGEN STORAGE

Hydrogen storage approaches presently being examined by scientists include compressed hydrogen gas[64], cryogenic gas[65] and liquid hydrogen[66], metal hydrides[67-73], high surface area sorbents[35,74-82], and chemical hydrogen storage media.[83-87] Figure 32 compares volumetric and gravimetric density of the many hydrogen storage media currently being considered for use. Compressed hydrogen gas and cryogenically stored liquid hydrogen are the most developed technologies and are currently utilized in the demonstration vehicles of several automotive manufacturers. [88] In all current compressed gas systems, the containment vessel accounts for 90% of the system's mass, but lightweight composite cylinders are presently being developed to alleviate this issue. In addition, the safety of pressurized cylinders is also a concern. A significant drawback of cryogenic storage is the large amount of energy needed for condensation. As a result, liquid nitrogen is used to cool hydrogen gas before liquefaction. The large amount of energy necessary for liquefaction and the continuous boil-off of hydrogen limits the possible uses of liquid hydrogen storage systems to applications where the cost of hydrogen is not an issue and the gas is consumed in a short time.

Metal Organic Frameworks (MOFs) have attracted attention recently as a possible hydrogen storage media because of their exceptionally high specific surface areas (1000-3000m^2/g) and chemically-tunable structures. MOFs absorb hydrogen within their vast internal network of surface area in a process known as physisorption. Physisorption is a Van der Waals interaction between hydrogen molecules and the surface atoms of the material. This weak interaction offers great kinetic advantages, but leads to low binding enthalpies, generally less than 10 $kJ \cdot mol^{-1}$. [89,90] While low binding enthalpies facilitate heat

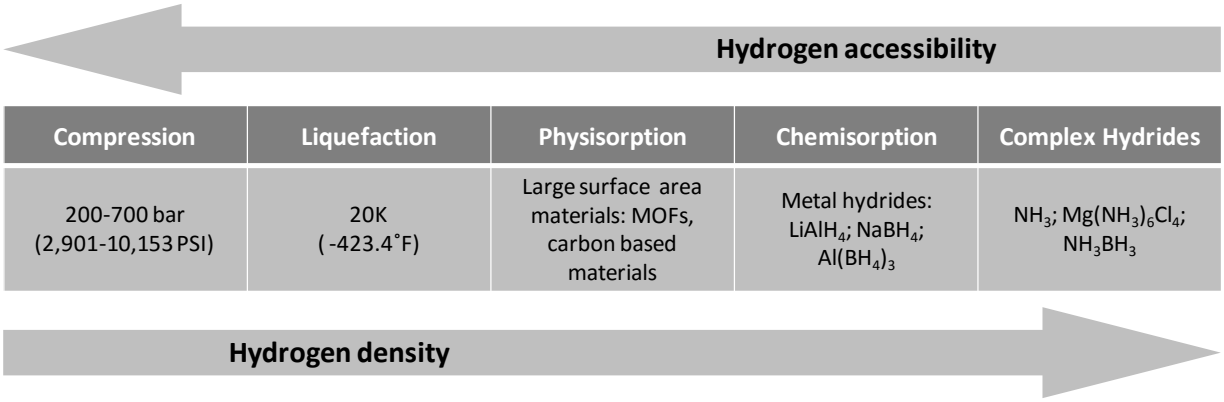

Figure 31: An illustration showing the relationship between hydrogen accessibility and hydrogen density of current methods for hydrogen storage.

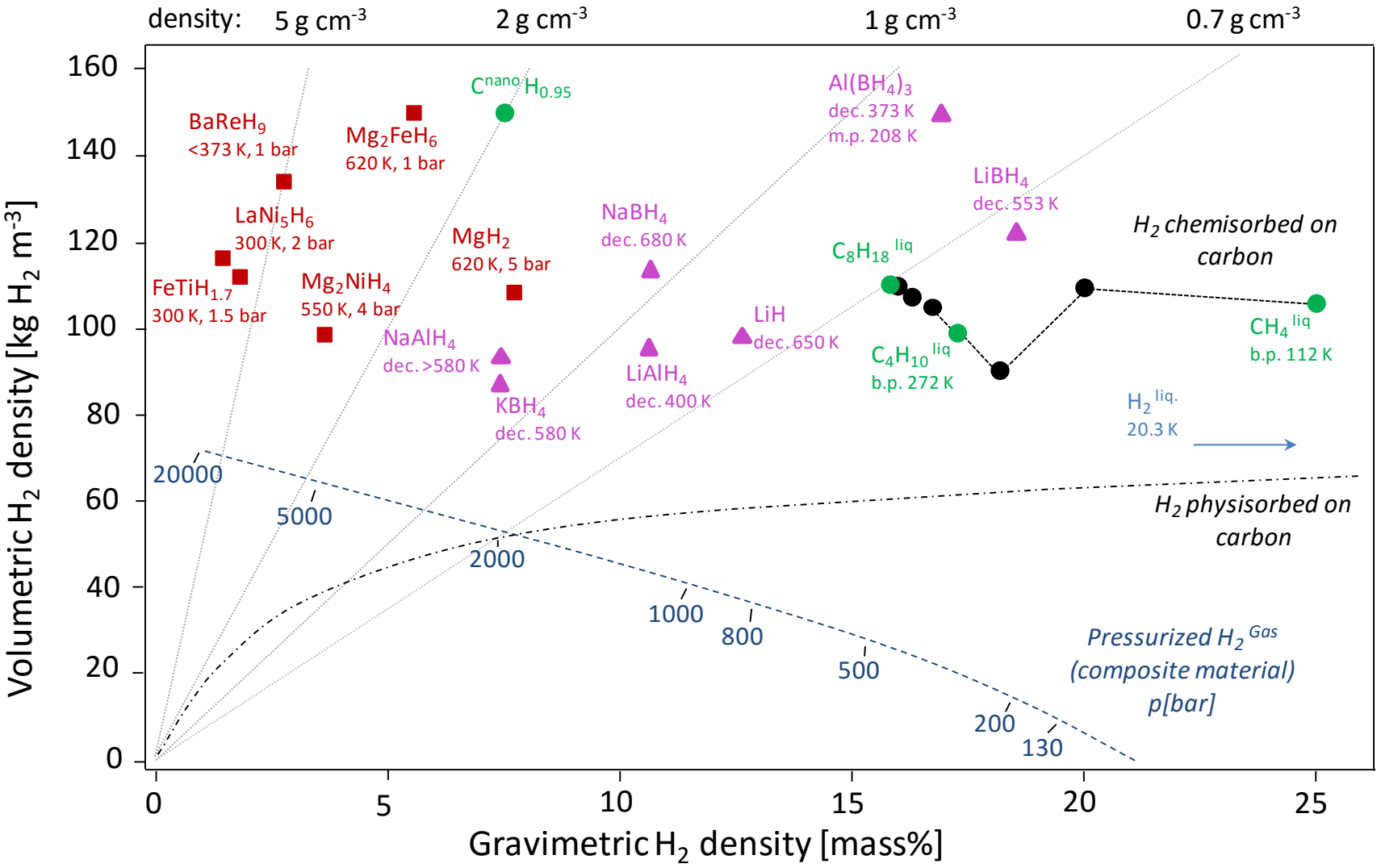

Figure 32: *A plot of the storage density (volumetric H_2 density vs. gravimetric H_2 density) for various hydrogen storage forms currently being investigated. [44]*

management on refueling, it becomes necessary to cool to 77 k for optimal performance, diminishing the energy storage capacity of the system. MOF-5 has been shown to bind upwards of 4.5 weight percent at liquid nitrogen temperatures.[91] More recent research has concentrated on creating MOFs with unsaturated metal site in expectation of enhancing the binding energy. To date, most MOFs lack tailored binding sites and relies on weak electrostatic interactions operative, making the surface area the decisive factor of the storage capacity.

Much like MOFs, porous carbon materials absorb hydrogen on their vast internal network of pores.[80] Research surrounding hydrogen uptake in carbon materials has produced conflicting results.[92] Currently, a controversy exists regarding carbon materials' ability to absorb hydrogen. To a large degree, the controversy is caused by insufficient characterization of the carbon materials used.[93,94] Often a mixture of opened and closed, single-walled and multi-walled tubes of various diameters and helicities together with other carbonous species are analyzed. These results have led to a greater appreciation of the importance of sample and measurement reproducibility, along with the necessity of establishing standard samples for instrumental calibration (especially for gravimetric methods where adsorbate contamination is a significant issue). Additionally, they emphasize the utility of theoretical studies to gain insight into the details of the uptake mechanism. The big advantages of physisorption materials for hydrogen are the low operating pressure and the simple design of the storage systems. However, the rather small gravimetric and volumetric hydrogen densities, together with the very low temperatures necessary to achieve substantial loadings, are significant current drawbacks to the use of carbon as hydrogen storage materials.

Complex hydrides such as $LiBH_4$, Na_3AlH_6, $Ti(BH_4)_3$, $Mg(AlH_4)_2$, etc., offer high gravimetric densities at room temperature (18 wt% for $LiBH_4$,), but exhibit binding enthalpies of 70 $kJ \cdot mol^{-1}$ and higher. They also release enormous amounts of heat on filling and require equally large amounts of energy to liberate the hydrogen when it is required as fuel. This creates problems with heat management and also drastically lowers the effective energy storage capacity of the system. The low dynamics of the hydrogen releasing process is a problem for complex hydrides. Hydrogen is released via cascade decomposition from the complex hydride, and the sequence of step reactions require different conditions. Therefore, there is a large difference between the theoretical and the practically attainable hydrogen with complex hydrides. Additionally, many of these decompositions are irreversible within the operating specifications of an onboard system, thus the depleted material would have to be exchanged, adding addition cost to refueling.

Currently, the most promising hydrogen storage routes involve porous solid materials, which chemically bind and/or physically adsorb hydrogen at volume densities greater than that of liquid hydrogen. These materials combine the bond enthalpies of chemisorption with the density of physisorption.

It has been proposed that materials with binding enthalpies between 20-30 $kJ \cdot mol^{-1}$ would be ideal for hydrogen storage applications.[95,96] These moderate heats of absorption do not cause as much difficulty in terms of heat management, but provide enough thermal stability for interactions between the hydrogen bound in the materials so that the material can bind/release hydrogen at temperatures higher than 77 k. One type of hydrogen interaction that is known to exhibit binding energies in this sweet spot

is that which occurs between the hydrogen molecules and a transition metal center. This is an example of the Kubas interaction.[97,98] A reasonable place to start looking for a material with binding enthalpies in this range is the first-row transition metals. For first-row transition metals, the 4s orbital is much larger than the 3d orbitals. In addition, due to symmetry, the 4s orbital is a logical orbital for acceptance of σ donation from the incipient H_2 ligand. Other more subtle factors can also affect bonding, most important of these is backbonding from filled d orbitals into the σ* orbital of H_2, an effect that is very important for the late first row metals. Another factor is d-σ repulsion if the orbital is filled on the metal. This effect is especially important in early metals due to the relatively large size of their orbitals. Effectively, a σ-π Kubas (Figure 33) type interaction between a hydrogen molecule and a metal center afford many hypothetical systems, with ideal enthalpies in conjunction with predicted high storage capacities, most involving early transition metals.[95,96,99]

In 2008, the first example of a material exhibiting an enthalpy within the targeted enthalpy range (between 20-30 $kJ \cdot mol^{-1}$) was reported by A. Hamaed *et al*.[100] This material was synthesized from grafting tetrabenzyl titanium onto a mesoporous silica followed by a reduction using heat and dynamic vacuum. This system is believed to be comprised of titanium(III) benzyl units on mesoporous silica which increased the performance of the system from 1.2 wt% (without Ti(III)) to 1.65 wt% (with Ti(III)). The targeted titanium fragments are believed to hold 3 H_2 molecules per metal center at 77 k, while also retaining 41% of their capacity at room temperature. In 2009, the same group optimized the performance of this titanium (III) system by adjusting synthetic parameters and exploring other titanium precursors leading to 2.45 wt% absorption at 77 k and 60 atmospheres, which is equivalent to 3.98 H_2 per metal center. This is close to the theoretical maximum of 5 H_2 per titanium atom predicted by the 18-electron rule with additional organic ligands on the titanium metal center. Porous materials with tailored metal centers constitute a substantial leap forward by the demonstration that Kubas binding may represent a potential answer to many hydrogen storage problems.

Theoretical [101-103] studies have shown that exposed, isolated titanium metal centers may bind hydrogen with a binding energy near the sweet spot. Puna's theoretical models indicated that it may be possible to bind as many as six hydrogen molecules to an exposed, reduced titanium center.[102] The model indicates the first hydrogen molecule binds strong enough to cause a dissociation of the sigma bond within the hydrogen molecule, producing two hydride species. Once two or more hydrogen molecules become associated with the titanium center they remain as molecular hydrogen and each appears indistinguishable from the other. Once the system is activated it is impossible to remove all six hydrogen molecules in a reversible manner as the final two hydrogens remain dissociated as two hydrides which are much more difficult to cleave from the titanium. Although the theoretical study involved an idealized system with spatially isolated titanium atoms simply surrounded by hydrogen, the promise of this model was sufficient to inspire this project to investigate synthetic routes to mimic this theoretical system. In fact, the theoretical model gives a total hydrogen gravimetric density above 20%, with 16.8% being easily accessed. Puna's work is widely cited as identifying an area where novel hydrogen sorbents might be discovered. Frequently there is a significant difference between what theory can imagine and our ability to synthesize something that approximates the theoretical models. All traditional methods of

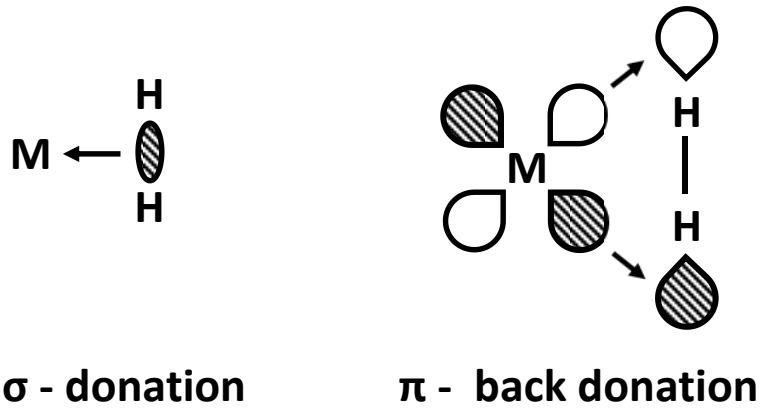

***Figure 33**: Components of Kubas binding between a metal atom and molecular hydrogen.*

grafting metals on surfaces would invariably lead to mixtures of surface species where the average connectivity would be greater than one, thus distancing these approaches from the theoretical models. However, the synthetic strategy outlined in Chapter 1 of this dissertation is ideal for this specific problem. The work presented in this chapter is an attempt to synthesize nanostructured, silicates with atomically isolated exposed titanium center ideal for Kubas interaction with hydrogen.

As discussed in chapter 1 the Barnes group has developed a synthetic methodology optimized for the synthesis of defined geometry, targeted single-site metal centers that are atomically dispersed within a porous amorphous silicate. Surface titanium assemblies synthesized using this methodology are ideal candidates for binding hydrogen, by virtue of the fact that they are the closest synthetic representations to isolated titanium site in space, studied in the theoretical work of *Chertihin et al* [101] discussed above. These isolated titanium(IV) sites serve as a well-defined starting point for a "complex" reduction, resulting in reduced titanium centers capable of binding H_2 reversibly. The reduction of these titanium sites should activate them for Kubas type interaction with molecular hydrogen.

The ability to start from well-defined and well-characterized precursors separates our synthetic strategy from that of others. The synthetic approach of A. Hamaed et al. uses grafting and heating. As discussed in Chapter 1 these methods can lead to the presence of multiple titanium centers and aggregated titanium sites. In addition, a well-defined starting point will assist in developing an understanding of the ligands and coordination geometry that exists around the titanium center after reduction.

Amorphous materials, like the ones synthesized in this chapter, are difficult to characterize fully due to the lack crystallinity. Instead of a single method such as diffraction for full structural characterization, this work relies on multiple methods to gain the amount of knowledge concerning both the local environment surrounding the titanium site on the support and the characteristics of the macrostructure in which it is located. Knowledge of both of these components is integral to obtain a material capable of effectively acting a hydrogen storage media. The following few paragraphs give an overview of the characterization techniques and what information was gathered from each.

INSTRUMENTATION

INFRARED SPECTROSCOPY

Fourier Transform Infrared Spectrometry (FTIR) gives vital information about the bonds within a sample and can also be used to observe changes over the course of several reactions. The most important regions to monitor for the materials discussed this chapter are shown in Figure 34. Two important stretches are seen between 2800 and 4000 cm^{-1}. First, aliphatic carbon-hydrogen stretches can be observed between 2800 and 3000 cm^{-1}. These features correspond to the methyl units of the trimethyltin, which decrease as trimethyltin chloride is lost during the synthesis. Additionally, evidence of hydrolysis can be seen between 3400 and 3800 cm^{-1} which can indicate exposure of the sample to air. The next important region to monitor is between 1500 and 1200 cm^{-1}. Literature indicates that within this region it may be possible to observe Ti-H stretches.[101] Between 1000 and 950 cm^{-1} are the Si-O-Si and Ti-O-Si stretches which are the linking groups between the building blocks in the material. These stretches are important to monitor as they can indicate the decomposition of the sample in the form of leaching of titanium sites or the

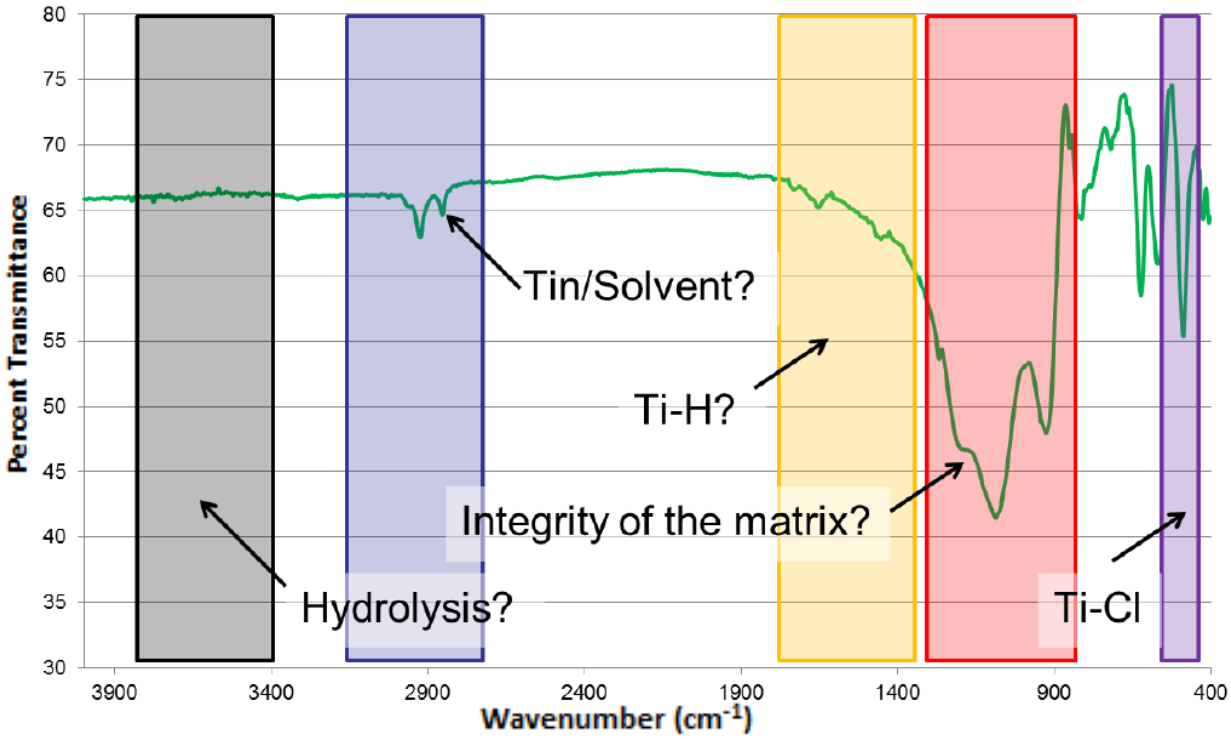

Figure 34: *A sample FT-IR spectrum showing the main areas of interest.*

decomposition of the cube structure. Finally, at 495-490 cm^{-1} is the Ti-Cl stretch, the presences of absences gives further information about the ligands bound to titanium sites in the matrix. For these reasons infrared spectrometry is an important characterization technique used to gain an understanding of the materials detailed below.

Infrared spectra were collected using a Thermo Nicolet IR100 in an MBraun LabMaster 130 N_2 dry box. 32 scans are collected using 4 cm^{-1} resolution from 400-4000 cm^{-1} for the background and samples. A KBr pellet is prepared and collected as the background spectrum. A KBr pellet containing sample material (~1-5 wt%) is prepared and collected as the sample spectrum.

X-RAY ABSORPTION SPECTROSCOPY

X-ray absorption spectroscopy (XAS) in the form of X-ray Absorption Near Edge Spectroscopy (XANES) and Extended X-Ray Absorption Fine Structure (EXAFS) was used to investigate the environment around the reduced titanium sites. As discussed in chapter 1, the XANES region of XAS gives information about the coordination geometry and oxidation state of the metal. The titanium k-edges (4966 eV) were obtained at the National Synchrotron Light Source (NSLS) at Brookhaven National Laboratory on beamlines X18B and X19A, operated at 2.8 GeV with a current of 300 mA. The beam dimensions (i.e. spot size) on sample was 10 x 1 mm (w x h) for X18B and 3 x 1 mm (w x h) for X19A. Spectra were collected at room temperature. X-rays were monochromatized via reflection from Si(111) crystals through a 1 mm entrance slit. The incident beam was detuned 40% to suppress harmonics. Samples were mounted 45° to the beam, to allow for the collection of fluorescence spectra. The intensity of the incident beam was measured with a 10 cm He-filled ion chamber detector (I_0). The fluorescence signal from the sample was recorded with a Canberra PIPS detector (I_{fluor}). Spectra were recorded at room temperature in four energy regions about the titanium k-edge at 4966 eV: -150 to -15 eV (below the edge) in 5 eV steps (1 s integration), -15 to 75 eV (through the edge) in 0.5 eV steps (2 s integration), 75 eV to 12 k in 0.05-k steps (3 s integration), and 12k to 16k in 0.05-k steps (4 s integration).

Sample powders were held in copper plates between windows of 7.5 µm polyimide (Kapton®) film (Chemplex 442) affixed with double sided tape to each side of the plate. Samples were loaded in an N_2 dry box to prevent hydrolysis. Two to three scans were collected for each sample. Data processing and analysis were performed using the IFEFFIT data analysis software suite (Athena & Artemis). The Athena program was used for XANES analysis and extraction of EXAFS from the smooth absorption edge background using standard procedures. The pre-edge background was modeled with a linear function. The post edge, smooth background was approximated with a stiff spline function and adjusted to minimize Fourier components that produce low R (< 1 Å) features in R-space plots. Low-frequency Fourier components were also filtered from the EXAFS via the R_{bkgd} parameter that was kept smaller than 0.5 times the distance of the closest backscattering shell. Merged files were generated after auto-aligning scans in Athena program.

As discussed in Chapter 1, XAS is an averaging spectroscopic technique that probes the immediate environment (~6 Å) around the absorbing element and provides both structural and electronic information about the element. Our strategy for using XAS focuses on the two regions of measure. In the XANES region, we expect to probe the approximate coordination geometry and the oxidation state of our

titanium species. As a titanium atom is reduced the energy needed to ionize (from the 1s orbital) is also reduced and is observed as a 2 - 4 eV shift for every unit change in oxidation state. Thus we would expect to observe edge position at approximately 4976 eV for titanium(III). Analysis of the EXAFS region required us to take an indirect approach. Since hydrogen ligands cannot be observed in radial distribution plots, EXAFS data were used as an indirect method for determining if hydrogen ligands were present. A low number of observable ligands around titanium seen in an EXAFS sample can be used as evidence for undetectable hydrogen that exist on titanium since low coordinate titanium species are highly reactive and therefore will not remain stable.

POROSITY ANALYSIS

Porosity analysis was used to monitor changes in the porosity over the course of synthesis and reduction of the surface titanosilicates. Nitrogen adsorption-desorption analysis was performed using a Micrometrics ASAP 2020 Physisorption and Chemisorption analyzer. The BET surface area was calculated using adsorption data in the relative pressure range from 0.05 to 0.35. The adsorption portion of the nitrogen gas adsorption/desorption isotherms was used to calculate the pore size distribution (BJH method) of the samples.

HYDROGEN ADSORPTION-DESORPTION ANALYSIS

Materials exhibiting hydrogen binding in the "sweet spot" should demonstrate hysteresis-like behavior on the absorption/desorption analysis with hydrogen gas. The difference between the desorption curve and adsorption curve signifies the amount of hydrogen chemisorbed (Figure 35). This analysis was the determining analysis for our reduced materials, materials that demonstrated hysteresis during desorption were further characterized, those that did not were set aside. Hydrogen adsorption-desorption analysis was performed using a Micrometrics ASAP 2020 Physisorption and Chemisorption analyzer.

EXPERIMENTAL AND RESULTS

MATERIALS: The general procedures for handling the chemicals used in the reactions reported here were described previously in Chapter 1. Several steps were taken to exclude all sources of water from reactants, solvents, and glassware as well as any hydroxyl groups present on glassware used in reactions. All Schlenk reaction vessels were silylated with a chlorotrimethylsilane/triethylamine solution followed by flame drying under vacuum prior to use. Toluene (Fisher Scientific) was dried using sodium-potassium alloy and distilled. Pyridine (Fisher Scientific) was distilled and dried using calcium hydride. Toluene and pyridine were kept in solvent bulbs equipped with high vacuum Teflon® stopcocks with the appropriate drying agent. The solvent bulbs were degassed using freeze-pump-thaw cycles and stored under vacuum prior to use. Trimethyltin cube, $Si_8O_{12}(OSnMe_3)_8$ was synthesized using previously reported procedures.[31] Prior to use, samples of trimethyltin cube were heated overnight at 100°C under vacuum to ensure removal of waters of hydration in the crystal. Silicon tetrachloride ($SiCl_4$, Acros, 99.8+%) and titanium tetrachloride ($TiCl_4$, Alfa Aesar, 99.6%) were distilled, degassed, and stored under vacuum in Schlenk vessels equipped with Teflon® stopcocks. The solid bispyridine complex of silicon tetrachloride, $SiCl_4 \cdot py_2$ was produced according to the literature and added to reaction vessels in a nitrogen atmosphere glove box.[33] All volatile solvents and reagents were delivered into reaction vessels using vapor transfer methods.

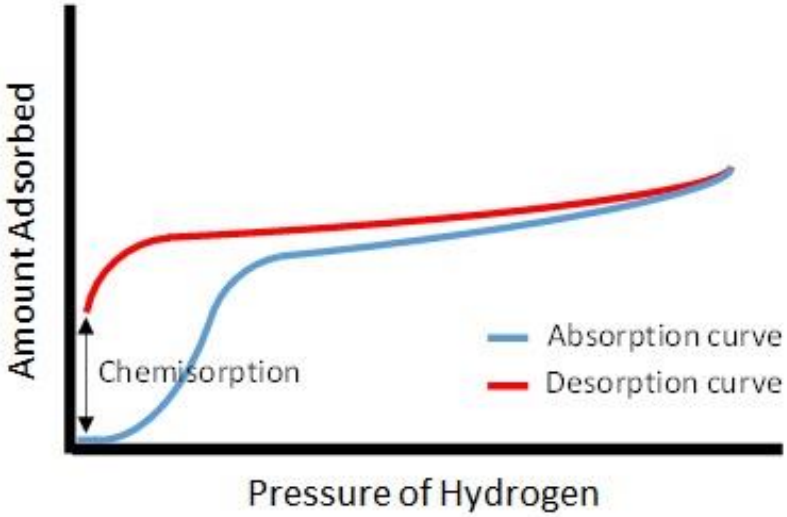

Figure 35: *A schematic illustration chemisorption found from the difference in adsorption and desorption curve.*

TRIMETHYLTIN CUBE BASED SILICATE PLATFORM In a Schlenk reaction vessel, 2.534 g (1.366 mmol) of dry trimethyltin cube, $Si_8O_{12}(OSnMe_3)_8$, was added to 1.163 g (3.545 mmol) of silicon tetrachloride bispyridine, $SiCl_4py_2$ [2.60:1 $SiCl_4py_2/Si_8O_{12}(OSnMe_3)_8$; 1.30:1 Cl/Me_3Sn] followed by the vapor transfer of approximately 30 mL of toluene. The sealed system was left under vacuum and heated at 80°C. A gel forms within 1 hour. The solution was allowed to react for 18 hours whereupon all volatiles were removed using heat and dynamic vacuum. Previous investigations indicated that both trimethyltin chloride and pyridine are quantitatively removed under these conditions. The resulting fine powder solid was used without further purification. Gravimetric analysis of the reaction indicated, on average, the inert silicon linkages were connected to 2.47 silicate cubes. By multiplying the reaction ratio and the experimentally determined connectivity; then subtracting it from the number of stannylated corners on the silicate cube it was determined that 1.58 trimethyltin groups remain per silicate cube. BET analysis indicated the platform has a broad pore size distribution with an average of 3.1 nanometers and a surface area of 630 square meters per gram. Table 5 outlines the approximate ratios and concentrations within trimethyltin cube based silicate platform. All values in Table 5 are after the completion of the reaction and based on gravimetric weight change. Pyridine and trimethyltin chloride formed during the reaction were assumed to account for the entire weight change. This assumption was verified by NMR analysis of the volatiles isolated from the reaction.

TITANYLATION OF SILICATE CUBE BASED PLATFORM WITH TITANIUM TETRACHLORIDE To the Schlenk reaction vessel from the previous reaction, approximately 30 mL of toluene was vapor transferred. Following the transfer of toluene, 0.5 mL (4.316 mmol) of titanium tetrachloride, $TiCl_4$, was vapor transferred into the reaction vessel. Based on the number of remaining trimethyltin groups in the sample, the ratio of $TiCl_4$:$SnMe_3$ was approximately 2.0. The solution was then stirred at 80° and allowed to react for 48 hours. Following the reaction, all volatiles were removed using heat and dynamic vacuum. Excess titanium tetrachloride in the system is removed from the reaction Schlenk under these conditions. A dark yellow red color developed in the cold trap, which is excess titanium tetrachloride complexed with toluene. The resulting off-white powder was used without further purification. Gravimetric data is consistent with the formation of 1.55 trichloro-titanium groups per silicate cube, giving a concentration of $1.55x10^{-3}$ moles of titanium per gram of solid. By varying the titanium precursor used in this protocol, a series of titanium surface species can be synthesized. Figure 36 displays the series of titanium surface species synthesized in the study.

The IR spectrum of titanated silicate platform is shown in Figure 37. Weak aliphatic carbon-hydrogen stretches can be observed between 2800 and 3000 cm^{-1}, indicating a few trimethyltin groups remain in the matrix. Additionally, there is no evidence of hydrolysis which would be seen between 3400 and 3800 cm^{-1}. The region between 1500 and 1200 cm^{-1} is clean, consistent with no Ti-H present in the sample. Between 1000 and 950 cm^{-1} there is a broad feature assigned as Si-O-Si groups. The shoulder observed at ~960 cm^{-1} has been assigned to the Ti-O-Si stretches found in the literature of similar titanosilicates.[104] Finally, a strong vibrational band at 495-490 cm^{-1} assigned to the Ti-Cl stretch, gives further confirmation to the composition of the matrix.

Table 5: *The approximate ratios and concentrations within trimethyltin cube based silicate platform.*

Substituent	Molality (mmol/gram)	Ratio of substituent to cubes
cube	0.98	1.00
linker	2.55	2.60
Sn	1.55	1.58
Cl	3.90	3.98

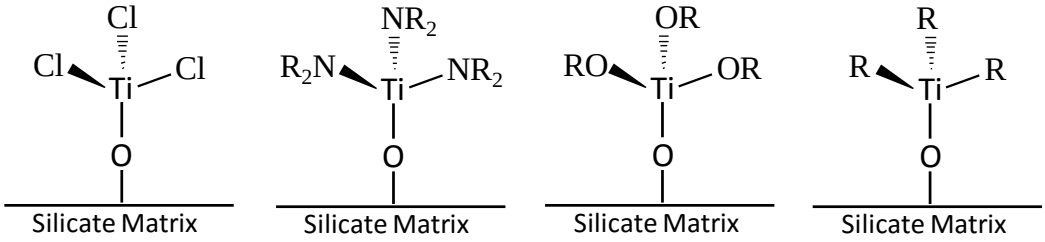

Figure 36*: series of surface titanium species synthesized from a trimethyltin silicate platform.*

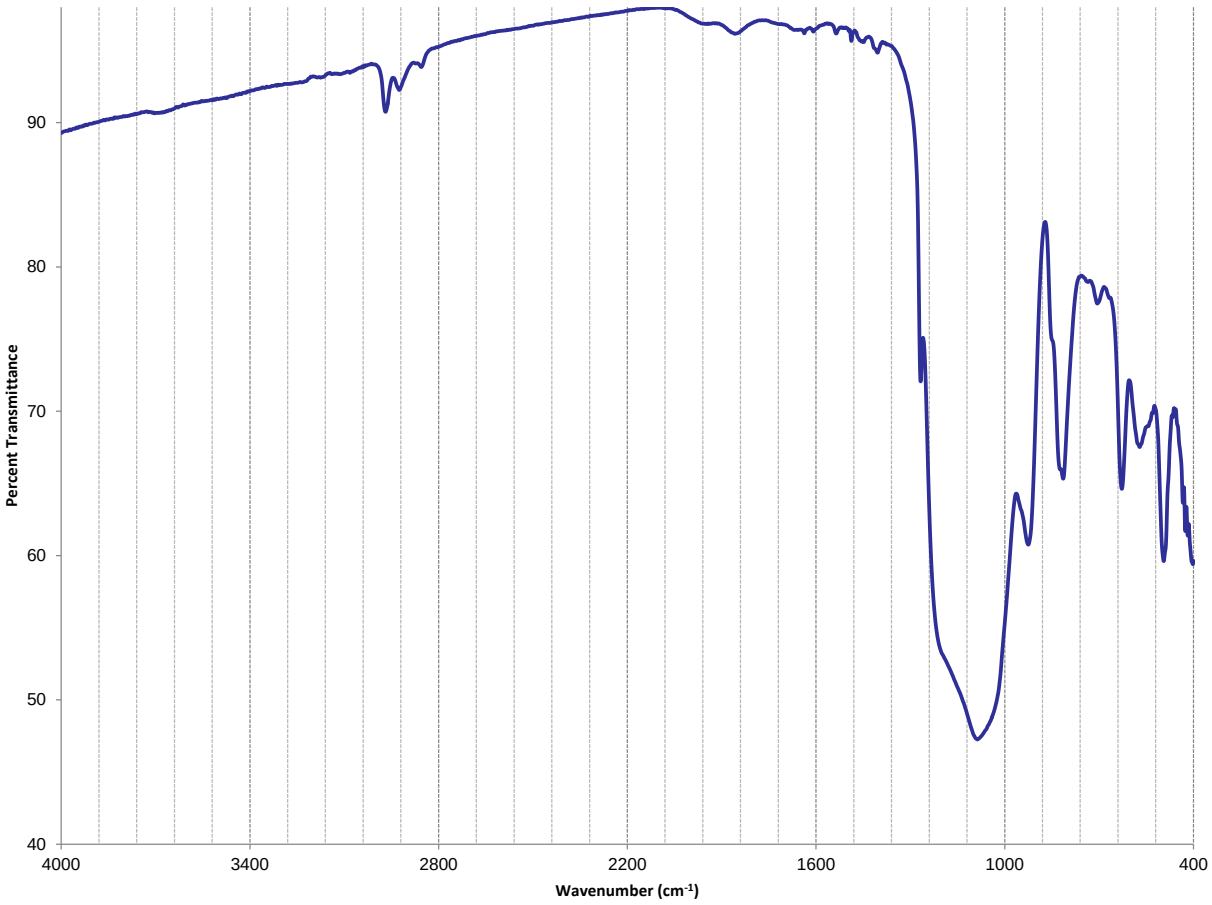

Figure 37: *The IR spectrum of titanated silicate platform.*

Titanium XANES data (K-edge) from the titanated silicate platform can be seen in Figure 38. It is important to note that a lightened image of the beam was observed on the sample after exposure to the X-ray beam. This photobleaching causes us to question the XAS data that was collected, as the titanium site may have. significantly changed from its interaction with the high intensity and high energy radiation. Furthermore, we observed significant differences between scans two and three compared with the data from scan one. As a result, the data presented is from only scan one, as it is the most likely to accurately reflect the nature of the sample as originally synthesized.

The 4978 eV edge position is consistent with titanium(IV) found in titanium dioxide. Additionally, a shoulder is seen superimposed on the edge indicative of a shake-up effect from titanium-chlorine bonds.[105] Finally, a single pre-edge feature with an intensity of approximately 0.5 can be seen. This pre-edge feature, assigned to a 1s -> 3d transition, can be quite sensitive to the coordinate geometry around the titanium site due to the Laporte selection rule. This bound transition is expected to have very low peak intensity (~0.1 of the normalized edge jump absorption) for titanium sites having a center of inversion (e.g. octahedral). For titanium sites without a center of inversion (e.g. tetrahedral) this feature frequently has much greater peak intensity (0.5- 1.0). The observed height of the pre-edge feature and edge position is most consistent with a titanium (IV) with no center of inversion (i.e. tetrahedral).

Even though we observed changes in the edge between the first and second scans, we performed a qualitative analysis of the EXAFS data for this sample**.** Figure 39, displays the EXAFS data (K-space and R-space) from the titanated silicate platform. The features shown in Figure 39 are not at real distances, as the spectra is not phase corrected and therefore features appear at distances ~0.3 lower than their true distances. Three features can be seen in the R space: (1) a feature at 1.30 Å, which is congruent with a titanium-oxygen bond, (2) a feature at 1.90 Å consistent with a titanium-chloride bond, and (3) a feature at 3.25 Å consistent with a second shell silicon.

The analysis above is somewhat suspect due to both the observed photobleaching as well as the observation in the absorption edge between the first and second scans. The sample could have changed the instant it was exposed to X-ray or more slowly as the scan progressed (~35 minutes per scan). While the chloride feature in the EXAFS is consistent with expected surface species, it is quite possible that the data reflects the presence of a mixture of species which, in most cases, makes a more detailed analysis of the EXAFS impossible.

The following sections discuss the reduction and activation of these surface titanium species in an attempt to obtain Kubas type interactions with molecular hydrogen. The reduction discussed below will be compared to this unreduced titanated silicate platform; as it is a well characterized, well-defined starting point for “complex” reduction that may have unforeseen consequences. The following paragraphs discuss our work to reduce and “activate” these surface titanium species for binding hydrogen. These protocols were carried out with the trichloro-titanium, as it is the readily synthesized.

REDUCTION WITH HYDRIDE REDUCING AGENTS

Lithium aluminum hydride ($LiAlH_4$) and sodium borohydride ($NaBH_4$) have been studied exhaustively as hydride reducing reagents in organic systems. Furthermore, some work has also been performed with

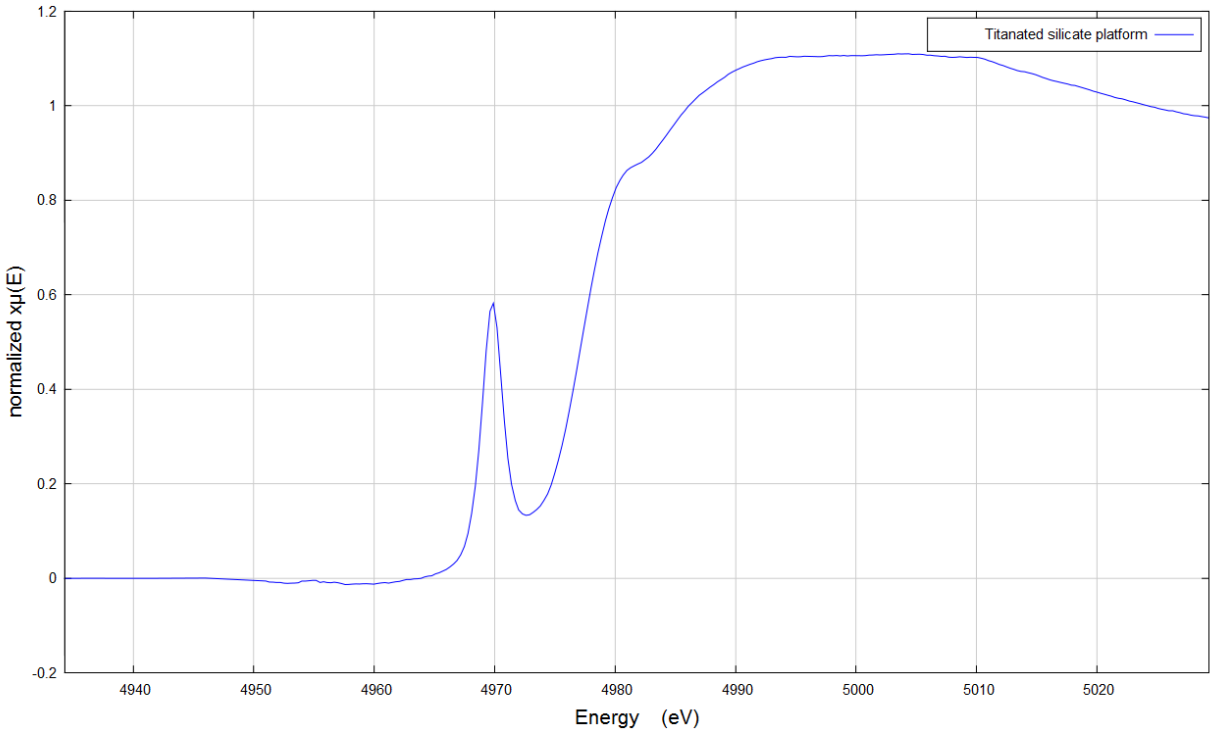

***Figure 38**: Titanium XANES data (K-edge) of titanated silicate platform.*

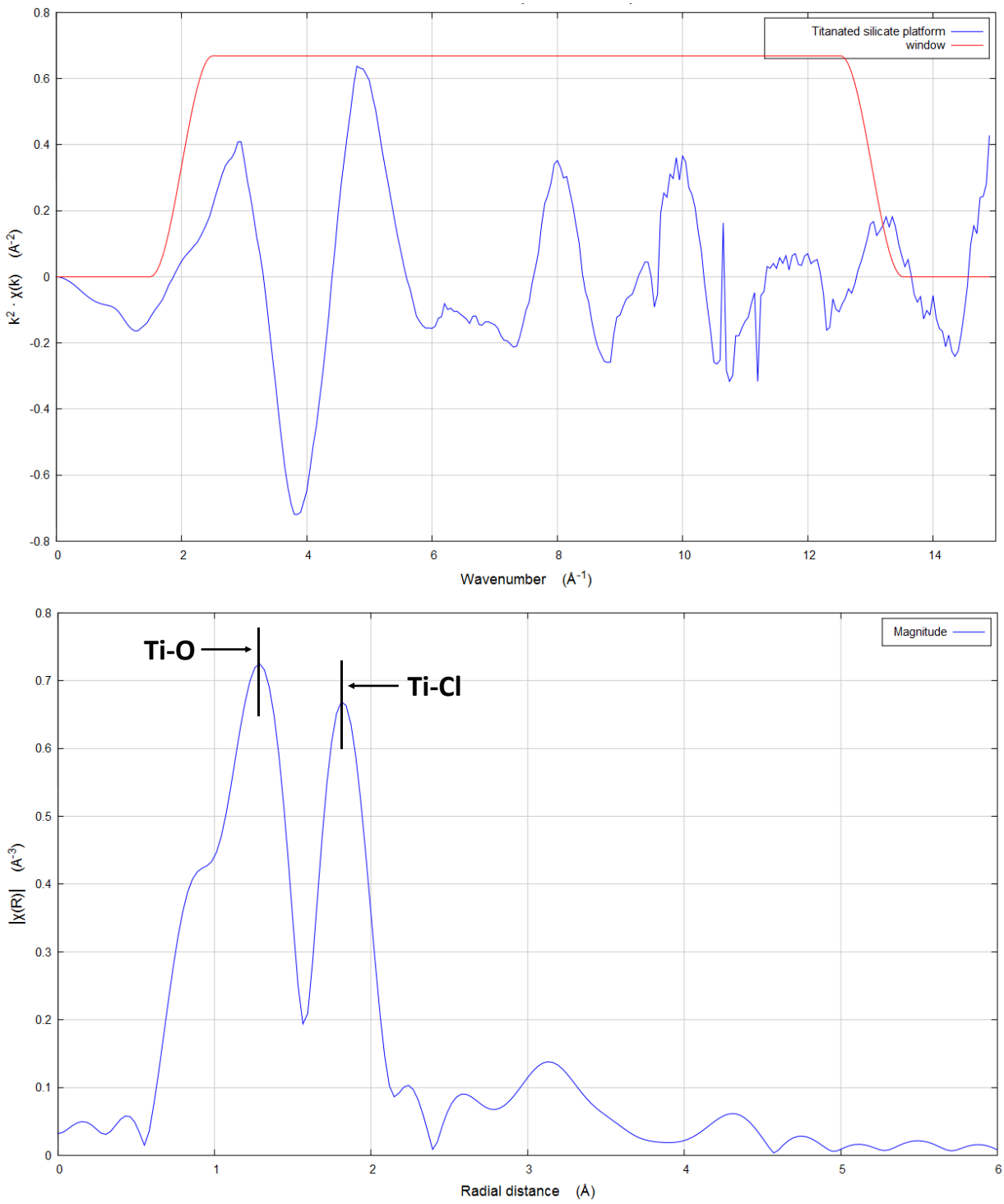

Figure 39: *The EXAFS data (K space and R space) of titanated silicate platform.*

both zeolites[106] and molecular titanium species.[107] In 1974, McMurry and Fleming reported reducing a molecular titanium species, $TiCl_4$ with $LiAlH_4$ producing low-valence titanium chlorides. This system is quite similar to our surface species and we theorized this reaction may extend to our system. Consequently, these traditional hydride reducing agents are excellent candidates for the reduction of the surface titanium(IV) species. Figure 40 illustrates schematically a possible sequences of steps in the reaction of a hydride base reducing reagent with our trichloro-titanium species; a hydride is transferred to titanium creating a high energy intermediate that then undergoes a reductive elimination to create a titanium(III) species. The following are the procedures used with these hydrides reducing agents: The exact stoichiometric amount of hydride reducing reagent is unknown. Therefore, the procedures below were carried out with estimates for one, two, four and five equivalents of hydride, one equivalent is used as an example.

PROCEDURES

LITHIUM ALUMINUM HYDRIDE

In a Schlenk reaction vessel, 0.500 grams of titanated silicate platform (0.775 mmol of titanium), was added to 0.029 grams (0.775 mmol) of lithium aluminum hydride, $LiAlH_4$ [1:1 $LiAlH_4$/Ti site] followed by the vapor transfer of approximately 30 mL of diethyl ether. The solution was then stirred at room temperature. The initially off white colored titanated silicate platform turned into a dark solid over the course of ~1 hour. The solution was allowed to continue to react for 18 hours whereupon all volatiles were removed using heat and dynamic vacuum. The resulting fine powder solid was characterized without further purification.

SODIUM BOROHYDRIDE

In a Schlenk reaction vessel, 0.500 grams of titanated silicate platform (0.775 mmol of titanium), was added to 0.029 grams of sodium borohydride, $NaBH_4$ [1:1 $NaBH_4$/Ti site] followed by the vapor transfer of approximately 30 mL of diglyme. The solution was then stirred at 80°C. The initially off white colored titanated silicate platform turned into a dark solid over the course of ~1 hour. The solution was allowed to continue to react for 18 hours whereupon all volatiles were removed using heat and dynamic vacuum. The resulting fine powder solid was characterized without further purification.

RESULTS AND DISCUSSION

The spectroscopic characterization of the sample exposed to sodium borohydride was identical to that the sample exposed to lithium aluminum hydride. For this reason, the results from a sample exposed to sodium borohydride will be discussed in detail.

The IR of a sample exposed to sodium borohydride is seen in Figure 41. The IR shows no evidence of hydrolysis which would be seen between 3400 and 3800 cm^{-1}. Additionally, there are no features in the region between 1500 and 1200 cm^{-1} suggesting no titanium hydrides have been created. Finally, the Ti-O-Si stretch at 960 cm^{-1} has decreased which is consistent with loss of titanium from the surface bound sites, i.e. the leaching of the titanium species from the matrix.

Titanium XANES data (K-edge) from the hydride reduced samples can be seen in Figure 42. Again, photobleaching was observed in this sample when placed into the X-ray beam and scan one was different from scans two and three. As a result, the data present is from scan one only.

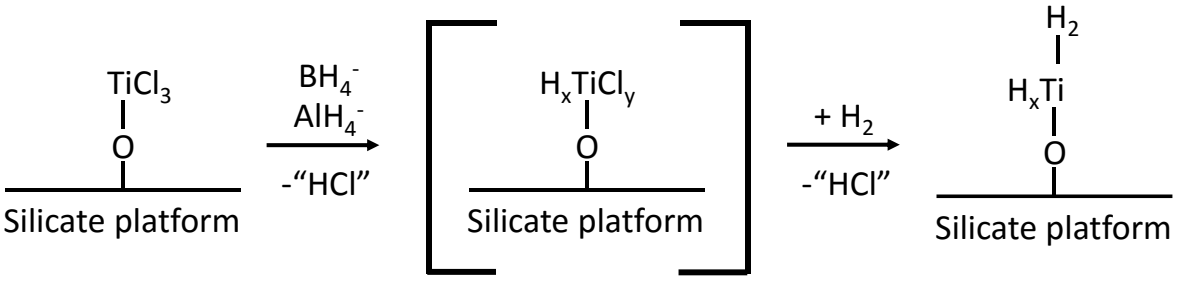

***Figure 40**: illustrates schematically a possible sequences of steps in the reaction of a hydride base reducing reagent with our trichloro-titanium species.*

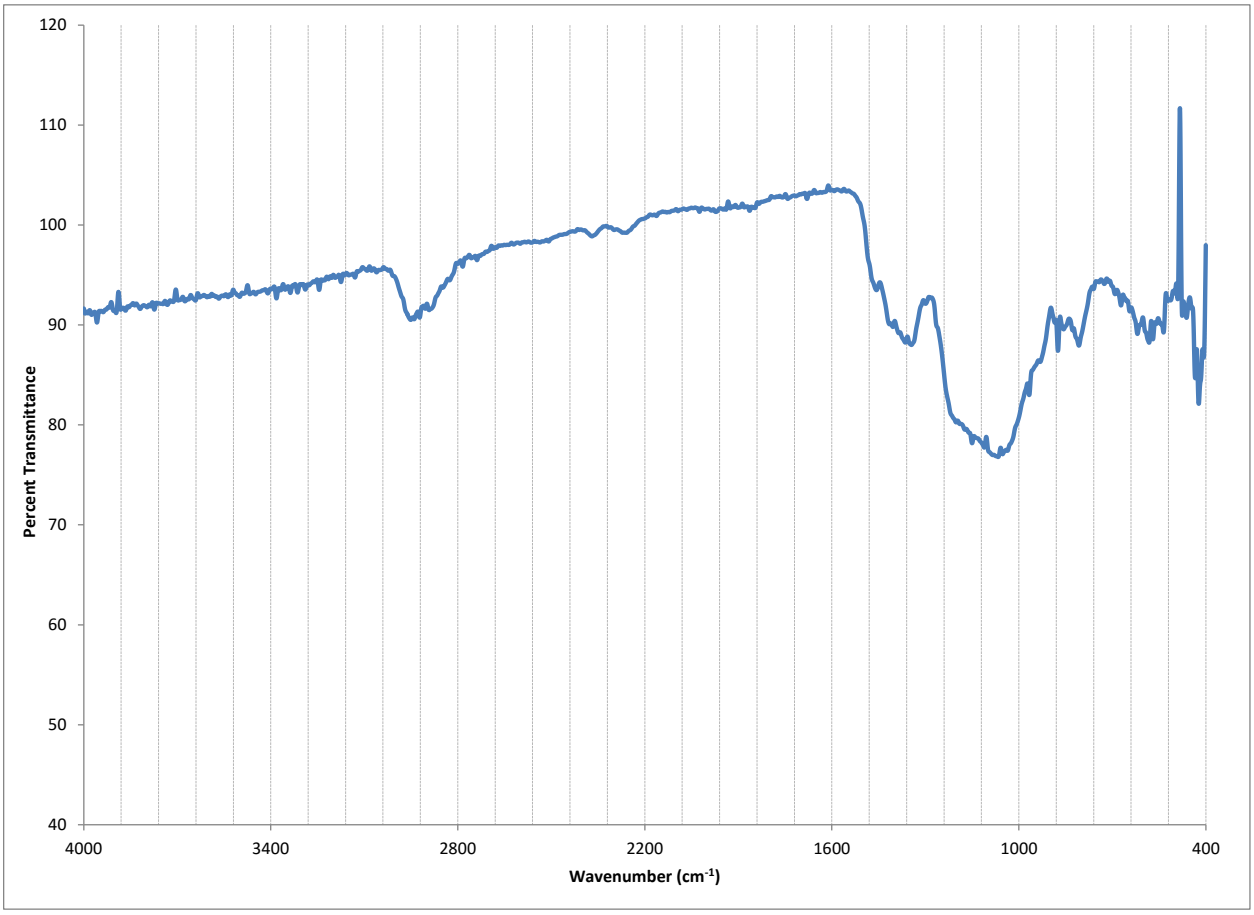

***Figure 41**: The IR spectrum of titanated silicate platform exposed to sodium borohydride.*

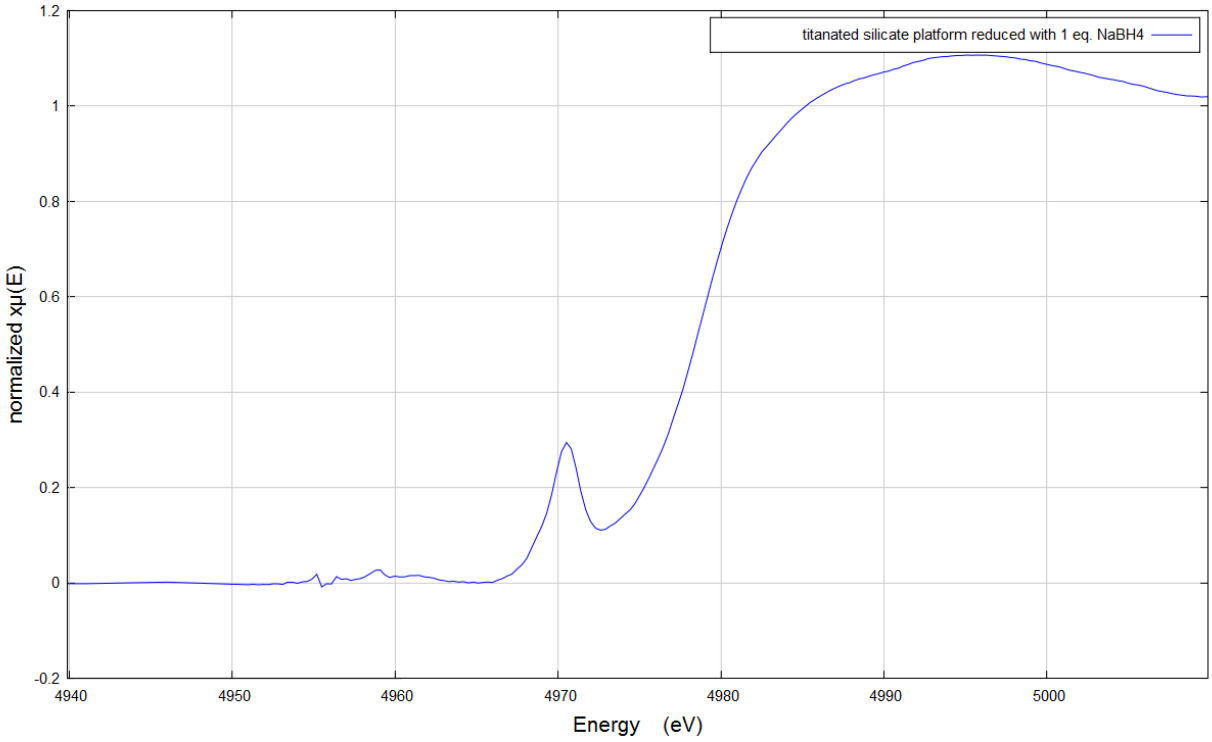

***Figure 42**: Titanium XANES data (K-edge) of titanated silicate platform exposed to sodium borohydride.*

Figure 43 displays the titanium XANES data (K-edge) from the hydride reduced samples as it compares to known standards. The ~4 eV shift in the edge position implies the titanium(IV) species have been reduced. Additionally, the loss of a chlorine shoulder on the edge suggests the loss of any chloride ligand on titanium. Finally, the decrease in the pre-edge feature, a 1s -> 3d transition, indicates a titanium coordination sphere with a center of inversion. EXAFS data from the hydride based reductants compared to unreduced titanated silicate platform, seen in Figure 39, indicates a lengthening of bond distances, which is incongruent with a reduced species. Also seen in EXAFS, the decrease in the 1.90 Å feature, consistent with the loss of chloride ligands. We attempted to develop structural models that could be used to fit the EXAFS data. Unfortunately, we were unsuccessful, probably due the presence of multiple species after reduction; the structural features of which are expected to overlap extensively in the EXAFS data.

A dark solution developed when two and four equivalents of lithium aluminum hydride and sodium borohydride were used. This is clear evidence of the titanium species leaching from the matrix during the reduction with hydride based reductants. This is most likely indicates that the reduction step was accomplished by breaking the bond to the surface. Both aluminum(III) and boron(III) are highly oxophilic. As titanium is reduced from +4 to +3 or lower, its oxophilicity is reduced which could facilitate breaking the bond to the surface and subsequent formation of solution species. As a result, the XAS quite possible reflects a mixture of species. Therefore, with this loss of control, we focused our efforts on other methods of the reduction that did not involve any oxophilic elements, such as boron and aluminum that may compete with titanium for surface sites.

REDUCTION WITH HYDROGEN

The reduction potential of hydrogen has been studied extensively in the literature.[108] Reactions with hydrogen offer the most direct approach to reducing titanium and obtaining titanium hydrides species. Hydrogen also removes the problems of oxophilic elements, like those seen in hydride based reductants. Figure 45 illustrations a theorized reaction of a hydrogen with our trichloro-titanium species; a sigma bond metathesis occurs, that then undergoes a reductive elimination to create a titanium(III) species. The following paragraphs discuss our work with hydrogen as a reductant for our trichloro-titanium species. The reduction using hydrogen was carried out in two different methods: pressure vessel and flow cell.

PROCEDURES

PRESSURE VESSEL

In a glass pressure vessel, seen in Figure 46, 0.500 grams of titanated silicate platform (0.775 mmol of titanium) was added and pressurized to two atmospheres of reagent grade hydrogen (99.999% pure). The pressure vessel was then placed in a molten salt bath (7% - $NaNO_3$: 40% - $NaNO_2$: 53% - KNO_3) at 350°C. A thermocouple placed into a side port allowed us to verify the hydrogen was at temperature. The pressure vessel was allowed to continue to react for 4 hours whereupon all volatiles were removed using heat and dynamic vacuum. The volatiles were found to be acidic with litmus paper. The resulting fine powder off-white solid was characterized without further purification.

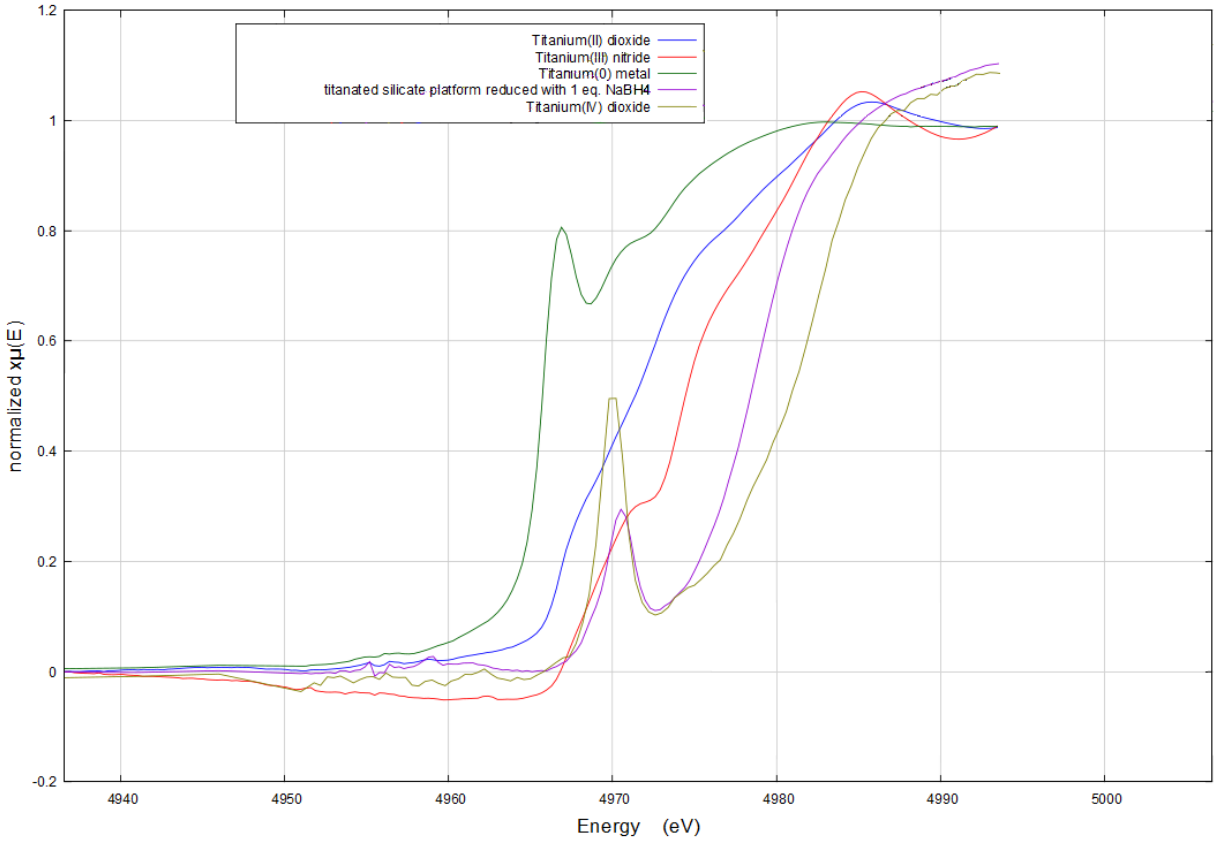

***Figure 43**: Titanium XANES data (K-edge)of titanated silicate platform exposed to sodium borohydride as it compares to known standards and titanated silicate platform.*

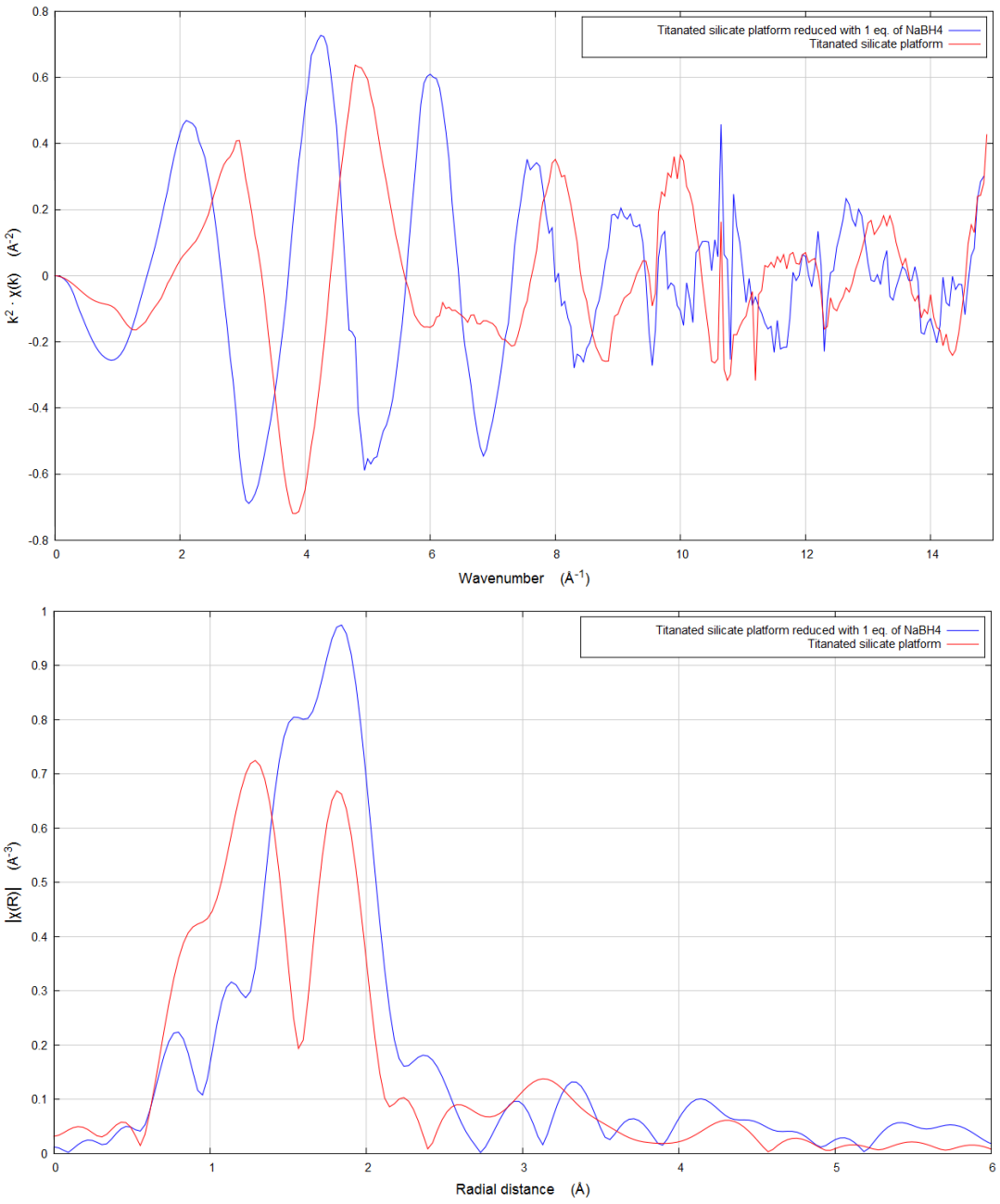

Figure 44: *The EXAFS data (K-space and R-space) of titanated silicate platform exposed to sodium borohydride.*

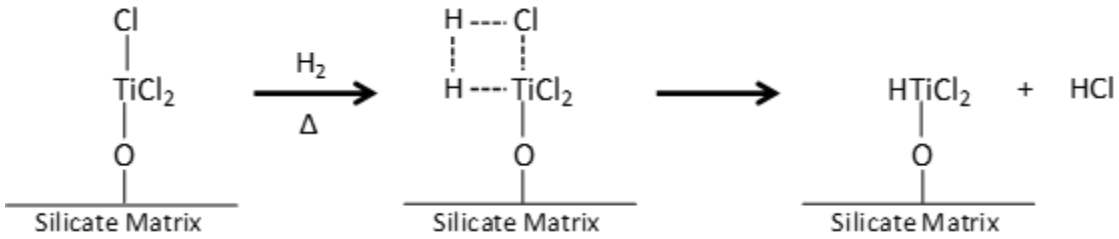

Figure 45*: illustrations a theorized reaction of a hydrogen with our trichloro-titanium species.*

Figure 46*: A picture of the pressure vessel used for the reduction with hydrogen.*

Figure 47: *A picture of the flow cell used for the reduction with hydrogen*

t FLOW CELL PROCEDURE

In a reactor U-tube reactor, seen in Figure 47, 0.500 grams of titanated silicate platform (0.775 mmol of titanium) was added and connected to a cylinder of reagent grade hydrogen (99.999% pure). The U- ube reactor was then placed in a molten salt bath at 350°C and a hydrogen flow (2mL per sec) was started. A thermocouple placed into a side port allowed us to verify the hydrogen was at approximately 340°C when in contact with the sample. The U-tube reactor was allowed to continue to react for 4 hours whereupon all volatiles were removed using heat and dynamic vacuum. The outflowing gas was found to be acidic with litmus paper. The resulting fine off-white powder solid was characterized without further purification.

RESULTS AND DISCUSSION

IR spectra of both the pressure vessel and flow cell samples exposed to hydrogen at 350°C can be seen in Figure 48. Both samples show no indication of titanium-hydride bands. The flow cell sample shows no significant amount of hydrolysis. The pressure vessel sample shows a significant about of isolated hydroxyl groups (seen at 3XXX cm^{-1}) compared with the flow cell. The reduction of titanium(IV) creates hydrochloric acid (HCl) as a byproduct. We theorize anhydrous HCl may attack Si-O-Si or Si-O-Ti linkages, leading to the formation of hydroxyl groups on the surface. The flow cell allows any HCl created during the reduction to be removed from the material, thus giving it less time to interact and break Si-O-Si or Si-O-Ti bonds. Additionally, the titanium-chloride feature at 490 cm^{-1} seen in the unreduced titanated has significantly decreased in both the flow cell and pressure vessel samples.

Titanium XANES data (K-edge) from both the pressure vessel and flow cell samples exposed to hydrogen can be seen in Figure 49. Again, photobleaching was observed in these samples and data shown are from the first scan only. The edge positions (4979 eV and 4980 eV; pressure vessel and flow cell respectively) implies the titanium(IV) species has not been reduced. Additionally, the loss of a chlorine shoulder on the edge suggests the loss of chloride ligand on titanium. Finally, the pre-edge feature is approximately the same height as the unreduced, indicates a titanium most likely has a tetrahedral coordination geometry.

Figure 50, displays the EXAFS data from both the pressure vessel and flow cell samples exposed to hydrogen. The sample in a flow reactor shows a single feature at 1.30 Å, which is incongruent with a titanium-oxygen bond. Whereas the sample in a pressure vessel has a feature at 1.30 Å consistent with titanium-oxygen and a feature at 1.90 Å consistent with titanium-chloride.

In our investigation, the samples exposed to hydrogen appear to remain in a high oxidation state but show the loss of coordinating chloride ligand. These coordinated unsaturated titanium species must be stabilized with alternative ligands that are not observable in XAS. These results are consistent with the presence of hydride ligands around titanium, although they are not visible in the IR spectrum.

These results indicate the activation energy to reduce our titanium species may be higher than previously anticipated. Two methods can be taken used to overcome this challenge. High temperatures (>500°C) may offer us the ability to reduce our titanium species with only hydrogen, but these temperatures can be difficult to reach and require extra precautions. An alternative method for reducing our titanium

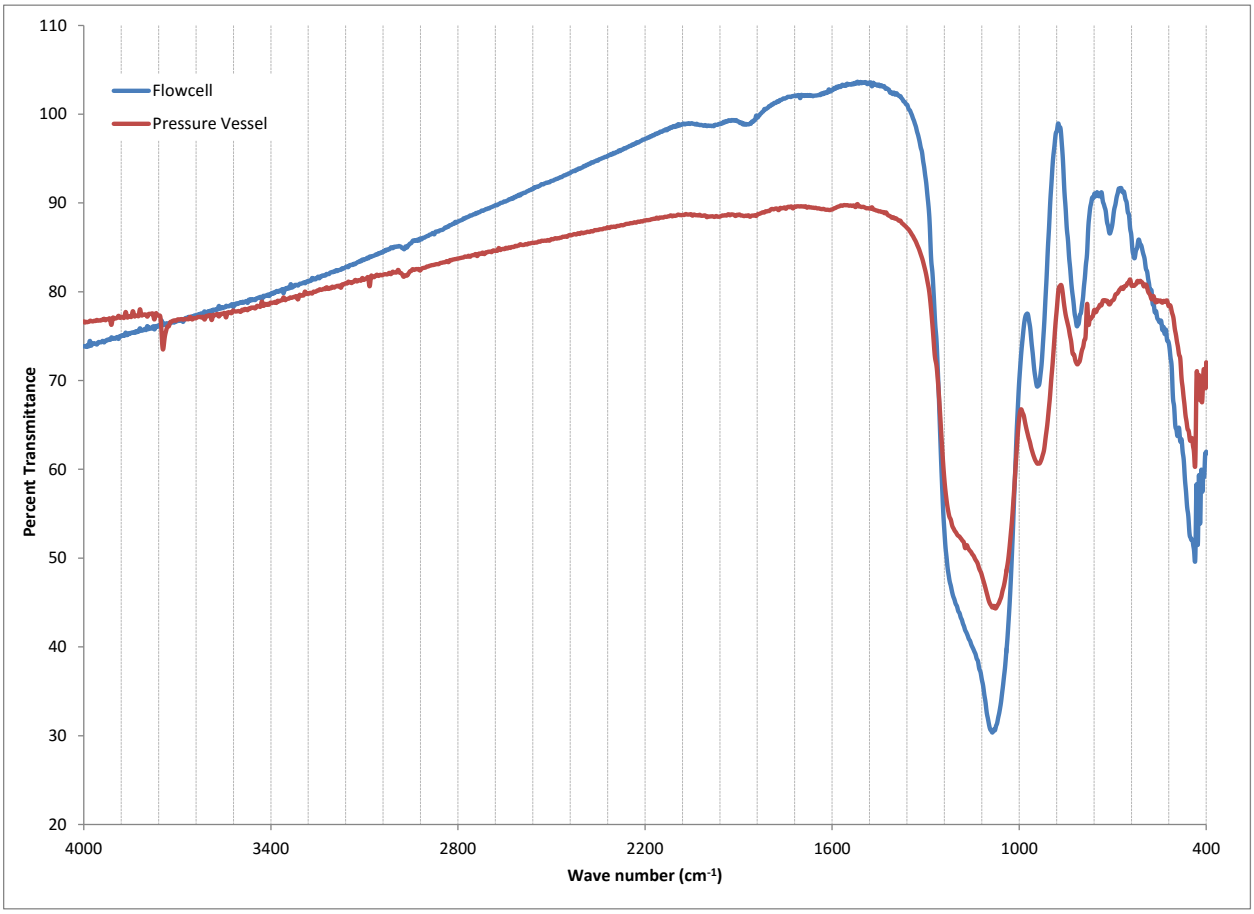

Figure 48: *An IR of both the pressure vessel and flow cell samples exposed to hydrogen at 350°C*

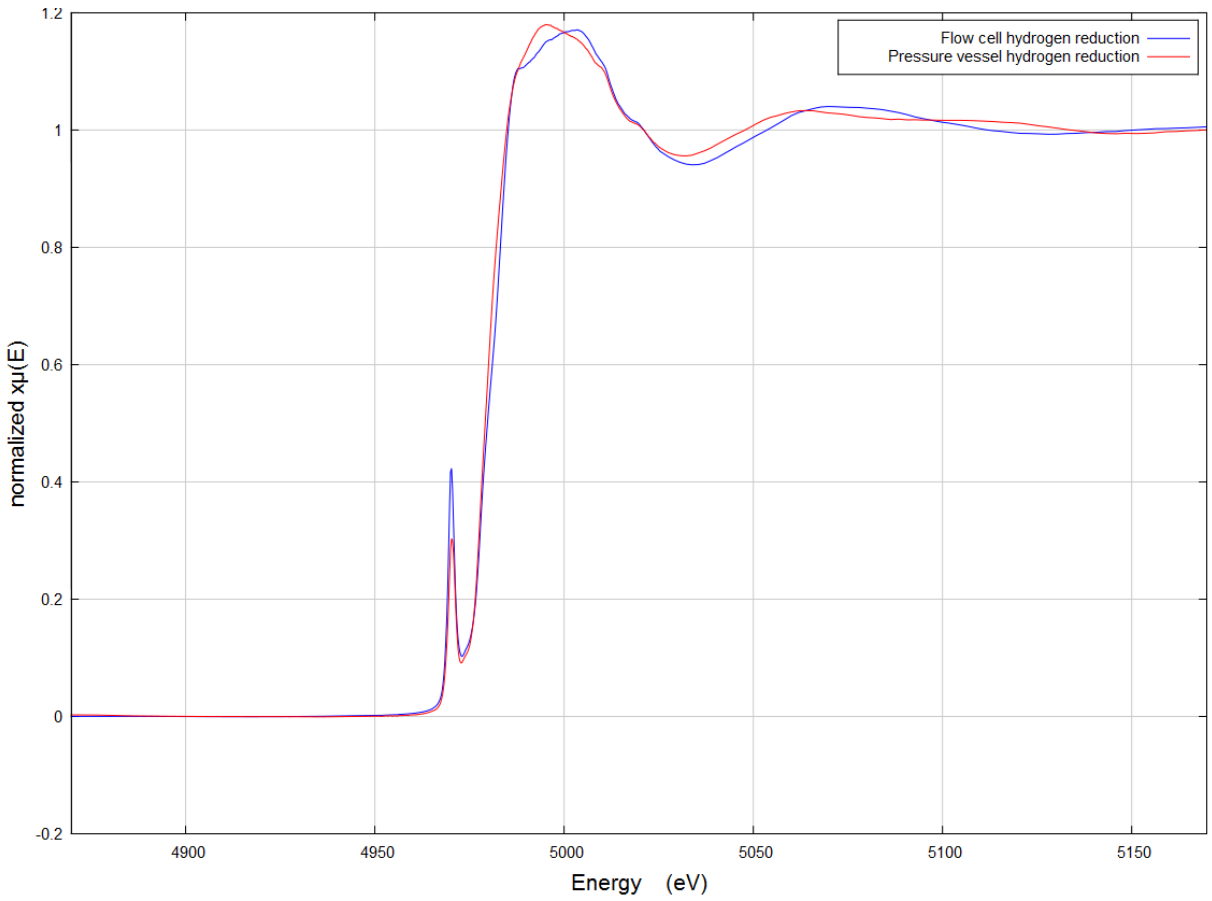

Figure 49: *Titanium XANES data (K-edge) from both the pressure vessel and flow cell samples exposed to hydrogen at 350°C*

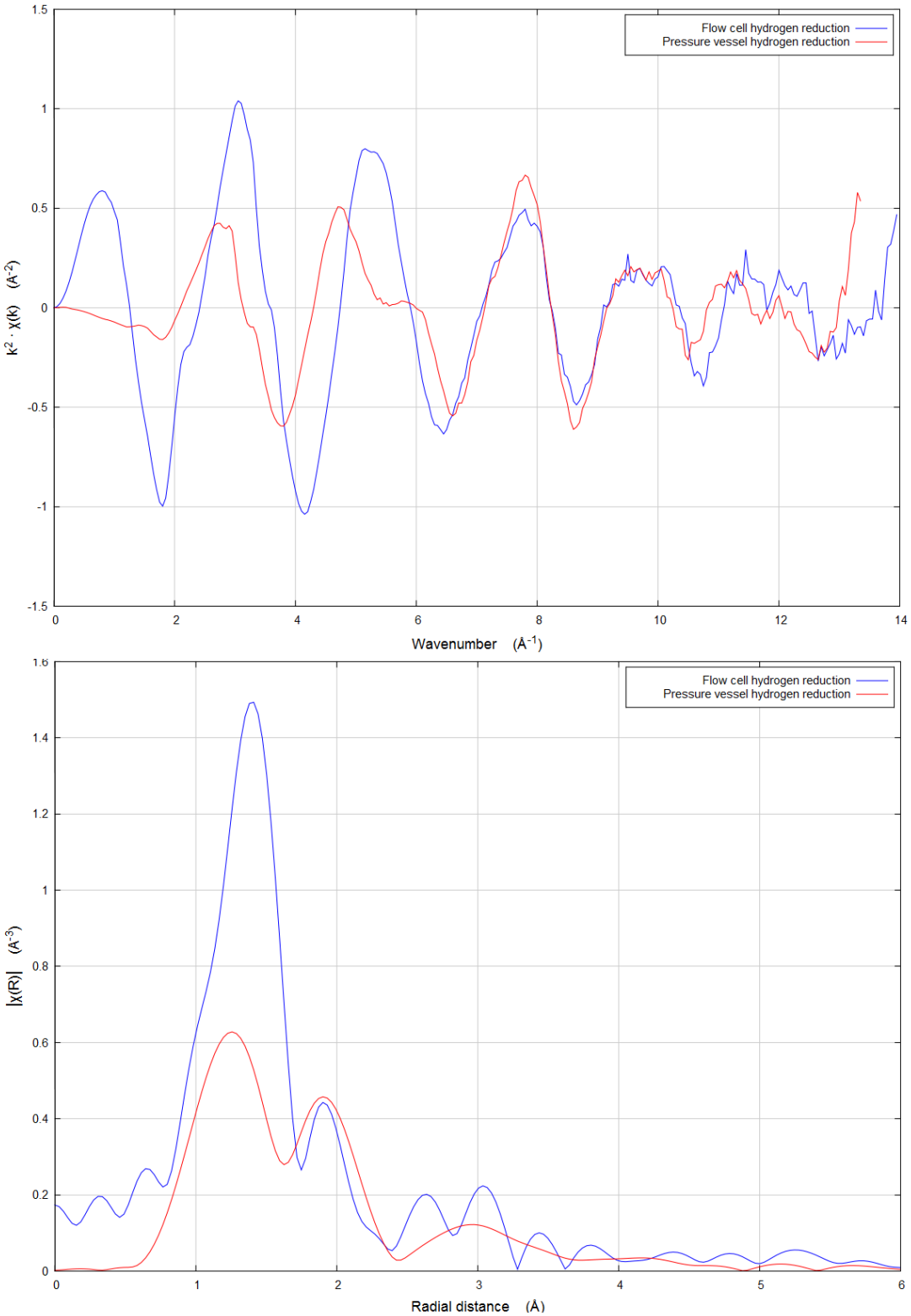

***Figure 50**: The EXAFS data (K-space and R-space) from both the pressure vessel and flow cell samples exposed to hydrogen at 350°C*

species is the addition of a hydrogen-activating agent that acts as a transfer agent creating an alternate mechanism to produce reduced titanium species.

REDUCTION WITH HYDROGEN WITH PLATINUM PROMOTER

The use of platinum promoters or activators for reductions with hydrogen is well documented in literature.[109] It is believed that a spillover phenomenon allows platinum to act as a hydrogen transfer agent. Figure 51 schematically illustrates a generalized hydrogen spillover mechanism. It was hoped that the addition of platinum to these titanium systems would help promote the creation of Ti-H by transferring hydrides from the platinum to the titanium. It is difficult to predict the platinum loading necessary to accomplish the reduction of our trichloro-titanium species. Therefore, two platinum loadings were investigated: a high loading (1Pt:10Ti) and a low loading (1Pt:100Ti). We speculate this method of reduction may follow a similar mechanism to that of only hydrogen reductions. As a result, this method may still produce significate amounts of anhydrous HCl, thus the reaction was carried out using the flow reactor designed for hydrogen reductions. The following summarizes our work with a platinum promoter and hydrogen for the reduction of our surface trichloro-titanium species.

PROCEDURE

To a Schlenk reaction vessel with 0.500 grams of titanated silicate platform (0.775 mmol of titanium), 0.003 grams (7.75×10^{-3} mmol) or 0.030g (7.75×10^{-3} mmol) of dichloro(1,5-cyclooctadiene) platinum(II), $Pt(cod)Cl_2$ was added to prepare low and high platinum samples respectively. This was followed by the vapor transfer of approximately 30 mL of methylene chloride. The solution was then stirred at room temperature for 1 hour. All volatiles were removed using heat and dynamic vacuum.

In a fritted U-tube reactor, 0.500 grams of material from the previous reaction was added and connected to a cylinder of reagent grade hydrogen (99.999% pure). The U-tube reactor was then placed in a molten salt bath at 350°C and a hydrogen flow (2mL per sec) was started. A thermocouple placed into a side port allowed us to verify the hydrogen was at approximately 340°C when interaction with the sample The U-tube reactor was allowed to continue to react for 4 hours whereupon all volatiles were removed using heat and dynamic vacuum. The resulting fine powder solid was characterized without further purification. At high platinum loading the sample turned from off-white to dark gray in color during the reaction. This is consistent with the reduction of platinum to platinum nanoparticles.

RESULTS AND DISCUSSION

The IR spectra of the samples exposed to hydrogen containing platinum promoter at 350°C were nearly identical to those obtained from titanated silicate samples exposed to hydrogen at the same temperature without platinum. IR spectra show no indication of titanium-hydride bands, but did show signs of the presence of hydrolysis. Additionally, the titanium-chloride feature at 490 cm^{-1} seen in the unreduced titanated species is not present in the reduced species.

Titanium XANES data (K-edge) from a sample exposed to hydrogen with high loading platinum promoter are shown in Figure 52. Once again, photobleaching was observed in these samples and data shown are from the first scan only. The edge position (4979 eV) implies the titanium species has not been reduced. The lack of a chlorine shoulder on the edge is consistent the loss of chloride ligand on titanium. Finally,

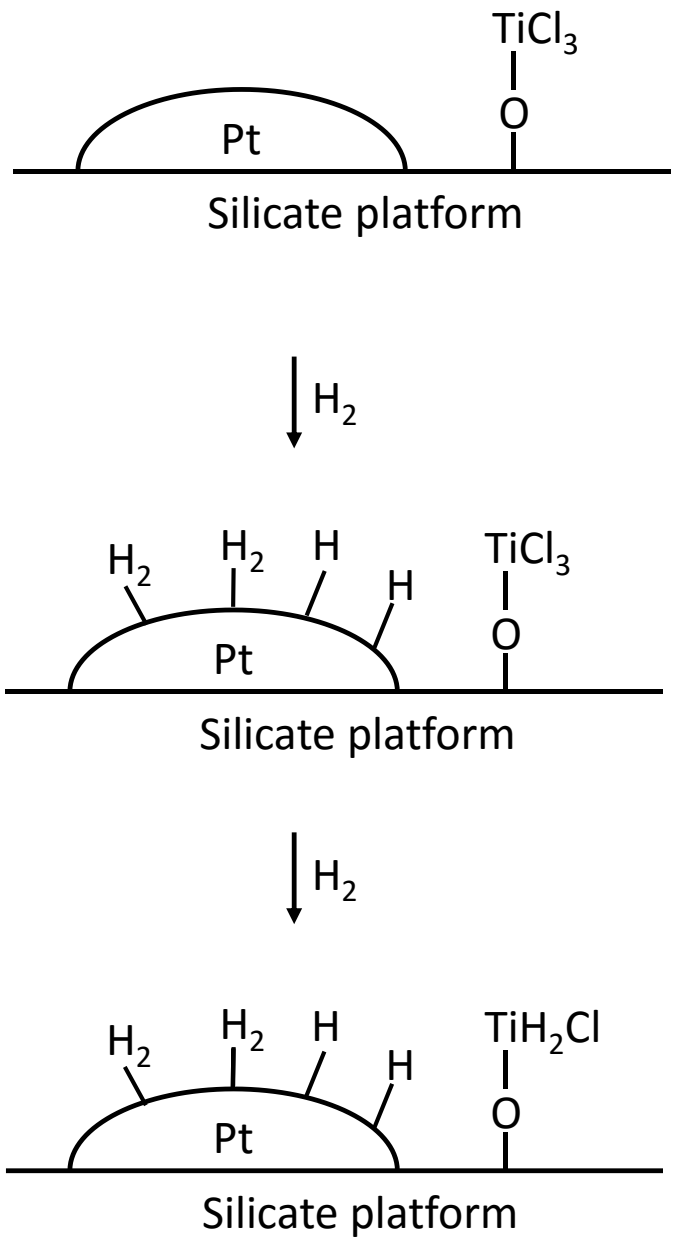

Figure 51*: schematically illustrates a generalized hydrogen spillover mechanism.*

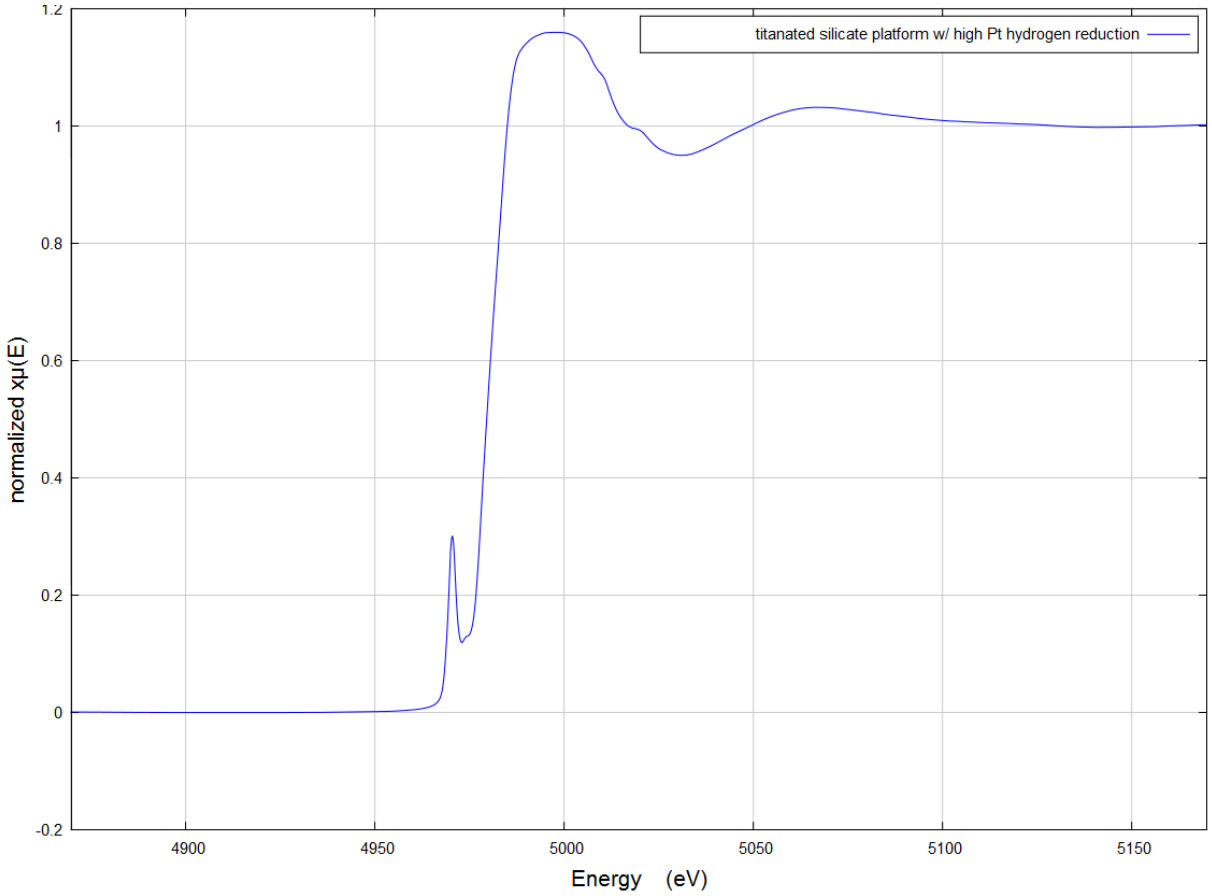

***Figure 52**: Titanium XANES data (K0edge) from a sample exposed to hydrogen with high loading platinum promoter.*

the decrease in the intensity of the pre-edge feature indicates a titanium with a geometry that has an inversion symmetry. Titanium EXAFS data from a high Pt loaded sample exposed to hydrogen, seen in Figure 53, shows two features. One strong feature at 1.30 Å consistent with a titanium-oxygen bond and a smaller feature at 1.90 Å consistent with a titanium-chlorine bond. Whereas the unreduced titanated platform has a Ti-O at 1.30 Å and Ti-Cl at 1.90 Å. XAS and IR indicate that the titanium sites appear to be identical with those without the addition of platinum.

Platinum XANES (L_{III} edge) spectra from a high Pt loaded sample before and after exposure to hydrogen can be seen in Figure 54. The unreduced high platinum loading sample has a white line approximate twice as intense as the edge jump. This white line, assigned to an electronic transition from $2p^{3/2}$ to a 5d orbital, can be quite sensitive to the oxidation state of platinum. The intensity of the white line observed at the L_{III} edge reflects the occupancy of the d orbitals of the absorbing atom.[110] Thus, reduced platinum with filled d-orbitals exhibits a suppressed white line. The platinum XANES (L_{III} edge) spectra from a high Pt loaded exposed to hydrogen has a white line slightly less than half the edge jump. These results are consistent with the reduction of platinum in our sample.

The data gathered from samples with high Pt load and exposed to hydrogen causef us to question the effects a platinum promoter has on our trichloro-titanium species. The data suggest that we obtained similar titanium species with and without platinum. It is unclear whether platinum influenced the reaction. The color change of the sample and the change in white line intensity in the platinum XAS are consistent with the reduction of platinum. The exact form platinum takes, nanoparticles or larger metal crystallites, is unclear. While there is good evidence that platinum has been reduced to metal there may be no effective way to transfer activated hydrides from platinum to titanium site, via the silicates support. Literature shows that silicates are very difficult to reduce, making them a very poor conduit for hydrogen atoms.

At this point in our attempts to reduce and active our titanium species for Kubas binding, we decided to take a more empirical approach to our reduction methods. Rather than attempting to understand the structural and electronic configuration of our “reduced” titanium species, we studied their interaction with molecular hydrogen to determine if any reduced species showed chemisorption behavior. Materials that exhibited chemisorption of hydrogen should demonstrate hysteresis-like behavior on the absorption/desorption analysis with hydrogen gas. The difference between the desorption curve and adsorption curve signifies the amount of hydrogen chemisorbed (Figure 35). This analysis became the determining analysis for our reduced materials. Materials that demonstrated hysteresis during desorption would be further characterized, others would be set aside.

REDUCTION WITH COBALTOCENE

Cobaltocene, a nineteen electron organometallic complex, has been extensively studied for its reduction potential.[111] Like hydrogen based reductions, cobaltocene was investigated as a chemical reductant without the presence of oxophilic elements. A general reaction of cobaltocene with a trichloro-titanium surface species is seen in Figure 55. This reaction may leave the titanium species coordinately unsaturated. As a result, these reactions was run under an atmosphere of hydrogen.

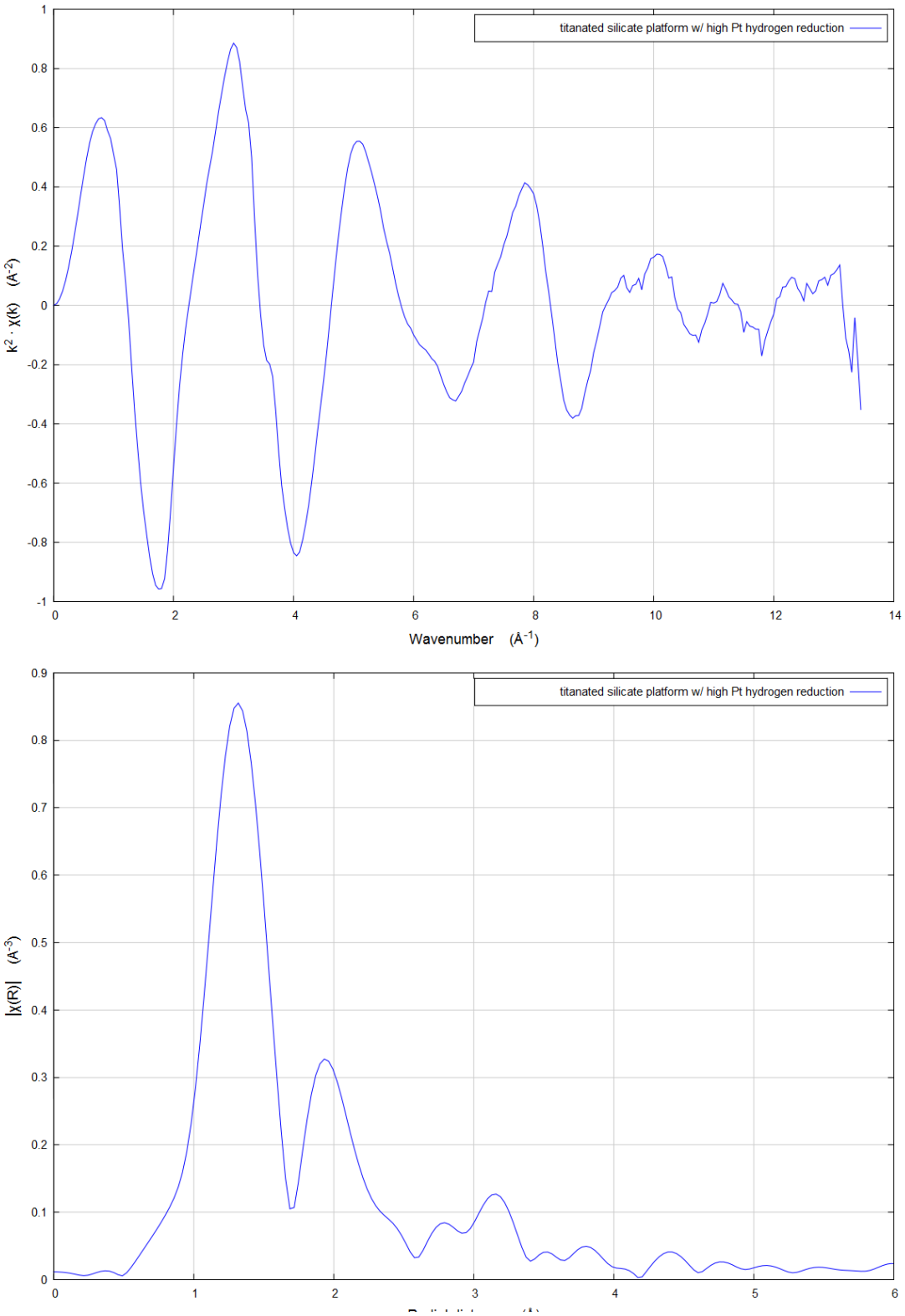

***Figure 53**: The EXAFS data (K-space and R-space) from a sample exposed to hydrogen with high loading platinum promoter.*

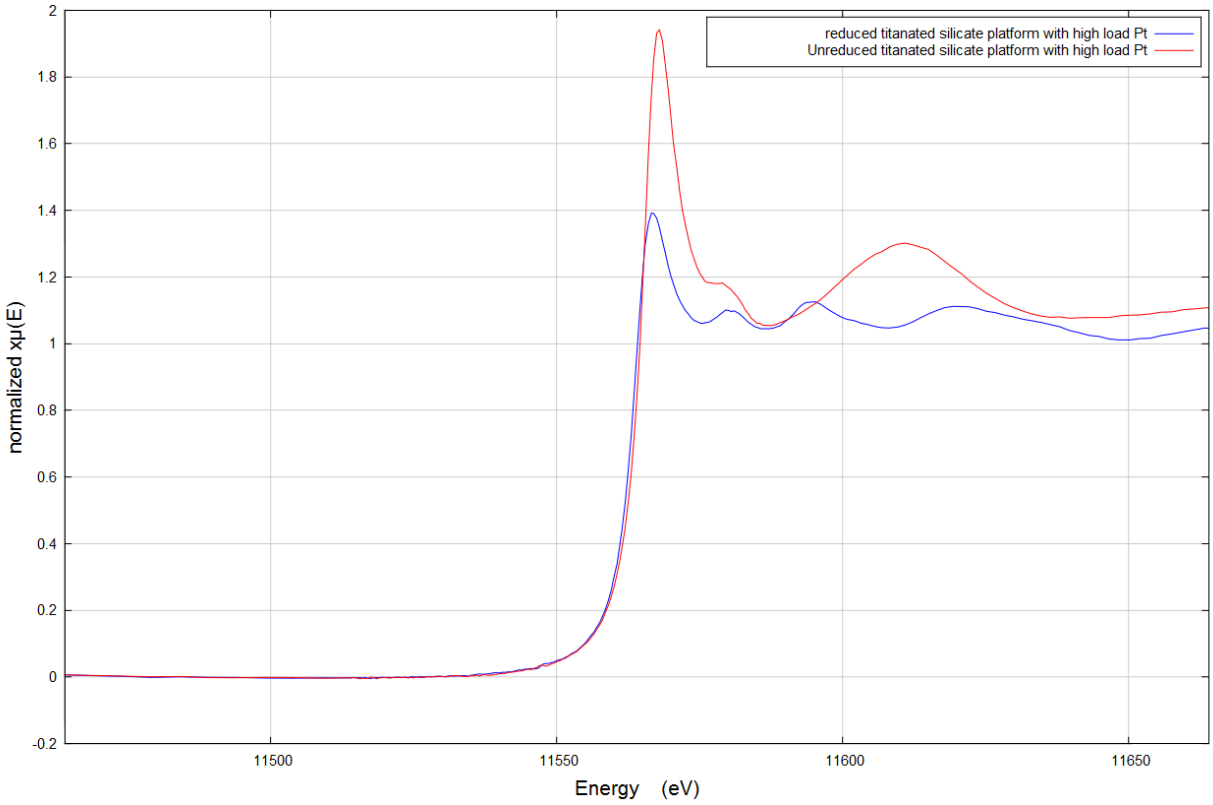

***Figure 54**: Platinum XANES (LIII-edge) spectra from a high Pt loaded sample before and after exposure to hydrogen.*

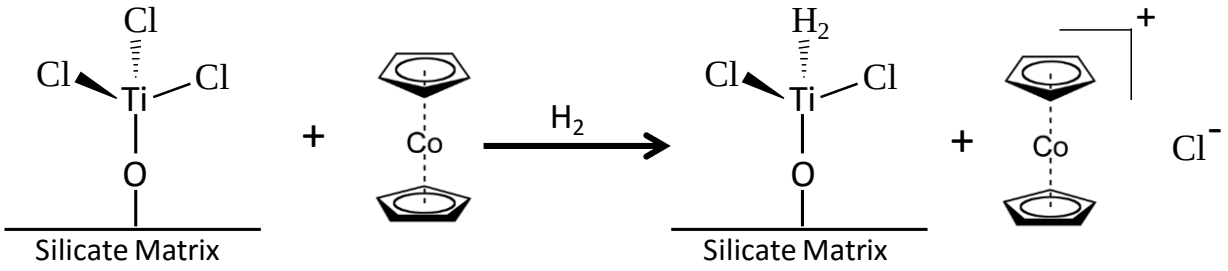

***Figure 55**: A general reaction of cobaltocene with a trichloro-titanium surface species*

PROCEDURE

In a Schlenk reaction vessel, 0.500 grams of titanated silicate platform ($7.75x10^{-1}$ mmol of titanium), was added to 0.147 grams ($7.75x10^{-1}$ mmol) of cobaltocene, $Co(C_5H_5)_2$ [1:1 $Co(C_5H_5)_2$:Ti site] followed by the vapor transfer of approximately 30 mL of hexane. 1 atm of hydrogen was then added. The solution was then stirred at room temperature. A dark purple solution indicative of cobaltocene in solution was seen within minutes and the solution developed a green color within 4 hours. The solution was allowed to continue to react for 18 hours whereupon all volatiles were removed using heat and dynamic vacuum. The resulting fine powder solid was characterized without further purification.

RESULTS AND DISCUSSION

An IR of the sample exposed to cobaltocene can be seen in Figure 56. Like previous methods, a sample exposed to cobaltocene shows no indication of titanium-hydride bands. Additionally, the sample showed signs of the presence of hydrolysis. A sharp feature at 1415 cm^{-1} may indicate the present of a titanium hydride. Finally, the titanium-chloride feature at 490 cm^{-1} is still present. No XAS data was collected on this sample.

It is extremely difficult to draw any conclusions about the oxidation state and coordinated ligands around titanium in these reactions from IR spectroscopic data. What we can observe is that the color change (purple to green) is consistent with cobaltocene reacting to become cobaltocenium. The counterion of the cobaltocenium complex is unknown, but a chloride species can be easily conjectured. There are two sources of chloride in our sample: 1) the titanium species 2) inert silicon linkers. With the data at hand, it is unclear which source produced the chloride.

The hydrogen adsorption-desorption isotherm can be seen in Figure 57. It shows a small hysteresis indicative of chemisorb hydrogen. To verify this finding the sample was heated (200°C) under vacuum and the measurement was repeated. Upon completion of the second hydrogen isotherm, the hysteresis was no longer observed and no further measurements were taken.

REDUCTION WITH UV LIGHT AND HYDROGEN

Prior methods used to reduce the surface titanium species indicated that the titanium reduction may have higher activation energy than initially suspected. As a result, we focused our efforts on photochemical reduction. Photochemistry has long been used to activate reactions with high activation energies.[112] As with the other methods that only involve hydrogen, we believe this method could reduce the chloro-titanium species cleanly. There are two common sources of UV radiation: mercury and xenon sources. Both offer strong intensity in the UV and visible regions, with xenon sources extending their spectra far into the infrared region. This Infrared radiation can be problematic for dark samples as it results in localized heating. As a result, a mercury lamp was used in the following procedures.

PROCEDURE

In a quartz, fritted U-tube reactor, 0.500 grams of titanated silicate platform was added and connected to a cylinder of reagent grade hydrogen (99.999% pure). The lower portion of the quartz U-tube reactor was then placed in a molten salt bath at 350°C and a hydrogen flow (2mL per sec) was started. A thermocouple placed into a side port allowed us to verify the hydrogen was at approximately 340°C when interaction

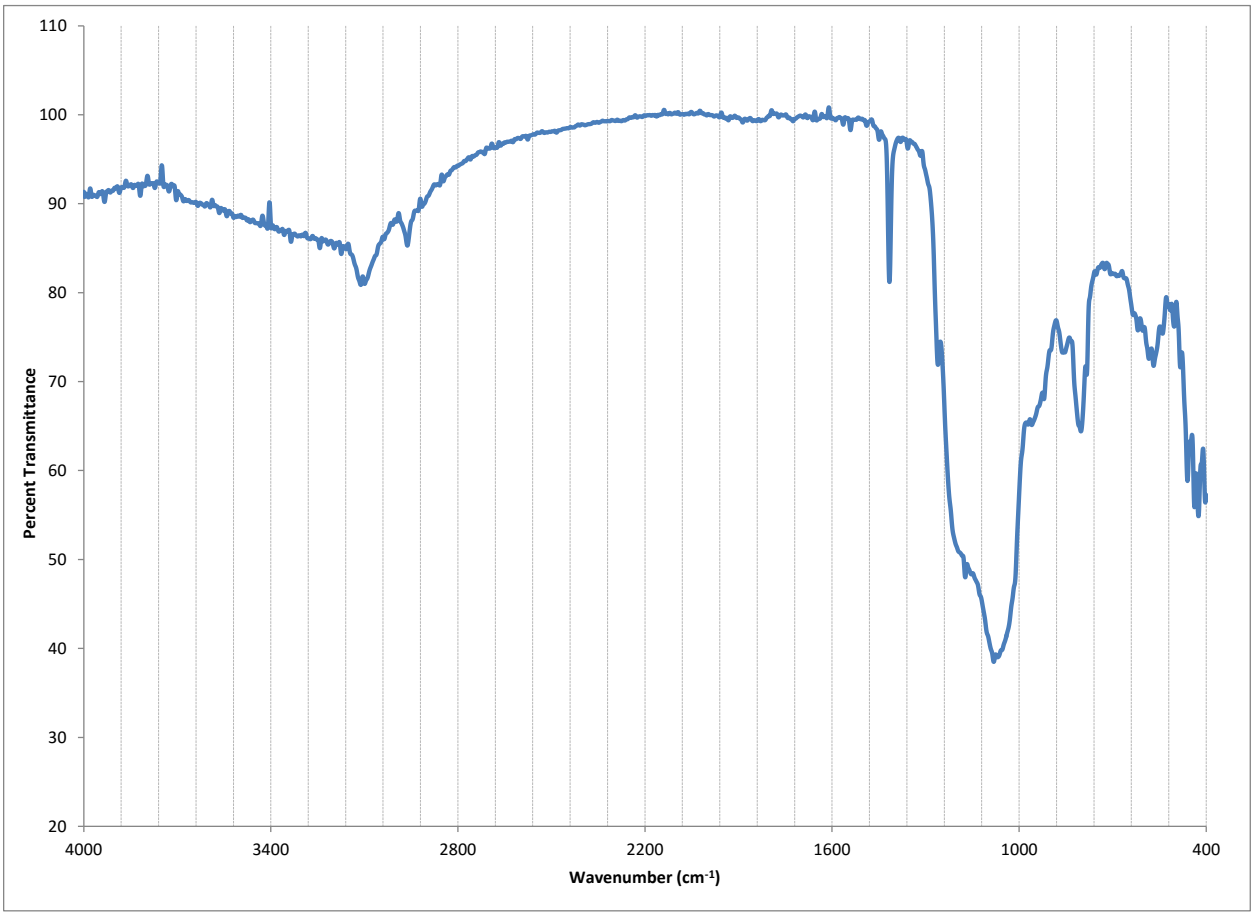

***Figure 56**: an IR spectrum of titanated silicate platform exposed to cobaltocene.*

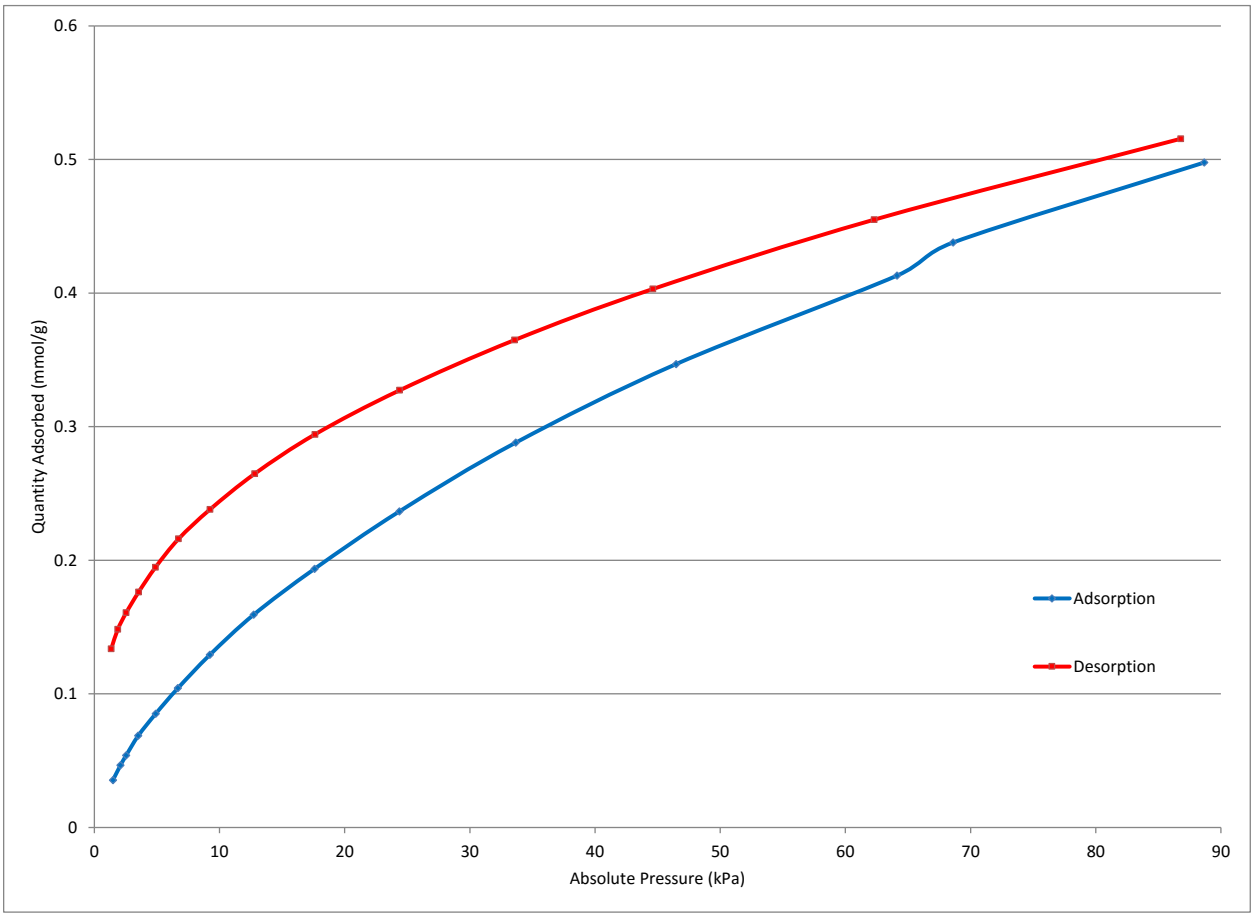

***Figure 57**: The hydrogen adsorption-desorption isotherm of titanated silicate platform exposed to cobaltocene.*

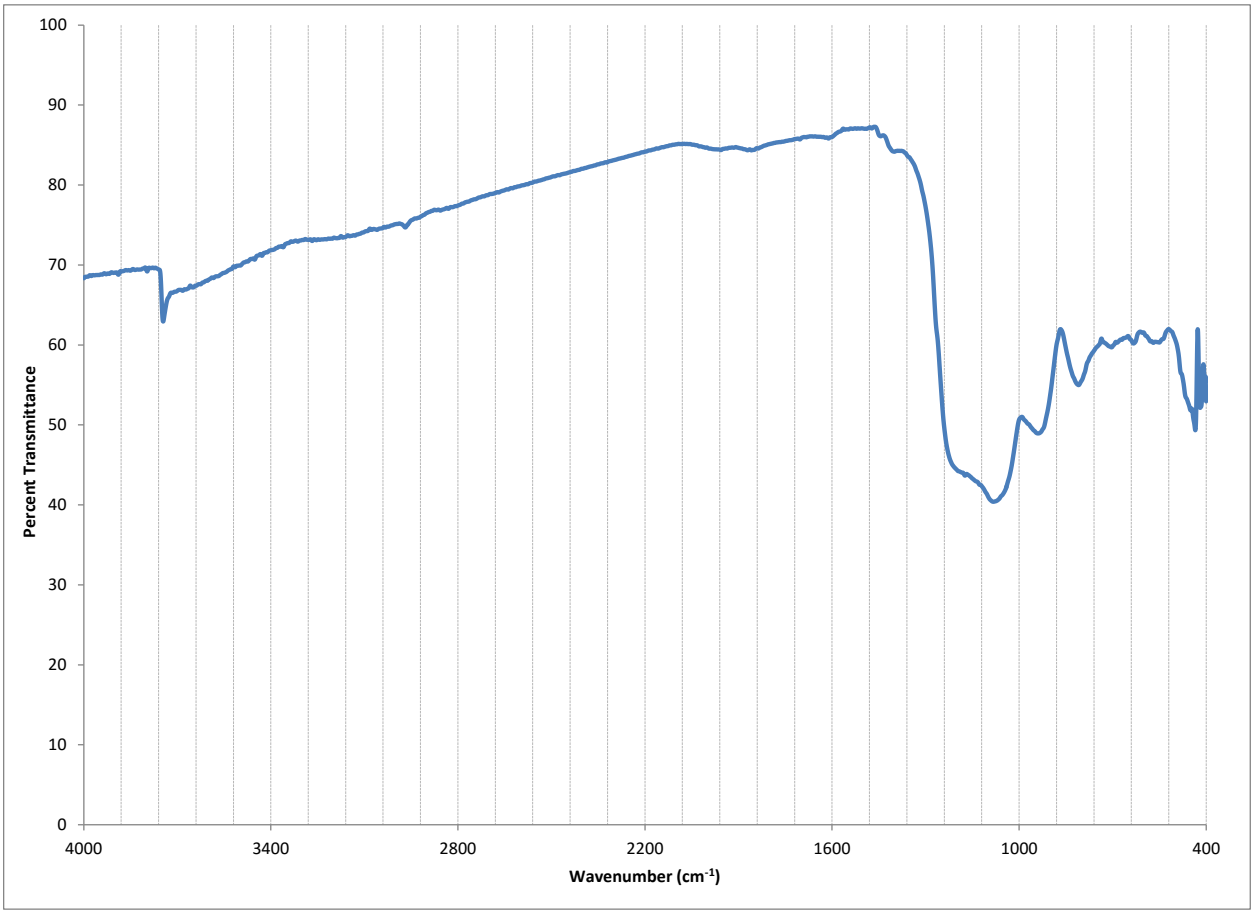

Figure 58: *An IR spectrum of titanated silicate platform exposed to UV light and hydrogen.*

with the sample. A mercury light source was the placed in front of the upper portion of the quartz U-tube reactor. The U-tube reactor was allowed to react for 4 hours whereupon all volatiles were removed using heat and dynamic vacuum. The resulting fine powder solid was characterized without further purification.

RESULTS AND DISCUSSION

Spectroscopic characterization of the sample exposed UV light and hydrogen was approximately identical to that of high-temperature hydrogen reduction. An IR of the sample exposed to UV light and hydrogen can be seen in Figure 58. Like previous methods, a sample exposed to UV light and hydrogen shows no indication of titanium-hydride bands. Additionally, the sample showed signs of hydrolysis. Finally, the titanium-chloride feature at 490 cm^{-1} is very weak. No XAS data was collected on this sample.

The hydrogen adsorption-desorption isotherm showed no indication of a hysteresis. To verify this, the sample was heated (200°C) under vacuum and the measurement was repeated. Upon completion of the second hydrogen isotherm, the presence of a hysteresis was not detected.

TITANIUM TRICHLORIDE

An alternative method for producing reduced titanium sites on our trimethyltin cube based support is to link an already reduced metal center of titanium. Titanium trichloride, $TiCl_3$, is a commercially available reduced titanium center that may be able to be activated for Kubas bind with an exchange of ligands. As discussed previously, as titanium is reduced its oxophilicity decreases. As a result, the titanium trichloride may not be oxophilic enough to exchange with trimethyltin on the corners of the cubes. The following paragraphs discuss the synthesis of a dichloro-titanium(III) surface species and our work to active it for Kubas binding.

TITANYLATION OF SILICATE CUBE BASED PLATFORM WITH TITANIUM TRICHLORIDE: In a Schlenk reaction vessel, 1.00 g ($1.55x10^{-3}$ mol of trimethyltin corners) of trimethyltin cube based silicate platform, was added to 0.167g (1.083 mmol) of titanium trichloride, $TICl_3$ [0.7:1 $TICl_3$/trimethyltin corners] followed by the vapor transfer of approximately 30 mL of acetonitrile. The solution was then stirred at 50°C. The solution was allowed to continue to react for 48 hours whereupon all volatiles were removed using heat and dynamic vacuum. The resulting fine powder solid was used without further purification. Gravimetric data is consistent with titanium trichloride having 0.82 connections to the surface. Although this is not ideal, as a small percent of the titanium trichloride is unbound, the decision was made to proceed to activate the sample for Kubas binding. The following procedure outline our activation attempt.

The IR of the titanated(III) silicate platform, seen in Figure 59, indicates some hydrolysis occurred during the titanylation method. Additionally, there is a feature at 2300 cm^{-1}. This feature is believed to be a bound acetonitrile, creating a four coordinated titanium(III) surface species. Between 1000 and 950 cm^{-1} there are broad features identified as Si-O-Si and Ti-O-Si stretches which make up the majority of the material. Finally, it is difficult to determine if the Ti-Cl stretch at 495-490 cm^{-1} is present.

ACTIVATION PROCEDURE

In a reactor U-tube reactor, 0.500 grams of titanated(III) silicate platform ($5.43x10^{-1}$ mmol of titanium) was added and connected to a cylinder of reagent grade hydrogen (99.999% pure). The U-tube reactor was then placed in a molten salt bath at 350°C and a hydrogen flow (2mL per sec) was started. The U-

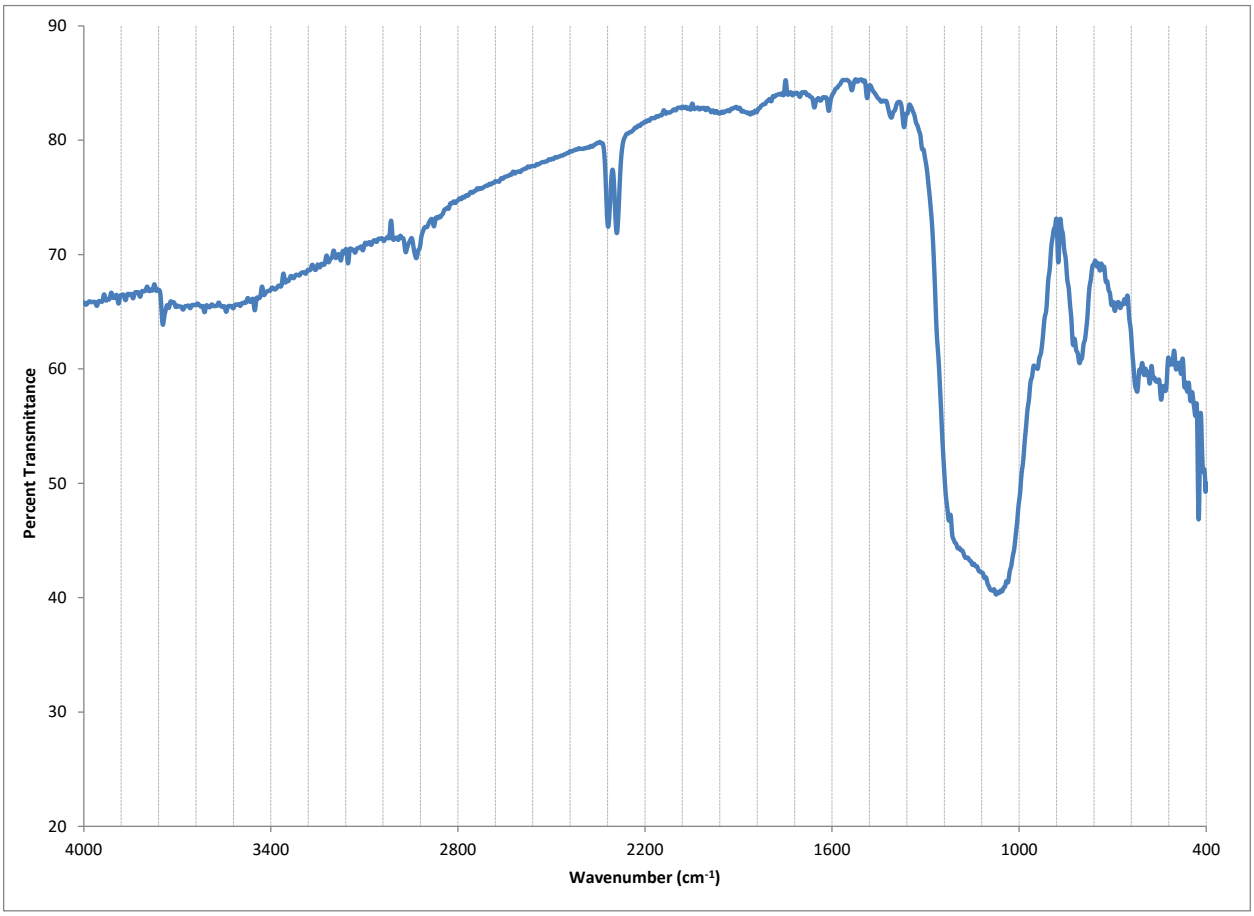

***Figure 59**: The IR spectrum of titanated(III) silicate platform.*

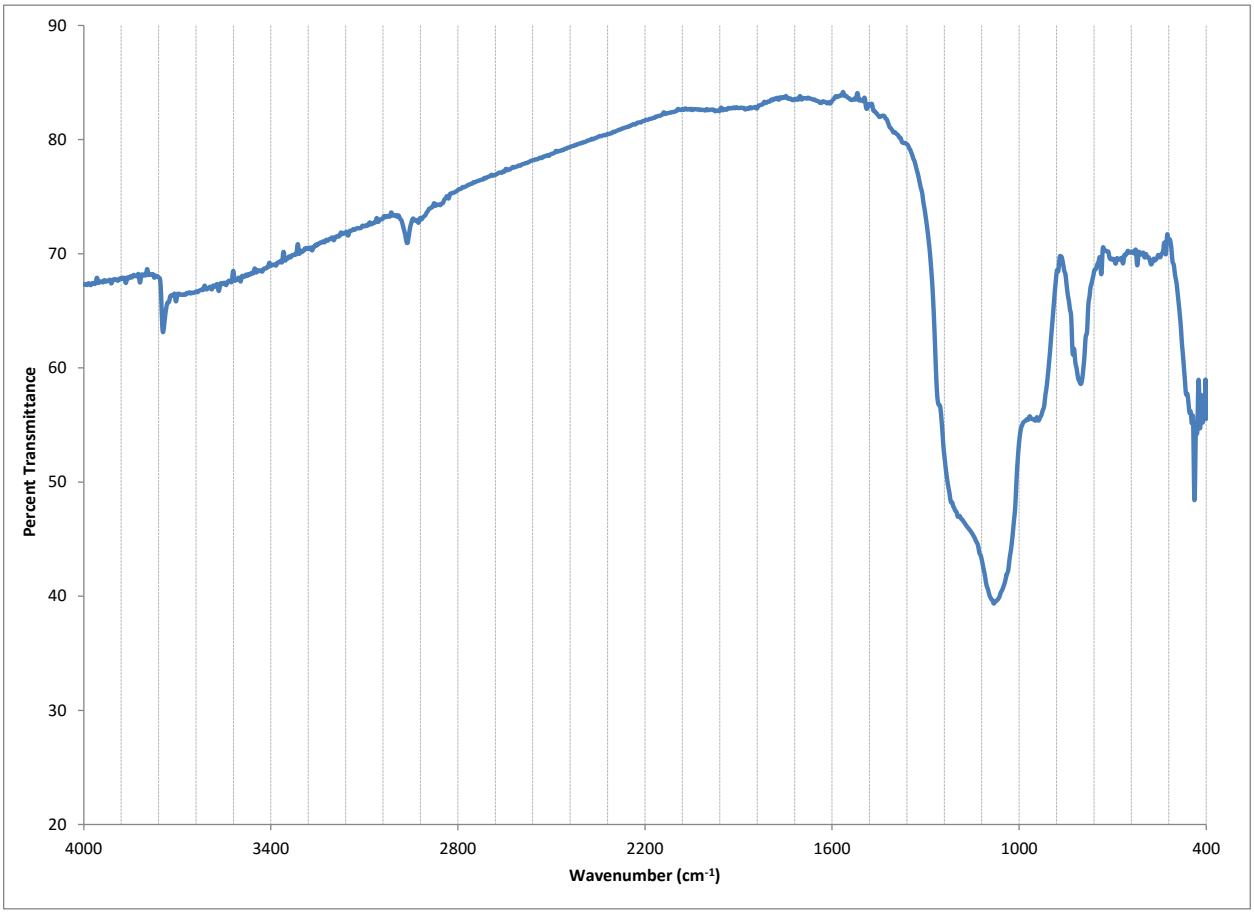

***Figure 60**: The IR spectrum of titanated(III) silicate platform exposed to hydrogen.*

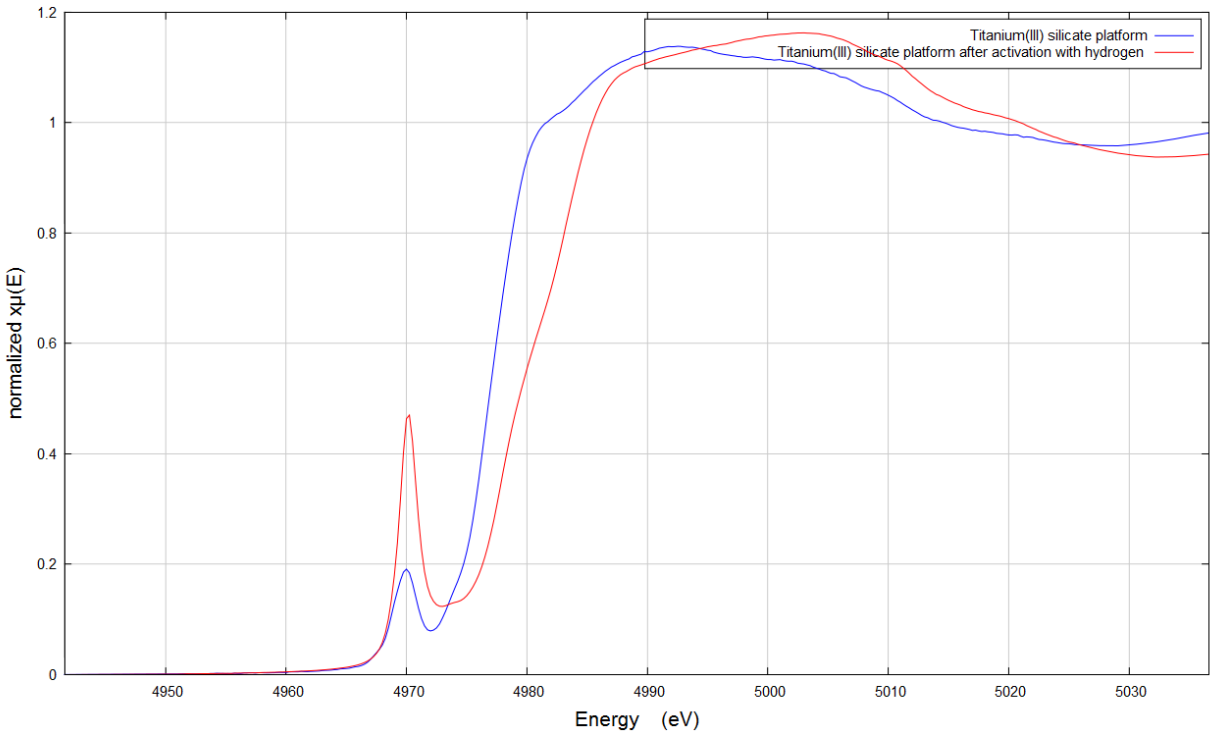

***Figure 61**: Titanium XANES data (K-edge) from titanium(III) silicate platform before and after exposure to hydrogen for activation.*

tube reactor was allowed to continue to react for 4 hours whereupon all volatiles were removed using heat and dynamic vacuum. The resulting fine powder solid was characterized without further purification.

RESULTS AND DISCUSSION

The IR spectra of the titanated(III) silicate platform exposed to hydrogen can be seen in Figure 60. The feature assigned to a bound acetonitrile at 2300 cm^{-1} seen in titanated(III) silicate platform (Figure 59) is not present in the sample activated by hydrogen. Additionally, the IR spectra show no indication of titanium-hydride bands. Finally, the titanium-chloride feature at 490 cm^{-1} is still undetected.

Titanium XANES data (K-edge) from the titanated(III) silicate platform before and after "activation" can be seen in Figure 61. Again, photobleaching was observed in this sample when placed into the X-ray beam and scan one was different from scan two and three. As a result, the data present is from scan one only. The 4977 eV edge position is inconsistent with a titanium(III) site. Additionally, a shoulder is seen on the edge, indicative of a shake-up effect from titanium-chlorine bonds. Finally, a single pre-edge feature with a low intensity of approximately 0.2 can be seen.

Figure 62, displays the EXAFS data from the titanated(III) silicate platform before and after exposure to hydrogen for activation. Two features can be seen for the titanated(III) silicate platform:(1) A feature at 1.30 Å, which is congruent with a titanium-oxygen bond. (2) A feature at 1.90 Å consistent with a titanium-chloride bond. A titanium-nitrogen bond was expected for the bound acetonitrile but was not seen in the data. The titanated(III) silicate platform exposed to hydrogen has an EXAFS spectra similar to that of titanated(IV) silicate platform exposed to hydrogen. The sample has a single feature at 1.45 Å, which is congruent with a titanium-oxygen.

SUMMARY

The goal of this research was to prepare a well-defined supported titanium species that would bind hydrogen reversibly. Some reports of theoretical modeling studies have appeared that describe how titanium atoms could bind significant numbers of hydrogen molecules (six hydrogens per titanium center). Based on these reports we hypothesized that the synthetic methodology developed previously in the Barnes group could be used to easily prepare a one-connected titanium species that approximated what the theoretical studies pointed to as a potential hydrogen binding site. An important difference between this starting point and the theoretical results is the formal oxidation state of the titanium species. Our synthetic methodology easily yielded well-defined, trichloro-titanium sites on a silica platform with the titanium oxidation state formally being +4 (d0) while titanium centers that would bind hydrogen should be in lower formal oxidation states having d electrons at the metal center. This difference was recognized from the outset of this project and our first major goal was to develop a synthetic methodology to reduce our titanium(IV) species on the surface of silica in a controlled fashion, preserving their connectivity to the surface. This proved to be challenging due to a number of reasons: As titanium is reduced, the bonding to the surface is weakened. As a result, the reduced species is more susceptible to leaching, or mobility on the surface that could produce aggregated species. As chloride ligands are removed from titanium, the desired hydride-hydrogen ligands are quite labile and very reactive frequently leading to reduced aggregates. The critical barrier to such reactions is to maintain site isolation of titanium centers on the support. At the start of this work it was understood that the reduction step would be quite difficult to

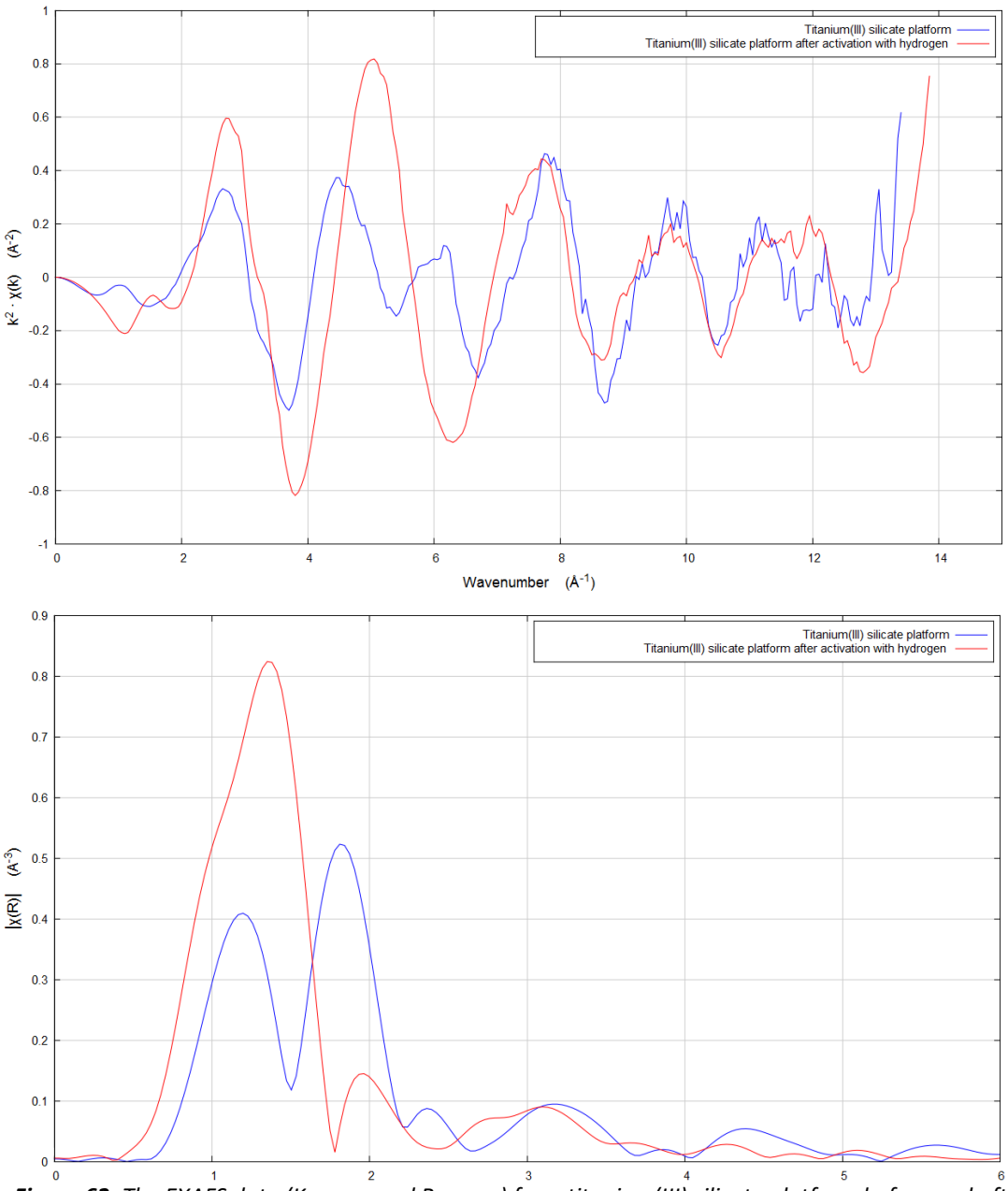

***Figure 62**: The EXAFS data (K-space and R-space) from titanium(III) silicate platform before and after exposure to hydrogen for activation.*

control and characterize. Our reduced titanium species would likely be unstable due to an unsaturated coordination sphere. As a result, the reductions were done under conditions where hydrogen was available to bind, filling the coordination sphere. Furthermore, finding a reducing agent that was strong enough was a concern, as the reduction potential of our surface trichloro-titanium species is not found in literature. We, therefore, used values for the closest analogs that we could find in the literature.

The work described in this chapter uses an empirical approach for finding a suitable reductant. By trial and error, we expected to find a reductant that would reduce our trichloro-titanium species without causing the species to become mobile. An alternative to this trial and error approach would have been to research the reduction potential of similar titanium complexes and base our choice of reductant off this literature. The following paragraphs describe our analysis in terms of reduction potential.

Titanium tetraisopropoxide represents probably the most difficult to reduce surface species that might be encountered in this research and has a reduction potential of -1.35 V.[113] We would expect our trichloro-titanium species to be easier to reduce that titanium tetraisopropoxide, due to fewer alkoxide ligands. Further researching into the literature demonstrates this to be accurate as titanium tetrachloride has a reduction potential of -0.32 V.[114] This 1.00 V difference can be taken as an estimate of the thermodynamical difference need to reduce titanium from +4 to +3 between the all-chloride and all-alkoxide species. When choosing a reductant based on this data, we could assume our surface trichloro titanium species has a reduction potential closer to that of the all-chloro complex. Additionally, to ensure complete reduction any reducing agent should have an over potential of ~200 mV.

The reduction potentials of hydride reducing agents such as lithium aluminum hydride are not usually listed in literature, although they are among the most potent reducing agents. [115] A rough estimate of their reduction potential would be to consider them as just hydrides and use the textbook potential of -2.25 V. [116] The large over potential seen between lithium aluminum hydride and our trichloro titanium species may have unexpected consequence during the reaction.

Samples reduced with lithium aluminum hydride show clear evidence for the titanium species leaching from the matrix during the reductions. This most likely indicates that the reduction step was accomplished by breaking the bond to the surface. The over potential discussed above could be the reason behind leaching. Reduction of titanium(III) to titanium(I) and metal with lithium aluminum hydrides have been described in the literature. Additionally, aluminum(III) is highly oxophilic. As titanium is reduced from +4 to +3 or lower, its oxophilicity is reduced which would facilitate breaking the bond to the surface and subsequent formation of solution species. As a result, the XAS quite possible reflects a mixture of species. Therefore, with this loss of control, we focused our efforts on other methods of the reduction that did not involve any oxophilic elements, such as boron and aluminum that may compete with titanium for surface sites.

Cobaltocene has a reduction of -1.33 mV, approximately half of that of lithium aluminum hydride allowing for a gentler reduction than chemical hydrides.[117] This reduction potential suggests cobaltocene may be an ideal reductant for titanium tetraisopropoxide but again, may have a large over potential compared with our surface trichloro species. Additionally, cobaltocene is a chemical reductant that has no oxophilic elements. The importance of this has been stated above.

It is extremely difficult to draw any conclusions about the oxidation state and coordinated ligands around titanium in these reactions from IR spectroscopic data. What we can observe is that the color change

(purple to green) is consistent with cobaltocene reacting to become cobaltocenium. The counterion of the cobaltocenium complex is unknown, but a chloride species can be easily conjectured. There are two sources of chloride in our sample: 1) the titanium species and 2) inert silicon linkers. With the data at hand, it is unclear which source produced the chloride.

Reactions with hydrogen offer the most direct approach to reducing titanium and obtaining titanium hydrides species. Hydrogen reduction potential is set as the reference (0.00 mV) that all other potentials are correlated to. As a result of hydrogen low reduction potential, reactions with hydrogen were run at high temperatures (300-500°C). High temperatures open up reaction channels involving initial bond fragmentation followed by reduction. It is entirely possible that hydrogen will only reduce our titanium species if enough thermal energy is provided to create hydrogen atoms or breaking Ti-Cl bonds. In addition, the use of hydrogen alone removes the problems of oxophilic elements, like those seen in hydride based reductants.

In our investigation, The samples exposed to hydrogen appear to remain in a high oxidation state (see XAS discussion below) but show the loss of coordinating chloride ligand. These coordinated unsaturated titanium species must be stabilized with alternative ligands that are not observable in XAS. These results are consistent with the presence of hydride ligands around titanium, although they are not visible in the IR spectrum.

Hydrogen alone may not have a reduction potential strong enough to reduce our titanium species, which is not unexpected. An alternative method for reducing our titanium species is the addition of a hydrogen-activating agent that acts as a transfer agent creating an alternate mechanism to produce reduced titanium species. An ideal activating agent would be easier to reduce than our trichloro species and be able to transfer hydride to our trichloro species. The textbook reduction potential of platinum(II) (+1.19) suggests platinum is much easier to reduce that our trichloro species. Additionally, platinum has a long history of being used as a hydride promotor. [109]

The data gathered from samples with high Pt load and exposed to hydrogen cause us to question the effects a platinum promoter has on our trichloro-titanium species. The data suggest that we obtained similar titanium species with and without platinum. It is unclear whether platinum influenced the reaction. The color change of the sample and the change in white line intensity in the platinum XAS are consistent with the reduction of platinum. The exact form platinum takes, nanoparticles or larger metal crystallites, is unclear. While there is good evidence that platinum has been reduced to metal there may be no effective way to transfer activated hydrides from platinum to titanium site, via the silicates support. Literature shows that silicates are very difficult to reduce, making them a very poor conduit for hydrogen atoms.

THE LOSS OF X-RAY ABSORPTION SPECTROSCOPY

Through several attempts were made to collect XAS data, it became apparent that all species discussed here were light (x-ray) sensitive. One possible light-induced decomposition pathway would involve the reoxidation of any reduced titanium species present in the sample. As a result, the oxidation would be quickly followed by the loss of any hydrogen on titanium. Light-induced reoxidation of the titanium centers in the sample could then lead to the conclusion that the reduction was not successful. This was indeed observed in several cases and therefore we were forced to abandon the only technique that could have allowed us to intuit the structures around titanium in these samples. Loss of this characterization

technique makes it much more difficult to understand what happened during the reduction and to identify the final products.

Other techniques could only give hints about the properties of the products of these reactions. IR can only show the presences of Ti-O, Ti-Cl and maybe Ti-H, but generally gives no information about the oxidation state or coordination geometry. Characterization of titanium(III) with EPR is generally only possible at liquid helium temperatures for non-octahedral geometries due to fast relaxation. While available at UTK, this requirement made the use of EPR as a tool to screen large numbers of samples impossible, and therefore, while a few preliminary samples were run at liquid nitrogen temperatures, no signals were observed. [118]

The work described in this chapter uses an empirical approach to evaluate a variety of reductants with a range of reduction potentials for their ability to reduces the surface trichloro species. The majority of the work with these systems has focused on characterizing the titanium species present in the systems to understand their composition. Due to the amorphous nature of our materials and instability of the reduced titanium species, we were unable to obtain a clear understanding of their composition and structure of the products of these reactions. Ultimately, we turned our focus to investigating whether any of the materials demonstrated reproducible chemisorption with molecular hydrogen. We found that none of the materials measured demonstrated chemisorption with hydrogen. These results are consistent with the results from our computational modeling collaboration. Regardless, this work represents a novel system with targeted isolated single sites.

PARALLEL COMPUTATIONAL MODELING

Parallel to the synthetic work discussed above, we collaborated with Dr. Nethika Suraweera, a member of Dr. Keffer's group who specializes in computational modeling of amorphous materials. In this collaboration, our colleagues sought to develop a model from the Si_8O_{20} cube-based matrices that we were preparing. Their models consisted of a volume containing Si_8O_{20} cubes with voids to represent the pores in our matrixes. The Si_8O_{20} cubes were randomly arranged to produce amorphous materials, linked together with oxy-silicon-oxy bridges. On the corners of Si_8O_{20} cube not linked to another cube, resided surface trichloro-silane or trichloro titanium. To help generate accurate models, Dr. Suraweera asked us to synthesize two experimental samples that were designed to be similar to their models. The experimental properties gathered from these samples allowed Dr. Suraweera to alter their models to matching our synthetic work. These titanium(IV) models were to be the first of many, as we planned to study the reduced species after obtaining models that accurately emulated the experimental properties. The synthesis procedures of the two samples are outlined in the following paragraphs:

Synthesis of trimethyltin silicate platform

In a Schlenk reaction vessel, 1.276 g (0.683 mmol) of dry trimethyltin cube, $Si_8O_{12}(OSnMe_3)_8$, was added to 0.582 g (1.773 mmol) of silicon tetrachloride bispyridine, $SiCl_4py_2$ [2.60:1 $SiCl_4py_2/Si_8O_{12}(OSnMe_3)_8$; 1.30:1 Cl/Me_3Sn] followed by the vapor transfer of approximately 30 mL of toluene. The sealed system was left under vacuum and heated at 80°C. A gel forms within 1 hour. The solution was allowed to continue to react for 18 hours whereupon all volatiles were removed using heat and dynamic vacuum. Previous investigations indicated that both trimethyltin chloride and pyridine are quantitatively removed

under these conditions. The resulting fine powder solid was used without further purification. Gravimetric analysis of the reaction indicated, on average, the inert silicon linkages were connected on average to 2.49 silicate cubes and 1.56 trimethyltin group remained per silicate cube. This material represents the unfunctionalized amorphous Si_8O_{20} structure found in our collaborator models. Functionalization of the surface with trichloro-silane or trichloro titanium would allow us to reproduce our collaborator's models.

Surface species treatment

After silicon linkers were incorporated into the Si_8O_{20} based building blocks solid matrix. Toluene was again delivered to the Schlenk vessel followed by $TiCl_4$ or Me_3SiCl via vapor transfer for the second dose treatment. The solution was allowed to react at 80°C for overnight (18h) followed by removal of the solvent and Me3SnCl byproduct under dynamic vacuum and heat (80°C). An off white solid and white solid were obtained, respectively. Gravimetric analysis indicated both samples contained an insignificant number of residual trimethyltin groups (1 Sn: 100 Ti) and the reactions had proceeded as expected.

Characterization

Surface area determinations were performed using data from a Micromeritics ASAP 2020 Surface Area and Porosity Analyzer using nitrogen gas adsorption. The nitrogen isotherms allowed our collaborators to determine density, surface area, and accessible volume, to generate the most accurate models possible. The surface area for trichloro-titanium and TMS surface species were found to 621 m^2/g and 565 m^2/g, respectively. The densities for trichloro-titanium and TMS surface materials were found to be 0.975 g/cm^3 and 0.985 g/cm^3, respectively. Carbon dioxide, methane, and hydrogen isotherms were then completed for comparison with the models.

Computational results on these oxidized models confirmed physisorption as the primary mechanism of interaction for all three gases.[119-121] The maximum gravimetric capacity of CH_4 was found to be 16.9 wt.%, occurring at 300 K and 97 bar and the maximum gravimetric capacity of CO_2 was 50.3 wt.%, occurring at 300 K and 51.6 bar. Both these maxima occurred on non-titanated silicate platform. Hydrogen's maximum gravimetric capacity occurred on a non-titanated silicate platform, as well, with 5.8 wt.% H_2 occurring at 77 K and 89.8 bar. [119] Furthermore, pair correlation functions illustrate that the most favorable adsorption sites for hydrogen are located in front of the faces of the spherosilicate cubes. Finally, it was found that titanium sites in the matrix did not enhance hydrogen storage capacity.[121]

CHAPTER 3: INVESTIGATION OF SINGLE SITE TITANOSILICATE MATERIALS FOR EPOXIDATION

Almost every facet of our daily lives depends on catalysis and its contributions to present day society cannot be overstated. The production of fuels, plastics, chemicals, and pharmaceuticals all rely on catalysis on an industrial scale.[122] This industrial scale demands not only larger scale production but, more importantly, catalysts with superior performance. Traditional heterogeneous catalysts are frequently quite primitive in both function and structure, compared to biological analogs. As a result, there is abundant potential for developing new and better catalysts.

Considering nitrogen fixation as an example, instead of the mild conditions needed for biological nitrogenase, high pressure (>30 MPa) and temperature (>450°C) are required for the industrial equivalent.[123] The catalyst used for industrial nitrogen fixation has not undergone any fundamental changes since its invention in 1918. Nitrogen fixation is a prime example of the importance to develop novel catalysts that are more efficient than current catalysts.

Catalysts play an important role in the petrochemical industry. Catalysts are used in many reactions from cracking of the major components for gasoline production, to reaction design to increase the value of minor components found in crude oil. The majority of crude oil will be transformed by a catalyst before it is consumed by society. Additionally, many of the value added chemicals produced would be quite expensive or nearly impossible to synthesize if it weren't for the petrol-based substrate and an effective catalyst. The desire for new novel catalysts has never been higher. New novel catalysts that are highly active and selective are the key to making the most of our limited petrochemical supply.

Selective oxidation of hydrocarbons to higher value chemical feedstocks represents a significant petrochemical process. Nonetheless, it remains a great challenge to achieve high activity and selectivity in these reactions. One selective oxidation reactions that has attracted tremendous attention in the scientific community due to its industrial importance is olefin epoxidation (Figure 63). Despite successes in homogeneous catalysis, there is a clear demand from industry for better performing heterogeneous materials that catalyze epoxidations with commercially available oxidants such, as H_2O_2 and organic peroxides.[124,125] In response to this, heterogeneous epoxidation remains an active field of research, with new and improved materials being developed over the past decade. However, the syntheses of the catalysts are often costly, and many possess poor selectivity due to a random mixture of active groups with geometries less conducive for catalysis in the solid matrix.[126,127]

The materials presented in this chapter possess many properties desired in a new heterogeneous epoxidation catalyst: (1) 100% of the titanium from each of the precursors is incorporated within the matrices and theoretically turns into an active center. (2) High site homogeneity of titanium centers with targeted connectivity. (3) Site isolation that prohibits titanium dimerization and leaching. (4) Meso-sized pore structures that accommodate large olefins substrates.

In ordered to keep up with ever-increasing needs for new engineered catalysts, new synthetic strategies are needed. The syntheses of these catalysts need to be more targeted and directed. These advanced engineered catalysts need their composition and structure controlled at many different length scales, allowing for the targeted synthesis of active sites with specific, desired characteristics. An approach in which the targeted site is identified initially and then built into the matrix as it is being created is one

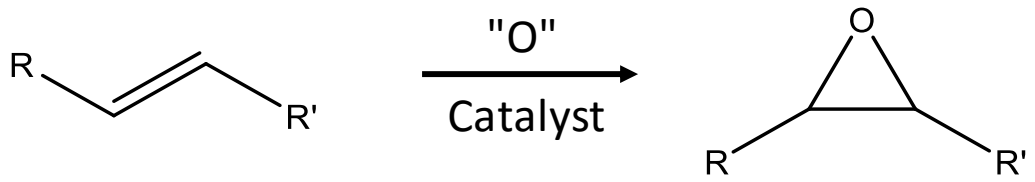

***Figure 63**: Generalized Epoxidation Reaction.*

approach to this idea. This sort of targeted synthesis is still quite difficult and there are relatively few synthetic strategies that can offer this control.

The synthetic methodology discussed in-depth throughout chapter 1 may have the potential to overcome the issues that plague current heterogeneous epoxidation catalysts. By targeting and synthesizing known geometry and connectivities we believe a better understanding of olefin epoxidation can be achieved. Using sequential additions with a building block-based synthetic approach we have been able to synthesize three unique single site titanosilicates (Figure 64). Each of these titanium active sites has a tetrahedral coordination sphere with a targeted connectivity to the surrounding silicate matrix. As discussed in Chapter 1, it is believed that the selectivity and activity of a catalyst is directly related to the number of different active sites within a "catalyst". As a consequence of each active site favoring a different reaction, catalysts with multiple active sites tend to have lower selectivities. Single site catalyst like the ones discussed here should have higher selectivity to their multi-site counterparts.

This chapter describes work, in which the goal was to determine if the family of single sites titanosilicates described above would be an effective catalyst in the epoxidation of olefins. In addition to targeting and synthesizing single-site heterogeneous titanosilicates for epoxidation, establishing a relationship between the structure of titanium sites in a silicate matrix and their catalytic properties is of great importance. Based on previous studies of titanosilicates, it is believed that new approaches, such as the synthetic methodology used here, are necessary in order to target specific active sites in these materials on the atomic level. The synthetic approach developed and described here allows the unique catalytic behaviors of titanium sites with well-defined connectivities to a silicate matrix to be studied and compared. As a result, we would expect a titanium site with four bonds to the matrix to react differently relative to that with only two bonds. As the number of bonds to the surrounding matrix decrease, the site becomes more assessable to substrates. This more open coordination sphere around titanium should contribute to a higher affinity for substrate, creating a catalyst with higher activity. However, as a consequence of lower connectivity, the likelihood of the site leaching from the matrix and becoming homogenous is increased. As a result, this work will focus on titanium sites with at least two connections to the matrix.

The work presented in this chapter is anticipated to increase our understanding of the active site in heterogeneous olefin epoxidation catalysts and be an example of a synthetic methodology that allows one to target and create catalytically active single site within silicate matrixes.

INSTRUMENTATION

The work presented in this chapter relies heavily on the characterization accomplished of Dr. Nan Chen and Dr. Richard Mayes. Both of their dissertations discuss the characterization of single site titanosilicates, generated from the synthetic methodology discussed in-depth in chapter 1. After extensive characterization with X-ray absorption spectroscopy, diffuse reflectance spectroscopy, gravimetric analysis and catalytic studies Dr. Chen and Dr. Mayes establish a relationship between the structure of titanium sites in silicate and their catalytic properties. For the first time, the unique catalytic behaviors of each type of catalyst titanium sites can be studied and compared. The work presented here uses the foundation created by Dr. Chen and Dr. Mayes to further show the advantages of single site engineered

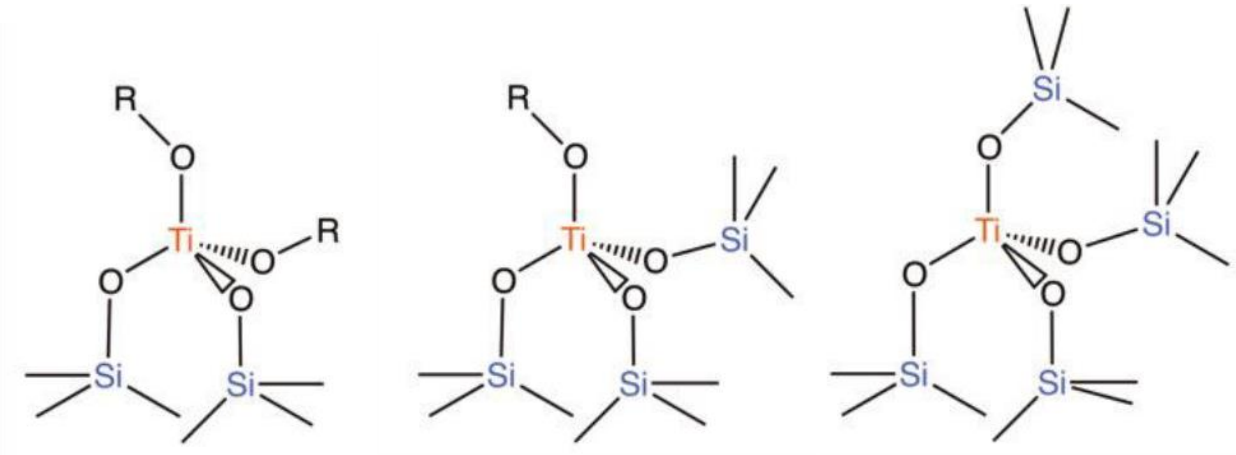

2-Connected **3-Connected** **4-Connected**

***Figure 64**: Titanium centers with different connectivity on silica matrices*

materials using a methodology of building blocks and sequential additions. The changes to their synthetic approach are as follows: 1) Instead for silicon tetrachloride, dimethyldichlorosilane was used for the second cross-linking reaction. This change removed most if not all of any remaining silicon-chloride groups in these matrices that react with protic species to produce hydrogen chloride that may heterogenize the carefully crafted titanium sites. 2) The second cross-linking reaction was allowed to react for 72 hours compared to the 48 hours presented in Dr. Chen's work. The additional time is to account for the lower ratios of chlorine to trimethyltin cube found in the work presented here. It is believed the rate at which the cross-linking proceeds is directly related to the concentration of reactive silicon-chlorides in solution, thus more time is needed to allow the reaction to reach completion. 3) As a result of the change in the second cross-linking agent, the surface of the materials discussed here are air stable. Thus the required methanol passivation found in Dr. Chen's work is not needed for these materials.

GRAVIMETRIC ANALYSIS

The reaction vessel is weighed before and after each reaction and the weight change is used to determine the amount of trimethyltin chloride (Me3SnCl) that is produced during the cross-linking reaction.

INFRARED SPECTROSCOPY

Infrared (IR) spectra were collected using a Thermo Nicolet IR100 in an MBraun LabMaster 130 N2 dry box. 32 scans are collected using 4 cm-1 resolution from 400-4000 cm^{-1} for the background and samples. A KBr pellet is prepared and collected as the background spectrum. A KBr pellet containing sample material (~1-5 wt. %) is prepared and collected as the sample spectrum. The IR is a fingerprint in characterizing our catalysts. Important bond formation and destruction within our matrices may be tracked by IR spectroscopy. Two important stretches are seen between 2800 and 4000 cm-1. First, aliphatic carbon-hydrogen stretches can be observed between 2800 and 3000 cm-1. These features correspond to the methyl units of the trimethyltin, which decrease as trimethyltin chloride is lost during the synthesis. Additionally, evidence of hydrolysis can be seen between 3400 and 3800 cm-1 which can indicate exposure of the sample to air. Between 1000 and 950 cm-1 are the Si-O-Si and Ti-O-Si stretches which are the linking groups between the building blocks in the material. These stretches are important to monitor as they can indicate the decomposition of the sample in the form of leaching of titanium sites or the decomposition of the cube structure. For these reasons infrared spectrometry is a major characterization technique used to gain information about the composition of the materials detailed below.

POROSITY ANALYSIS

Porosity analysis was used to monitor changes in the porosity over the course of synthesis. Nitrogen adsorption-desorption analysis was performed using a Micrometrics ASAP 2020 Physisorption and Chemisorption analyzer. BET surface area was calculated using adsorption data in the relative pressure range from 0.05 to 0.35. The adsorption portion of the nitrogen gas adsorption/desorption isotherms was used to calculate the pore size distribution (BJH method) of the samples.

NUCLEAR MAGNETIC RESONANCE (NMR)

Proton NMR was used for qualitative analysis of catalyst precursors and quantitative analysis of catalytic test reactions. NMR spectra were taken on Varian VNMRS 500 MHz. 16 scan with 10-second delays were used to assure quantitative accuracy. Spectra were worked up on MestreNova V10.0.

ELEMENTAL ANALYSIS

Elemental analysis for titanium was collected using a Perkin Elmer Optima 2100 DV ICP - Optical Emission Spectrometer equipped with a Scott spray chamber. Typically, 25 mg of material was digested/dissolved into approximately 50 mL of solution (~1.5 mL HNO_3, ~1.5 mL HF (50 w/w %) and ~47 mL ultrapure (18MΩ) deionized water). The procedure for sample preparation is as follows. Three sample solutions are analysis for each material. For each solution, an empty 60 mL plastic bottle is weighed. In a glovebox, the appropriate amount of material (~25 mg) is added to the plastic bottle. The exact mass of material added to the plastic bottle must be known. An aliquot of each material is digested in an HNO_3 (~1.5 mL) and HF (~1.5 mL) solution for 2 hours followed by dilution to the appropriate volume (50 mL) using ultrapure deionized water. The amount of water needed for dilution was measured gravimetrically on an analytical balance with the assumption the density of the final solution was approximate 1.00 g/mL, Thus, 50 grams of solution is 50 mL of solution. The data collection procedure is as follows. Emission data for three replicates were collected and averaged for each solution. A series of at least 5 standard solutions are used to construct a calibration curve for each metal being analyzed. Each sample solution is then collected and the concentration of the metal in solution determined using the corresponding calibration curve.

EXPERIMENTAL

Materials: The general procedures for handling the chemicals used in the reactions reported here have previously been described in chapter 1. Several steps were taken to exclude all sources of water from reactants, solvents, and glassware as well as any hydroxyl groups present on glassware used in reactions. All Schlenk reaction vessels were silylated with a chlorotrimethylsilane/triethylamine solution followed by flame drying under vacuum prior to use. Toluene (Fisher Scientific) was dried using sodium-potassium alloy and distilled. Pyridine (Fisher Scientific) was distilled and dried using calcium hydride. Toluene and pyridine were kept in solvent bulbs equipped with high vacuum Teflon® stopcocks with the appropriate drying agent. The solvent bulbs were degassed using freeze-pump-thaw cycles and stored under vacuum prior to use. Trimethyltin cube, $Si_8O_{12}(OSnMe_3)_8$ was synthesized using previously reported procedures.[31] Prior to use, samples of trimethyltin cube was heated overnight at 100°C under vacuum to ensure removal of waters of hydration in the crystal. Titanium tetrachloride ($TiCl_4$, Alfa Aesar, 99.6%), Silicon tetrachloride ($SiCl_4$, Acros, 99.8+%), and dimethyldichlorosilane, ($Si(CH_3)_2Cl_2$ Acros, 99.8+%) were distilled, degassed, and stored under vacuum in Schlenk vessels equipped with Teflon® stopcocks. Titanium tetraisopropoxide ($Ti(OiPr)_4$, Alfa Aesar, 99.6%), was distilled, stored, and added to reaction vessels in a nitrogen atmosphere glove box. All volatile solvents and reagents were delivered into reaction vessels using vapor transfer methods.

Dichlorodiisopropoxytitanium (2-connected precursor): 1.000 g (4.220 mmol) of titanium tetraisopropoxide, $Ti(OiPr)_4$, was added to Schlenk reaction vessel followed by the vapor transfer of approximately 30 mL of pentane with a dry ice/isopropanol bath. Then while stirring and cooling in a dry ice/isopropanol 0.804g (4.220 mmol) bath titanium tetrachloride, $TiCl_4$, was vapor transferred. A yellow precipitance formed during the vapor transfer of titanium tetrachloride. The sealed system was covered from light, warmed to room temperature, and left under vacuum. Upon reaching RT the solution became translucent yellow. The solution was allowed to continue to react for four hours whereupon all volatiles were removed using dynamic vacuum. The resulting fine yellow powder solid was sublimed (60°C) under vacuum for further purification. Proton NMR exhibits two broad singlets at 1.03 and 4.38 ppm. These proton shifts match those found in literature.[128]

Trichloroisopropoxytitanium (3-connected precursor): 0.500 g (2.110 mmol) of titanium tetraisopropoxide, $Ti(OiPr)_4$, was added to Schlenk reaction vessel followed by the vapor transfer of approximately 30 mL of pentane with a dry ice/isopropanol bath. While stirring and cooling in a dry ice/isopropanol 1.201g (6.235 mmol) bath titanium tetrachloride, $TiCl_4$, was vapor transferred. A yellow precipitance formed during the vapor transfer of titanium tetrachloride. The sealed system was covered from light, warmed to room temperature, and left under vacuum. Upon reaching RT the solution became translucent yellow. The solution was allowed to continue to react for four hours whereupon all volatiles were removed using dynamic vacuum. The resulting fine light yellow powder solid was sublimed (60°C) under vacuum for further purification. Proton NMR exhibits a doublet at centered at 0.82 and a septet centered at 4.10 ppm. These proton shifts match those found in literature.[128]

4-connected Embedded tetrahedral titanium silicate: 1.500 g (0.809 mmol) of dry trimethyltin cube, $Si_8O_{12}(OSnMe_3)_8$, was added to Schlenk reaction vessel. followed by the vapor transfer of approximately 30 mL of toluene. 0.092g (0.485 mmol) of titanium tetrachloride, $TiCl_4$, [0.60:1 $TiCl_4$/ $Si_8O_{12}(OSnMe_3)_8$; 0.30:1 Cl/Me_3Sn] was vapor transferred from a capillary. The sealed system was left under vacuum and heated at 80°C. The solution was allowed to react for 18 hours whereupon all volatiles were removed using heat and dynamic vacuum overnight. A white powder remained in the Schlenk. Gravimetric analysis of the reaction indicated on average the titanium atom linkers were connected to 3.96 silicate cubes. The following day approximately 30 mL of toluene was vapor transfer onto the powder. Then from a capillary 0.209 g (1.618 mmol) of dimethyldichlorosilane, $Si(CH_3)_2Cl_2$, was vapor transferred. The sealed system was left under vacuum and heated at 80°C. The solution was allowed to react for 48 hours whereupon all volatiles were removed using heat and dynamic vacuum overnight. The resulting fine powder solid was used without further purification. Gravimetric analysis of the reaction indicated on average the inert silicon linkages were connected to 1.98 silicate cubes. The weight percent titanium was found to be 2.76 wt. % via ICP-OES.

3-connected Embedded tetrahedral titanium silicate: In a Schleck reaction vessel, 1.500 g (0.809 mmol) of dry trimethyltin cube, $Si_8O_{12}(OSnMe_3)_8$, was added to 0.147 g (0.687 mmol) of Trichloroisopropoxytitanium, $TiCl_3(OiPr)$, [0.85:1 $TiCl_3(OiPr)$/ $Si_8O_{12}(OSnMe_3)_8$; 0.32:1 Cl/Me_3Sn] followed by the vapor transfer of approximately 30 mL of toluene. The sealed system was left under vacuum and heated at 80°C. The solution was allowed to react for 18 hours whereupon all volatiles were removed using heat and dynamic vacuum overnight. A white powder remained in the Schlenk vessel. Gravimetric analysis of the reaction indicated on average the inert titanium linkages were connected to 2.99 silicate cubes. The following day approximately 30 mL of toluene was vapor transfer onto the powder. Then from a capillary 0.209 g (1.618 mmol) of dimethyldichlorosilane, $Si(CH_3)_2Cl_2$, was vapor transferred. The sealed system was left under vacuum and heated at 80°C. The solution was allowed to continue to react for 48 hours whereupon all volatiles were removed using heat and dynamic vacuum overnight. The resulting fine powder solid was used without further purification. Gravimetric analysis of the reaction indicated on average the inert silicon linkages were connected to 1.94 silicate cubes. The weight percent titanium was found to be 4.68 wt. % via ICP-OES.

2-connected Embedded tetrahedral titanium silicate: In a Schlenk reaction vessel, 1.500 g (0.809 mmol) of dry trimethyltin cube, $Si_8O_{12}(OSnMe_3)_8$, was added to 0.287 g (1.213 mmol) of Dichlorodiisopropoxytitanium, $TiCl_2(OiPr)_2$, [1.50:1 $TiCl_2(OiPr)_2$/ $Si_8O_{12}(OSnMe_3)_8$; 0.37:1 Cl/Me_3Sn] followed by the vapor transfer of approximately 30 mL of toluene. The sealed system was left under vacuum and heated at 80°C and allowed to react for 18 hours whereupon all volatiles were removed using

heat and dynamic vacuum overnight. A white powder remained in the Schlenk. Gravimetric analysis of the reaction indicated on average the inert titanium linkages were connected to 2.01 silicate cubes. The following day approximately 30 mL of toluene was vapor transfer onto the powder. Then from a capillary 0.209 g (1.618 mmol) of dimethyldichlorosilane, $Si(CH_3)_2Cl_2$, was vapor transferred. The sealed system was left under vacuum and heated at 80°C. The solution was allowed to continue to react for 48 hours whereupon all volatiles were removed using heat and dynamic vacuum overnight. The resulting fine powder solid was used without further purification. Gravimetric analysis of the reaction indicated on average the inert silicon linkages were connected to 1.97 silicate cubes. The weight percent titanium was found to be via 6.83 wt. % ICP-OES.

Embedded silicon silicate: 1.500 g (0.809 mmol) of dry trimethyltin cube, $Si_8O_{12}(OSnMe_3)_8$, was added to Schlenk reaction vessel. followed by the vapor transfer of approximately 30 mL of toluene. Then from a capillary 0.082g (0.485 mmol) of silicon tetrachloride, $SiCl_4$, [0.60:1 $SiCl_4/Si_8O_{12}(OSnMe_3)_8$; 0.30:1 Cl/Me_3Sn] was vapor transferred. The sealed system was left under vacuum and heated at 80°C. The solution was allowed to react for 18 hours whereupon all volatiles were removed using heat and dynamic vacuum overnight. A white powder remained in the Schlenk. Gravimetric analysis of the reaction indicated on average the inert titanium linkages were connected to 3.99 silicate cubes. The following day approximately 30 mL of toluene was vapor transfer onto the powder. Then from a capillary 0.209 g (1.618 mmol) of dimethyldichlorosilane, $Si(CH_3)_2Cl_2$, was vapor transferred. The sealed system was left under vacuum and heated at 80°C. The solution was allowed to continue to react for 48 hours whereupon all volatiles were removed using heat and dynamic vacuum overnight. The resulting fine powder solid was used without further purification. Gravimetric analysis of the reaction indicated on average the inert silicon linkages were connected to 1.93 silicate cubes.

Grafted (G) Ti-MCM-41: 0.594g (0.002 mol) of titanium isopropoxide, $Ti(OiPr)_4$, was added to Schlenk reaction vessel. Followed by the vapor transfer of approximately 30 mL of pentane. Then approximately 2.000 grams of dry MCM-41 (ACS Materials) was added to the Schlenk. The reaction was stirred at RT for 18 hours whereupon all volatiles were removed using heat and dynamic vacuum. A white powder remained in the Schlenk. The white powder was removed from the Schlenk and placed into a crucible and heated to 580°C for 18 hours. The resulting fine white powder was used without further purification. The weight percent titanium was found to be via 4.45 wt. % ICP-OES

TS-1: 1730 µL of 1.0 M aqueous solution of tetrapropylammonium hydroxide, TPAOH, was added to the mixture of 3.00 g (0.0144 mol) tetraethyl orthosilicate $Si(OEt)_4$, in isopropanol (4 mL) and water (11 mL). Subsequently, a solution of 0.351g (1.728 x 10-3 mol) titanium butoxide $Ti(OBu)_4$ in dry isopropanol (~15 mL) was added under vigorous mixing. The solution had the approximate ratios: 25 $Si(OEt)_4$: 0.25 $Ti(OBu)_4$: 3 TPAOH : 1000 H_2O. The resulting clear solution was stirred and heated to approximately 60°C for 1 hour. The resulting sol (clear solution) was heated to 80°C and stirred for 4 hours. A titanium-silicate gel was obtained. The gel was transferred into a Teflon-lined autoclave and crystallization was carried out for 14 days at 170°C. The white solid was washed with deionized water and dried at 120°C overnight. Following the drying, the white solid was calcined at 500°C for 16 hours. The weight percent titanium was found to be via 1.72 wt. % ICP-OES

CHARACTERIZATION OF SINGLE SITE CATALYSTS

As stated previously, this chapter relies heavily on the prior characterization of single site titanosilicate, synthesized using the methodology discussed in-depth in chapter 1. X-ray absorption spectroscopy,

diffuse reflectance spectroscopy, gravimetric analysis and catalytic studies of "identical" single site titanosilicates have established a relationship between the structure of titanium sites in silicate and their catalytic properties. As a result of the extensive characterization of a catalyst's physical properties, this work will only summarize the physical properties, and focus more on understanding their catalytic activities.

Figure 65 shows the IR spectrum for the 4-connected embedded titanium centers. These materials were synthesized under non-aqueous aprotic conditions which results in the production of a hydroxyl- free surface. As expected no evidence for the presence of silanol groups (3600-4000 cm^{-1}) is observed in the IR spectrum. IR spectroscopy is again used to verify the Ti-O-Si linkage remained intact throughout the second cross-linking reaction. Both the Si-O-Si band (1080 cm^{-1}) and the Ti-O-Si shoulder (~960 cm^{-1}) were observed in the IR spectrum. The IR is consistent with the continued presence of Ti-O-Si groups in the matrix thus the Ti-O-Si linkage was not disrupted during the cross-linking reaction with Me_2SiCl_2. The IR spectra of both the 3-connected and 2-connected embedded titanium centers are virtually identical to that of 4-connected embedded titanium centers.

CATALYTIC TEST REACTIONS

As important as the characterization of a catalyst's physical properties is, it is meaningless if the material is incapable of acting as a catalyst. For this reason, every research program focused on catalytic test reactions in parallel with more classic characterization methods. These test reactions attempt to define important quantities that can be used to determine the effectiveness of a catalyst.

Activity is a measure of the amount of substrate that is converted during the reaction over a specified time interval. Percent conversion is sometimes considered an appropriate measure of activity. However, percent conversion data generally does not take into account the number of active sites present in the catalyst. As a result, these numbers can be easily manipulated by simply adding more catalyst, decreasing the concentration of substrate, or changing the temperature and time. Consequently, the observation of increased conversion does not necessarily mean a catalyst is more active. More accurate measures of activity are turnover number and turnover frequency. Turnover number, TON, (Equation 19) measures the number of substrate molecules converted per active site. Turnover frequency, TOF, (Equation 20) quantifies the activity of a catalytic site occurring at the site per unit time. At early time points where concentrations are not changing quickly, TOF can be an accurate representation of the rate of reaction whereas, at later time points, TOF becomes a more averaged value due to the changes in concentrations. TOF present here will be at two minutes. In addition to determining conversion, researchers must be able to quantify the number of active sites in a sample of the material in order to determine turnover numbers and turnover frequency. Counting the number of active sites in a heterogeneous catalyst can present a number of challenges which is the reason that many catalysis studies still only report percent conversions.

$$\boldsymbol{TurnOver\ Number} = \frac{\Delta\ moles\ of\ product}{moles\ of\ catalytic\ sites} \qquad \text{Eq. 19}$$

$$\boldsymbol{TurnOver\ Frequency} = \frac{turnover\ number}{\Delta\ time} \qquad \text{Eq. 30}$$

Selectivity measures how well a catalyst produces a specific product relative to all of the products of a reaction. Selectivity is generally represented as the percent yield of a specific product relative to the

***Figure 65**: IR spectrum for the 4-connected embedded titanium centers*

stoichiometric yield from the substrate. Selectivity is a property of great importance in industry because high selectivity means the yield of a desired product will be high and there will be less cost associated with the separation from unwanted byproducts. Single site catalysts are widely considered to have higher selectivity than their multi-site counterparts. This is justified by the concept that each individual type of site is will exhibit a unique reactivity and potentially a different product. Therefore, fewer types of sites should give rise to higher selectivity by a catalytic material. Selectivity is easy to determine as long as researchers can detect and quantify the products of a reaction.

As discussed previously one selective oxidation reaction that has attracted tremendous attention in the scientific community due to its industrial importance is olefin epoxidation. The test substrate of choice for epoxidation tends to be small, relatively stable olefins. Many previous studies have had great success with the epoxidation of cyclohexene with a variety of oxidants.[129,130] Other studies have indicated that the selection of solvents plays a critical role in the activity and selectivity of the epoxidation. As a result of these published works, our studies will investigate the epoxidation of cyclohexene with cumene hydroperoxide in a solution of decane. A generalized chemical equation can be seen in Figure 66.

The catalysis runs were performed on a Fisher Sci stirring and heating hotplate. An aluminum block with milled cavities designed to fit the reaction vial was submerged in a silicon oil. Temperature of the oil was monitored via a K-type thermocouple. The tip was submerged into a well within the aluminum block. The thermocouple reader could be read to ± 0.1°C. The temperature change over the course of a catalysis run was no more than ±0.5°C. Time was monitored on a Fisher Sci Triple-Display Timer, allowing multiple time points to be set and monitored. Figure 67 displays the catalytic run setup.

CATALYTIC PROTOCOL

An empty vial with a 10 mm stir bar and septa cap was tared. The vial was then taken into a glove box and approximately 50 mg of catalyst was added. The vial with catalyst was then weighed to determine the exact amount of catalyst. The approximate volume of decane need to create a 0.006 M titanium solution was added to the vial. Calculations were accomplished to determine the volumes needed to obtain the mole ratio of 1 : 25 : 250, Ti : Cyclohexene : Cumene hydroperoxide in the final reaction mixture. All amounts were dependent on the actual amount and titanium wt.% of catalyst weighed into the vial. After the addition of decane, 261 µL of mesitylene (Internal Standard) via a calibrated Wheaton™ Socorex Acura™ 835 Pipet and the calculated volume of cyclohexene were added to the vial. The vial was then put into an oil bath at 40°C. The calculated volume of cumene hydroperoxide was placed into a second vial in the oil bath. Both vials were allowed to come to temperature equilibrium for 20 minutes. After the vials reached temperature equilibrium, the cumene hydroperoxide vial was removed from the oil, wiped with a paper towel and poured into the vial with catalyst, cyclohexene, decane, and mesitylene. The total volume of the reaction varied between three to seven milliliters depending on the wt. % and the total mass of catalyst used. The reaction was allowed to stir for approximately 2 seconds (the time it takes to get a homogeneous mixture) at which point a 50 µL aliquot was removed and placed into an NMR tube. Once the aliquot was removed the septa cap was placed back onto the vial. To the NMR tube with the reaction aliquot, 600 µL of deuterated chloroform was added. The NMR tube was then placed into liquid nitrogen to halt the reaction. Additional aliquots were taken at 2, 5, 10, 30, 60, 120 minutes after the addition of the cumene hydroperoxide.

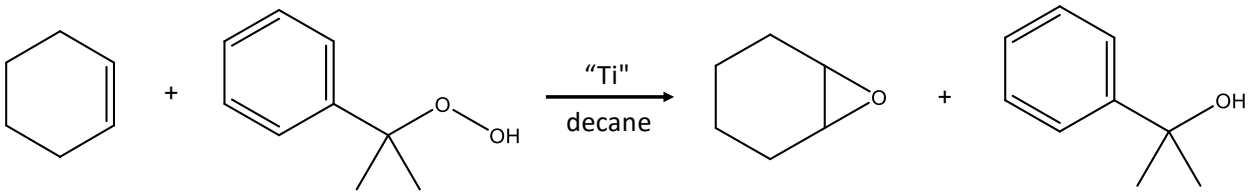

Figure 66: *Generalized epoxidation of cyclohexene with cumene hydroperoxide catalyzed by titanium.*

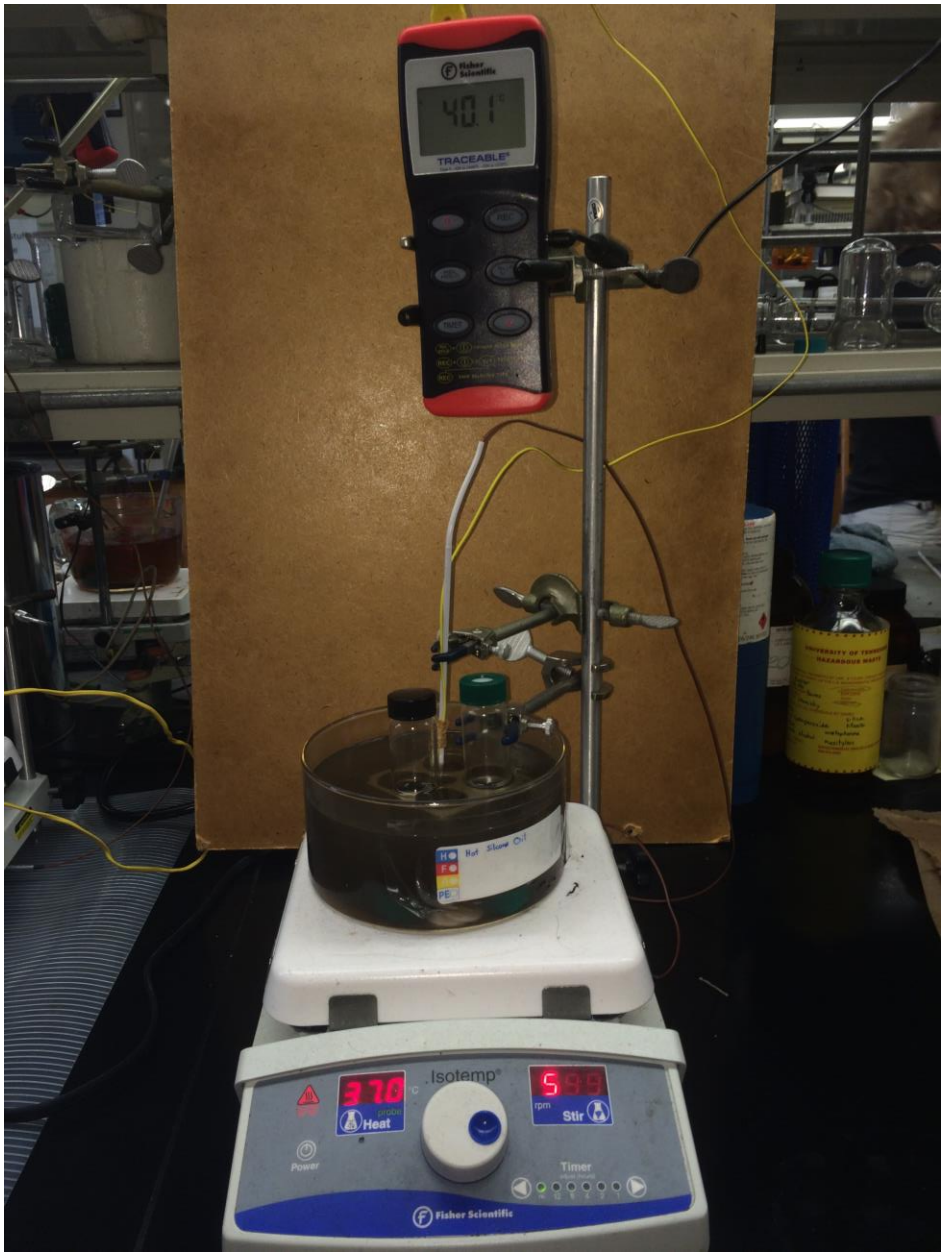

***Figure 67**: Image of catalytic test reaction set-up*

CHARACTERIZATION OF ALIQUOTS

Proton NMR spectra of each aliquot were taken on Varian VNMRS 500 MHz. 16 scan with 10-second delays were used to assure quantitative accuracy. MestreNova V10.2 was used to work up spectra. Each spectrum was manually phased, baseline corrected (Whittaker smoother filter-5.0, 0.61 Hz) and line broadened (0.5 Hz) before integrated. Integration regions were as follows: mesitylene 6.75-6.90 ppm, cyclohexene 5.64-5.735 ppm, cyclohexene oxide 3.10-3.16 ppm, cumene hydroperoxide 1.609-1.66 ppm, and cumene alcohol 1.585-1.608 ppm. An example NMR from an aliquot can be seen in Figure 68. From the data collected a plot showing the mole fraction at each time point can be generated. An example of this plot can be seen in Figure 69.

RESULTS & DISCUSSION:

The results of the epoxidation of cyclohexene with cumene hydroperoxide catalyzed with titanosilicates are summarized in Table 6.

The results from the embedded silicon silicate sample demonstrate that the epoxidation of cyclohexene does not occur without a titanium-containing catalyst. No conversion is observed for the embedded silicon silicate, a titanium-free analog that shares similar mesoporous structures with our targeted connectivity titanium catalysts. In contrast, all titanium containing catalysts exhibit considerable activity for the epoxidation of cyclohexene. Therefore, the lack of catalytic activity in the comparison reactions demonstrates that titanium atoms in the matrices are the only active centers in this reaction.

Different catalytic activities and selectivities were observed for our single site titanium catalysts. Under the same reaction conditions, 2-connected titanium silicate shows significantly higher conversion toward cyclohexene oxide than 3-connected and 4-connected titanium silicate. Additionally, all our single site titanium catalysts show significantly higher selectivity than currently commercially used catalysts ((G)Ti-MCM-41 and TS-1). The data indicates that our 2-connected titanium silicate is twice as fast as our 3-connected and three times as fast as (G)Ti-MCM-41 and our 4-connected. Finally, significant differences in TOF's can be observed for each of our single site titanium catalysts.

The structural differences between our single site titanium catalysts may explain the different TOFs. Given that all catalysts in this work are made up of similar building block matrices, the different accessibility of titanium sites is believed to play a key role in the catalytic activity. Compared to 3-connected and 4-connected titanium silicate, fewer silicon atoms are present around the titanium centers in 2-connected titanium silicate. The higher connectivity in 3-connected and 4-connected may result in steric hindrance, and as a result, less accessible titanium centers. In Figure 70, 4-connected tetrahedral embedded titanium site is shown. In most proposed mechanisms for epoxidation, an initial step involves coordination of a peroxide with the simultaneous breaking of a Si-O-Ti link to silicate support. From both a steric and electronic perspectives this is potentially a high energy step and as a result, may limit the effectiveness and efficiency of our 4-connected titanium silicate consistent with its reactivity being the lowest among the new catalysts tested. Furthermore, to coordinate peroxide or substrate may also require significant movement of the titanium atom with respect to the cage of Ti-O-Si bonds that surrounds it. We would expect significantly lower energy barriers for both 3-connected and 2-connected relative to 4-connected titanium catalyst for the same reasons.

(G)Ti-MCM-41 and TS-1, both well-known heterogeneous epoxidation catalysts, were also investigated in the epoxidation of cyclohexene and the catalytic properties compared with those reported above. As

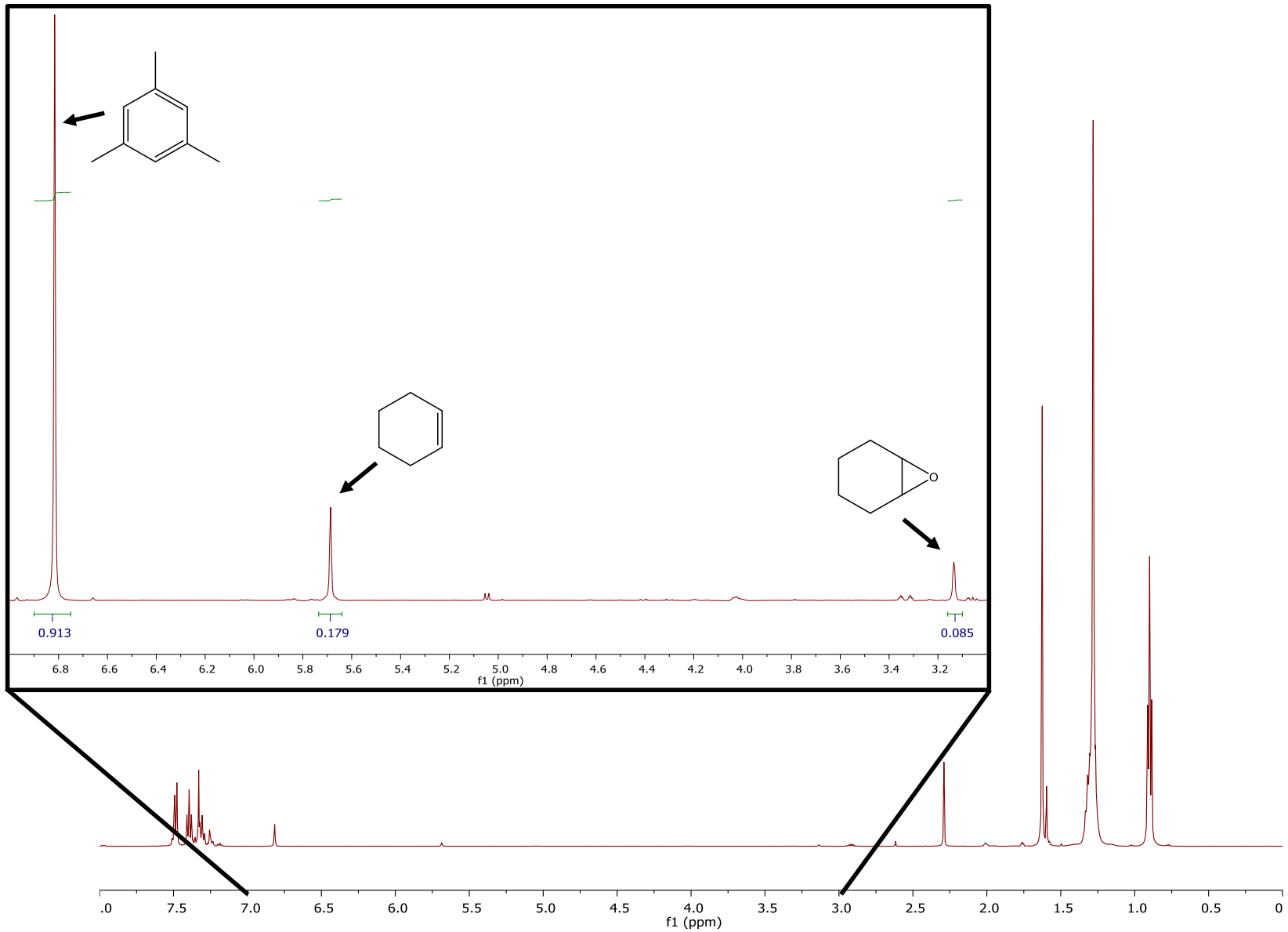

Figure 68: *An example NMR spectrum from an aliquot of the catalytic test reaction.*

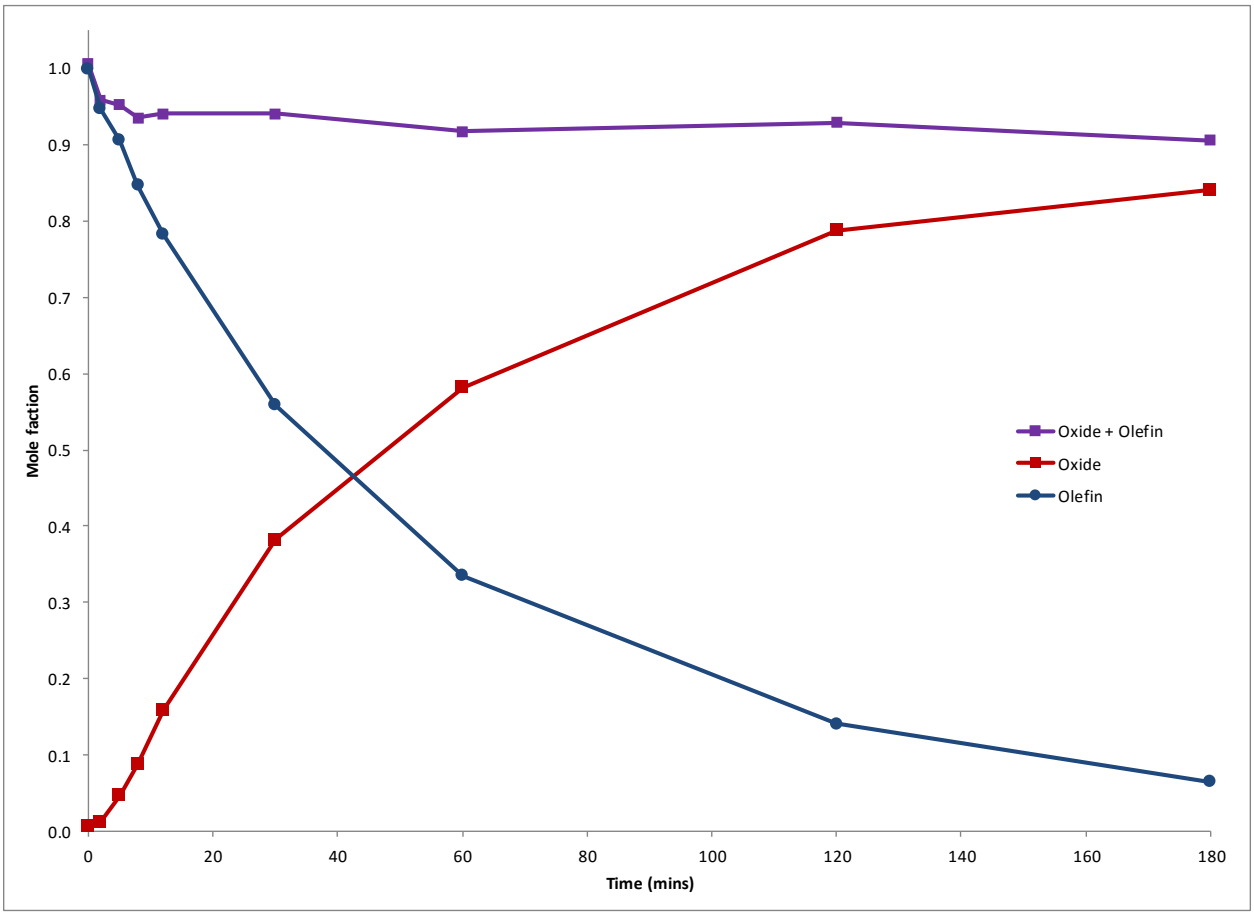

Figure 69: *An example mole fraction plot generated from the quantitative NMR data collected from the catalytic test reaction.*

Table 6: *Results of catalytic properties in the epoxidation of cyclohexene to cyclohexene oxide.*

Catalyst	Initial TOF (2 mins)	% Conversion at 2h ±4.0 (avg.)	Selectivity at 2h ±4.0 (avg.)
(G)-Ti-MCM-41	0.45	28.33, 36.4, 26.77 (30.50)	(74.66)
TS-1	0.09	1.25, 0.75, 1.87 (1.29)	(25.00)
4-Connected	0.28	27.35, 28.67, 27.47 (27.83)	(100.00)
3-Connected	0.38	39.81, 38.72, 39.34 (39.29)	(100.00)
2-Connected	0.47	91.13, 91.74, 93.19 (92.02)	(100.00)

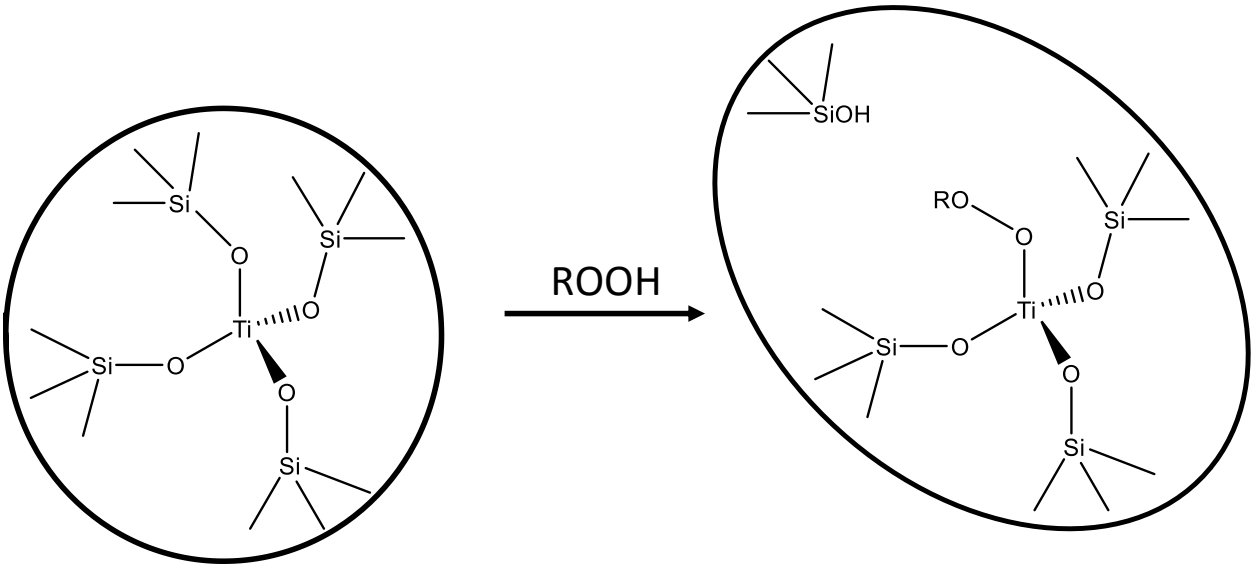

***Figure 70**: A 4-connected tetrahedral embedded titanium site reacting with a peroxide.*

described in chapter 1, TS-1 is a crystalline zeolite titanosilicates with relatively small pores (<1.5nm). (G)Ti-MCM-41 was prepared by grafting a titanium precursor onto surface silanol groups and then calcining. MCM-41 is an amorphous mesoporous matrix with pores large enough to accept a wide range of substrates. Unfortunately, through both the grafting and calcining steps of the synthesis all control of the site connectivity is lost and even polynuclear titanium sites are possible.

The conversion and selectivity of cyclohexene by TS-1 are both very low. The poor catalytic performance of TS-1 is expected because of the small micro-pore that prohibits the diffusion of bulky substrates such as cyclohexene to the titanium sites. Ultimately, the activity seen by TS-1 can be accounted for by the limited number of "surface" titanium species that cyclohexene can diffuse too. (G)Ti-MCM-41 exhibits mediocre conversion and selectivity, similar to that of our 3-connected titanium silicate. The catalytic behavior is likely to result from the local environment around titanium, possibly a mixture of multiple types of titanium centers with different connectivities to the silicate surface.

STABILITY

A component of catalytic test reactions involving heterogeneous catalysts that is less frequently studied is stability. The apparent reactivity of a catalyst frequently can decline over the course of a run due to several factors. Important pathways by which catalyst deactivate are leaching, active site decomposition, or blocking access to the active site. Leaching studies arguably provide information that is more critical in the determination of the effectiveness and longevity of a heterogeneous catalyst than activity and selectivity. The ideal case is that the active sites do not leave the support surface to become potentially soluble homogeneous active sites. If leaching does not occur, then the observed catalysis is truly heterogeneous in nature. However, if the components of the active sites of a heterogeneous catalyst leach during reaction one can envisage three different consequences: (1) the leached species is an active homogeneous catalyst and the apparent activity of the catalyst system is not an accurate measure of the sites initially present. (2) The leached species is an inactive homogeneous catalyst and the apparent activity of the catalyst system decreases. (3) The leached species produces undesired byproducts, reducing the selectivity of the overall reaction.

A modified activity protocol was used to investigate the stability of our catalysts. The catalyst of interest was placed in the same condition as our activity protocol and allowed to react for 20 minutes (2C - 15.3%, 3C - 6.7%, 4C - 3.9%, and (G)Ti-MCM-41 - 5.1%). At that point, the reaction mixture was filtered and aliquots were taken to monitor the progress of the reaction without the heterogeneous catalyst. If the reaction solution continued to produce cyclohexene oxide after filtration, this would suggest an active homogenous species exists within the solution. Thus we could conclude the catalyst leaches. If after filtration the production of cyclohexene oxide is terminated this suggest two results: 1) no leaching has occurred. 2) Titanium has leached from our substrate, but has become an inactive homogenous species. To determine the amount of homogeneous titanium in solution, the residue from the solution was analyzed by ICP-OES spectroscopy after calcination. The following paragraphs detail our work to understanding the stability of our single site catalysts and the (G)Ti-MCM-41 we synthesized.

PROTOCOL:

An empty vial with a 10 mm stir bar and septa cap was tared. The vial was then taken into a glove box and approximately 50 mg of catalyst was added. The vial with catalyst was then weighed to determine the exact amount of catalyst. The approximate volume of decane need to create a 0.006 M titanium solution was added to the vial. Calculations to determine the volumes needed to have the mole ratio of 1 : 25 :

250, titanium : cyclohexene : cumene hydroperoxide. After the addition of decane, 261 µL of mesitylene (Internal Standard) via a calibrated Wheaton™ Socorex Acura™ 835 Pipet and the calculated volume of cyclohexene were added to the vial. The vial was then placed in an oil bath at 40°C. The calculated volume of cumene hydroperoxide was placed into a second vial in the oil bath. Both vials were allowed to come to temperature equilibrium for 20 minutes. After the vials reached temperature equilibrium, the cumene hydroperoxide vial was removed from the oil, wiped with a paper towel and poured into the vial with catalyst, cyclohexene, decane, and mesitylene. The reaction was allowed to stir for 20 minutes at which point the entire reaction solution was sucked into a 12 mL syringe. A 0.3-micron filter was placed onto the tip of the syringe and the reaction solution was forced through the filter into a clean vial. At this point, a 50 µL aliquot was removed and placed into an NMR tube. The septa cap was placed back onto the vial and the vial was placed back into the oil bath at 40°C. To the NMR tube with the reaction aliquot, 600 µL of deuterated chloroform was added. The NMR tube was then placed into liquid nitrogen to halt the reaction. Additional aliquots were taken at 20 and 60 minutes from the addition of the cumene hydroperoxide. Characterization of aliquots follows the protocol outlined above.

RESULTS & DISCUSSION:

The results of the leaching study are summarized in Table 7. Within the hour after the removal of the solid catalyst, little to no change in cyclohexene oxide concentration was seen for all titanosilicates catalyst. This result suggest that all active titanium species are truly heterogeneous and if any titanium leaches into the solution, it became inactive. ICP-OES analysis of the mother liquor indicated no detectable amounts of titanium to be present.

SUMMARY:

Single site titanium silicates with unique connectivities have been synthesized and tested for the epoxidation of cyclohexene to cyclohexene oxide with cumene hydroperoxide. High conversion and selectivity were observed for all single site titanium silicates. Under the reaction conditions investigated, 2-connected exhibit distinctly higher activity (turnover frequency) than that of 3-connected, 4-connected and commercially used catalysts ((G)Ti-MCM-41 and TS-1). The data indicates that our 2-connected titanium silicate is twice as fast as our 3-connected and three times as fast as (G)Ti-MCM-41 and our 4-connected. Turnover frequencies (TOFs) for the different connectivities are in the sequence of 2-connected > 3-connected > 4-connected. All single site titanium silicates exhibited significantly higher selectivity than commercially used catalysts. Additionally, the stability of the catalysts was investigated by removal of any “solid” catalyst. Proton NMR of the mother liquor indicates little to no change in cyclohexene oxide concentration occurs after the removal of any heterogeneous catalyst. These results are consistent with all active titanium species remain bound to the silicate support and if any titanium leaches into the solution, it becomes inactive. Additionally, elemental analysis of the mother liquor indicated no detectable amounts of titanium.

The results described here represent only a small fraction of the work needed to completely characterize the catalytic activity if these single site titanium silicates. Furthermore, investigation continue on these single sites catalyst by others members in the group.

Catalytic test reaction with a variety of substrates would help strengthen the argument that our catalysts are superior to current commercially available ones. In addition to cyclohexene, 1-hexene and styrene are commonly used as comparative substrates in the literature.[131-133] It is important that we study the

***Table 7**: Results of the leaching study in the epoxidation of cyclohexene to cyclohexene oxide.*

Catalyst	Percent conversion after filtration	Percent conversion after 1 hours	Percent change
(G)Ti-MCM-41	5.10	5.06	0.83
4-Connected	3.81	3.71	2.5
3-Connected	6.57	6.62	0.78
2-Connected	15.33	15.47	0.89

reaction of these substrates with our catalysts before publishing and conclude our work with these titanosilicates.

Probing the sterics and electronic properties of these single site catalyst may offer a better understanding of the properties of titanium sites in silicates. Linear alkenes with internal double bonds such as 3-hexane would allow one to study the sterics properties of an active site. As an active site becomes more embedded in silicate, we would expect that its sterics would increase and therefore reaction with sterically hindered substrates would slow or even halt. A series of test reactions with 1-hexene, 2-hexene and 3-hexene would allow us to establish a relationship between the structure of titanium site in silicate and the sterics aossicated with the site. As substituents become coordinated to an olefin the electron density of said olefin increase, as a result we expect that a tertiary olefin would react faster than a secondary and a primary. a series of test reaction with cyclohexene, 1 methlycyclohexene and 1,2 dimethlycyclohexene would allow us to probe the electronics and sterics of these single sites catalyst.

Replacing cumene hydroperoxide with aqueous hydrogen peroxide would allow one to study these catalysts in a more industrial form factor, as aqueous hydrogen peroxide is the preferred industrial oxidant. We hypothesize these conditions would increase the vulnerability of the active sites to leaching and therefore it would be important to continue our elemental analysis of the solution to verify that our active sites remain within the silicate matrix. Additionally, we would expect the probabilities of the diol byproduct to increase, as the epoxide may react with water.[133]

Developing a quantitative protocol for analyzing the solid material for both continuous activity (reusability) and titanium content would be valuable. The work presented here doesn't discuss the activity of the catalyst once used. Currently, it is unknown if that these catalysts survive more than one catalytic batch cycle. It is imperative that we test recycled catalysts multiple times to develop an understanding of the robustness and activity of these catalysts. Furthermore, the work presented here doesn't discuss the titanium content of the used catalyst. If the catalyst does not leach the weight percent of titanium in the catalyst will be the same (within ICP error) before and after use.

It has been stated in the literature that the solvent used during the epoxidation has a strong impact on the activity and selectivity of the reaction.[131] Moving from decane to a more polar solvent like acetonitrile may alter the activity and selectivity observed. It is important that we study the effects of solvent polarity with our catalysts before publishing and conclude our work with these titanosilicates.

The amorphous porous structure seen in these materials may limit the variety of substrates suitable for epoxidation with these catalysts. Since these catalysts were created without any form of templating agent, the pore structure can narrow at points creating "choke points" that can block substrate from reaching active sites. Studying the epoxidation of larger, more rigid alkene (such as cyclooctene) would help Identify if this would be a limitation of these materials. If, under the same condition, large changes in activity between cyclodecene, cyclooctene, and cyclohexene were seen, we could conclude that access to some active sites were blocked and the porosity is limiting the effectiveness of the materials. Alternatively, adding a templating agent such as plutonic 123, or CTAB to our synthetic approach may allow us to minimize the "choke points" within our materials. Washes and rinsing would be the preferred method for removing the templating agent after synthesis, as calcination may alter the carefully crafted active sites. Testing these templated catalysts under these same conditions and determining their rate would allow us to see if "choke points" were a limitation of our current synthetic procedure.

Limonene, a diene, has both a 1,1-disubstituted olefin and a 1,1,2-trisubstituted olefin, allowing us to examine our catalysts preference of epoxidation. Often the most electron-rich double bond can be selectively epoxidized.[134] It would be ideal if these catalysts were able to selectively epoxidize a designated bond within a diene or triene. Catalytic test reaction with limonene and similar dienes substrates would allow use to study these preferences.

Catalysts that create 2,3-epoxyalcohols from primary and secondary allylic alcohols from functionalized alkenes such as vinyl alcohol are of great interest and important. Studying the epoxidation of vinyl alcohol and other functionalized olefins with our catalyst would significantly broaden the applicability of these catalysts.

We hypothesize this reaction proceeds with a mechanism similar to that of a Sharpless epoxidation. An in-depth kinetic study would allow use to determine the overall order of the reaction and compare it with that found in a Sharpless epoxidation. By changing the concentration of the reagents in the reaction and determining the rate we can determine the order of the reaction for each reagent and the overall rate. This data could prove/disprove our postulation about our mechanism.

Single site catalysts allow us the rare chance to study activation energies of heterogeneous catalysts. Because of the unique nature of our synthetic approach were have been able to create catalysts that only have a single type of titanium; 2-connection, 3-connections, or 4-connections to the support, but all have tetrahedral geometries. We would expect each species to have a different activation energy for epoxidation. In most proposed mechanisms for epoxidation, an initial step involves coordination of a peroxide with the simultaneous breaking of a Si-O-Ti link to silicate support.[133] From both a steric and electronic perspectives this is potentially a high energy step and as a result may limit the effectiveness and efficiency of our 4-connected titanium silicate consistent with its reactivity being the lowest among the new catalysts tested. Furthermore, to coordinate peroxide or substrate may also require significant movement of the titanium atom with respect to the cage of Ti-O-Si bonds that surrounds it. We would expect significantly lower energy barriers for both 3-connected and 2-connected relative to 4-connected titanium catalyst for the same reasons. By running kinetic studies at multiple temperatures and plotting the rate constants for each temperature we can determine the activation energy for each catalyst.

CHAPTER 4: CONCLUSION AND FUTURE WORK

This dissertation describes work aimed at synthesizing, characterizing and demonstrating applications for novel single site nanostructured titanosilicate. This work was part of an ongoing research program to develop new synthetic methodologies for the targeted preparation of advanced engineered materials. One area of focus was demonstrating how this new synthetic methodology is able to create well-defined single site surface titanium species that when reduced, could be capable of reversibly binding molecular hydrogen. A second focus of this work aimed at demonstrating how this synthetic methodology could be applied to constructing single-site heterogeneous catalysts. These catalysts were demonstrated to be active in the epoxidation of cyclohexene.

APPLICATIONS IN HYDROGEN STORAGE:

One of the primary focuses of this dissertation was the preparation of surface titanium ensembles for hydrogen applications. Surface titanium(IV) ensembles, were synthetically targeted by reacting a premade silicate building block support with a limiting amount of titanium tetrachloride, $TiCl_4$. The premade support initially contained spatially isolated surface functionalities which ensured that the generated surface catalyst ensembles were also spatially isolated. The local environment around all of the metal titanium sites in the matrix is identical which means the nanostructured catalysts again can be classified as single site.

These isolated titanium(IV) sites serve as a well-defined starting point for a "complex" reduction, resulting in reduced titanium centers that may be capable of Kubas's binding of hydrogen. The ability to start from well-defined and well-characterized precursors separates our synthetic strategy from those previously found in the literature. These isolated titanium(IV) sites were exposed to a variety of reductants including lithium aluminum hydride, sodium borohydride, cobaltocene, hydrogen, and UV radiation with hydrogen. The majority of the work with these systems focused on characterizing the titanium species after reduction in the systems to understand their composition. Due to the amorphous nature of our materials and instability of the reduced titanium species, we were unable to develop a clear understand of their composition. Ultimately, we turned our focus to investigating if any of the materials demonstrated chemisorption with molecular hydrogen. We found that none of the materials studied demonstrated chemisorption with hydrogen. These results were consistent with the computational modeling collaboration. Regardless, this work represents a novel system with targeted isolated single sites.

APPLICATIONS IN HETEROGENEOUS CATALYSIS:

Another primary focus of this dissertation was the preparation of nanostructured catalysts where one can control all of the necessary components of the catalyst ensembles in the material. Isolated metal cation centers, specifically titanium(IV), were incorporated into the framework of silicate building block matrices.

A series of catalyst ensembles, from partially and fully embedded, were synthetically targeted by reacting the octa-trimethyltin molecular building block with a limiting amount of metal chloride ($Ti(OiPr)_2Cl_2$, $Ti(OiPr)Cl_3$, $TiCl_4$). The local environment around all of the metal cation centers in the matrix (TiO_4) is identical which means the nanostructured catalysts contain only one type of metal cation center. These titanosilicate materials were further cross-linked using a dimethyldichlorosilane linking agent which resulted in the generation of a high surface area material around the embedded ensembles. The local environment around the ensembles remained unchanged during the generation of the high surface area

support and therefore the catalysts still contain only one type of metal cation center and can be classified as single site catalysts.

These single site catalysts were then shown to be active for the epoxidation of cyclohexene with cumene hydroperoxide. Like prior research with similar single site titanosilicates, a relationship between the structure of titanium sites in silicate and their catalytic properties was established. Leaching studies of these catalysts indicated that there was no significant loss of titanium from the silicate matrix. Furthermore, these single site catalysts were compared to two commercially used catalyst ((G)Ti-MCM-41 and TS-1) and found to be superior in both activity and selectivity.

In addition to targeting and synthesizing single-site heterogeneous titanosilicates for epoxidation, establish a relationship between the structure of titanium site in silicate and its catalytic properties is of great important. Based on the previous studies on titanosilicates, it is believed that new synthetic approaches such as the synthetic methodology used here are necessary in order to be able to target synthetically specific active sites in these materials on an atomic level. The synthetic approach developed and described here allows, the unique catalytic behaviors of each type of catalyst titanium sites to be studied and compared. The materials synthesized have a well-defined number of connections to the silicate matrix. As a result, we would expect a titanium site with four bonds to the matrix to react differently to that with only two. A more open coordination sphere around titanium should contribute to higher efficiency substrate, allowing for a faster more efficient catalyst

These result demonstrate the strengths of this synthetic methodology and represents a novel method for targeted isolated single sites and applying them to catalysis.

FUTURE WORK

The synthetic methodology discussed in-depth in chapter 1 and the example work presented in chapters two and three provides researchers with the ability to target specific catalytically active ensembles. The synthetic methodology discussed in this dissertation is applicable to a wide variety of active sites. As a result, this methodology can be used to target active sites for a range of reactions. As long as the active site precursor is high valent and oxophilic in nature this synthetic strategy will allow one to target a site of interest. A broad assortment of future work could focus on applying this synthetic approach to high valent transition and main group elements that have shown active in reactions of great importance.

INCORPORATION OF METAL CLUSTERS

An area which future work could be devoted focuses on incorporating metal clusters into the synthetic methodology discussed in this dissertation. This would allow researchers to address such questions as whether isolated single metal cation sites are more or less active than isolated collections of metal cations (i.e. metal clusters). An example of a few possible metal clusters that could be incorporated into the building block matrices can be seen in Figure 71. Preliminary work with the tetra-nuclear titanium cluster has indicated that when it is reacted with cube both trimethyltin chloride and trimethyltin benzoate are seen in the volatiles. In theory, this indicates the formation of multiple linkages to the support.

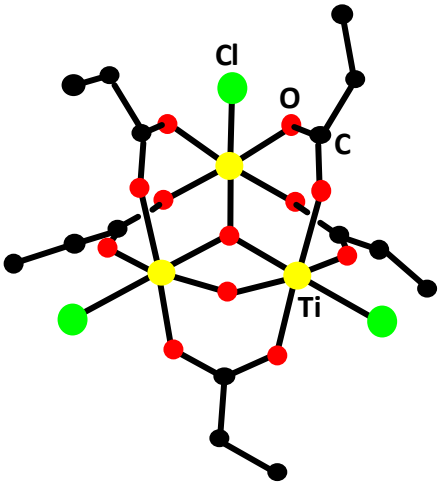

$Ti_3Cl_3O_2(O_2CEt)_5$

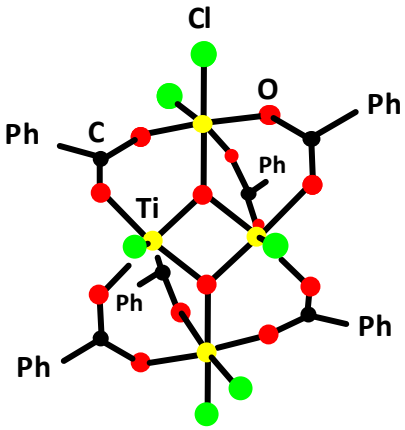

$Ti_4Cl_6(\mu\text{-}O_2)(O_2CPh)_6$

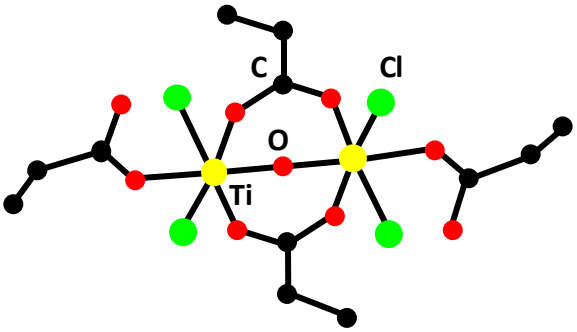

$\{TiCl_2(O_2CEt)(EtCO_2H)\}_2O$

Figure 71*: Titanium metal clusters capable of reacting with trimethyltin cube.*

HETEROGENEOUS CATALYSTS WITH NON-EQUILIBRIUM GEOMETRIES VIA IMPRINTING

Another area of future work involves the synthesis novel catalysts with non-equilibrium geometries controlled via imprinting and templating. For example, titanium tetrachloride bispyridine (Figure 72) can be reacted with trimethyltin cube to create an embedded titanium site with a square planar geometry once pyridine is removed. This square planar geometry would, in theory, be of higher energy than that of the equilibrium based tetrahedral and as a result may have substantially different activity.

Another area that may produce interesting results would be creating single site chiral catalysts. Chiral precursors placed within the trimethyltin cube silicate matrix may create catalyst with an inherent affinity for chiral-based reactions. Additionally, one could study how the size of the pores affects the observed catalytic activity of the nanostructured catalysts in selective oxidation reactions. The synthetic methodology presented in this dissertation allows one to synthetically target nanostructured catalysts with non-equilibrium geometries and catalysts that contains pore which might only allow certain substrates to be catalytically converted.

DEVELOPMENT OF METHODS TO REMOVE RESIDUAL TRIMETHYLTIN GROUPS

The development of a method for the removal of residual trimethyltin groups from the silicate matrices is an ongoing challenge facing our research program. The approach used in this dissertation was to reduce the trimethyltin groups as low as possible by varying the ratio and stoichiometry used in the synthesis. One of the risks of leaving trimethyltin groups in the matrices is that these groups could be catalytic active or be transformed into active species and therefore our “single site” catalysts would really become “multisite” catalysts. Finally, organotins like trimethyltin are often used as biocides and would deter industry interest for our novel methodology. Therefore, the development of a method for the removal of residual trimethyltin groups is vital to the overall success of this methodology.

DEVELOPMENT OF NEW BUILDING BLOCK APPROACH

The development of a new building block approach would solve the trimethyltin challenge just mentioned. A new building block approach would require the discovery of a new building block, new linking agents, and new cross-linking reaction. Some exploratory work has been conducted trying to use other nonhydrolytic sol-gel reactions (e.g. alkyl halide elimination and ester elimination) however these tests did not provide enough synthetic control to target specific catalyst ensembles. The development of a Trimethyltin free building block approach would reduce the cost and health hazard that are currently associated with the building block approach discussed in this dissertation.

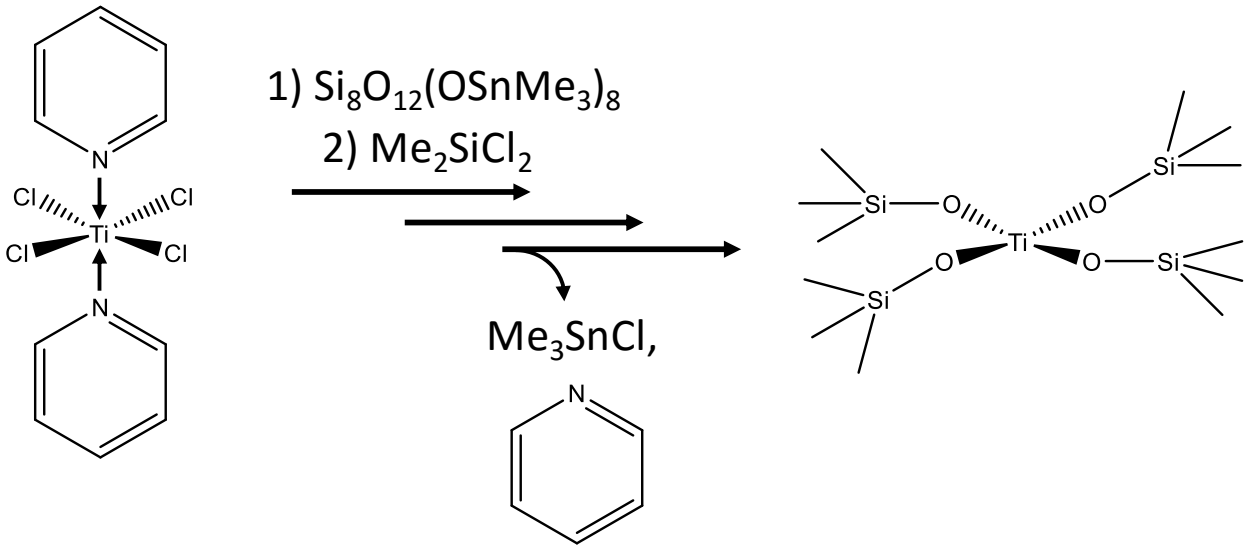

Figure 72*: Titanium tetrachloride bispyridine reacting with trimethyltin cube, followed by dimethyldichlorosilane to produce a square planar titanium site.*

REFERENCES

(1) Moulijn, J. A.; van Leeuwen, P. W.; van Santen, R. A. *Catalysis: an integrated approach to homogeneous, heterogeneous and industrial catalysis*; Elsevier, 1993; Vol. 79.
(2) Gerlt, J. A.; Kreevoy, M. M.; Cleland, W.; Frey, P. A. Understanding enzymic catalysis: the importance of short, strong hydrogen bonds. *Chemistry & biology* **1997**, *4*, 259.
(3) Gates, B. C.; Huber, G. W.; Marshall, C. L.; Ross, P. N.; Siirola, J.; Wang, Y. Catalysts for emerging energy applications. *MRS bulletin* **2008**, *33*, 429.
(4) Chatterjee, D.; Deutschmann, O.; Warnatz, J. Detailed surface reaction mechanism in a three-way catalyst. *Faraday Discuss.* **2001**, *119*, 371.
(5) http://www.scrapmetaljunkie.com/274/catalytic-converters-2.
(6) Barnes, C. E. Building Block Approaches to Nanostructured, Single Site, Heterogeneous Catalysts. *Modern Surface Organometallic Chemistry* **2009**, 137.
(7) http://sarahssureshots.wikispaces.com/file/view/figure06-14.jpg/105957707/figuer06-14.jpg.
(8) Dal Santo, V.; Liguori, F.; Pirovano, C.; Guidotti, M. Design and use of nanostructured single-site heterogeneous catalysts for the selective transformation of fine chemicals. *Molecules* **2010**, *15*, 3829.
(9) Hoveyda, A. H.; Morken, J. P. In *Metallocenes*; Wiley-VCH Verlag GmbH: 2008, p 625.
(10) Hench, L. L.; West, J. K. The sol-gel process. *Chemical Reviews* **1990**, *90*, 33.
(11) Brinker, C. J.; Scherer, G. W. *Sol-gel science: the physics and chemistry of sol-gel processing*; Academic press, 2013.
(12) Sakka, S.; Kamiya, K. Glasses from metal alcoholates. *Journal of Non-Crystalline Solids* **1980**, *42*, 403.
(13) Yoldas, B. E. Formation of titania-silica glasses by low temperature chemical polymerization. *Journal of Non-Crystalline Solids* **1980**, *38*, 81.
(14) Yamane, M.; Inoue, S.; Nakazawa, K. Preparation of gels to obtain glasses of high homogeneity by low temperature synthesis. *Journal of Non-Crystalline Solids* **1982**, *48*, 153.
(15) Cheng, F.; Tao, Z.; Liang, J.; Chen, J. Template-Directed Materials for Rechargeable Lithium-Ion Batteries†. *Chemistry of Materials* **2007**, *20*, 667.
(16) Kresge, C.; Leonowicz, M.; Roth, W.; Vartuli, J.; Beck, J. Ordered mesoporous molecular sieves synthesized by a liquid-crystal template mechanism. *nature* **1992**, *359*, 710.
(17) Zhao, D.; Feng, J.; Huo, Q.; Melosh, N.; Fredrickson, G. H.; Chmelka, B. F.; Stucky, G. D. Triblock copolymer syntheses of mesoporous silica with periodic 50 to 300 angstrom pores. *science* **1998**, *279*, 548.
(18) Vartuli, J. C.; Roth, W. J.; Degnan, T. In *Dekker Encyclopedia of Nanoscience and Nanotechnology*; Marcel Dekker New York: 2004, p 1797.
(19) Kim, J. M.; Stucky, G. D. Synthesis of highly ordered mesoporous silica materials using sodium silicate and amphiphilic block copolymers. *Chemical Communications* **2000**, 1159.
(20) Chen, S.-Y.; Jang, L.-Y.; Cheng, S. Synthesis of Zr-incorporated SBA-15 mesoporous materials in a self-generated acidic environment. *Chemistry of materials* **2004**, *16*, 4174.
(21) Klepel, O.; Böhlmann, W.; Ivanov, E.; Riede, V.; Papp, H. Incorporation of tungsten into MCM-41 framework. *Microporous and mesoporous materials* **2004**, *76*, 105.
(22) He, X.; Antonelli, D. Recent Advances in Synthesis and Applications of Transition Metal Containing Mesoporous Molecular Sieves. *Angewandte Chemie International Edition* **2002**, *41*, 214.
(23) Egeblad, K.; Christensen, C. H.; Kustova, M.; Christensen, C. H. Templating Mesoporous Zeolites. *Chemistry of Materials* **2007**, *20*, 946.
(24) http://www.iza-structure.org/databases/.

(25) Kamfjord, T.; Wester, T. S.; Rytter, E. Supported metallocene catalysts prepared by impregnation of MAO modified silica by a metallocene/monomer solution. *Macromolecular rapid communications* **1998**, *19*, 505.
(26) Brown, G. E.; Henrich, V. E.; Casey, W. H.; Clark, D. L.; Eggleston, C.; Felmy, A.; Goodman, D. W.; Grätzel, M.; Maciel, G.; McCarthy, M. I. Metal oxide surfaces and their interactions with aqueous solutions and microbial organisms. *Chemical Reviews* **1999**, *99*, 77.
(27) Basset, J.-M.; Psaro, R.; Roberto, D.; Ugo, R. *Modern surface organometallic chemistry*; John Wiley & Sons, 2009.
(28) Peretich, M. E. "Targeted Synthesis and Characterization of Nanostructured Silicate Building Block Supports and Heterogeneous Catalysts with Tungsten(VI) or Zirconium(IV) Centers. . *PhD diss., University of Tennessee,* **2011**.
(29) Vansant, E. F.; Van Der Voort, P.; Vrancken, K. C. *Characterization and chemical modification of the silica surface*; Elsevier, 1995; Vol. 93.
(30) Feher, F. J.; Weller, K. J. Synthesis and characterization of labile spherosilicates:[(Me3SnO) 8Si8O12] and [(Me4SbO) 8Si8O12]. *Inorganic chemistry* **1991**, *30*, 880.
(31) Clark, J. C.; Saengkerdsub, S.; Eldridge, G. T.; Campana, C.; Barnes, C. E. Synthesis and structure of functional spherosilicate building block molecules for materials synthesis. *Journal of organometallic chemistry* **2006**, *691*, 3213.
(32) Feher, F. J.; Weller, K. J. Phosphorus (III)-containing silicates via a new aprotic building-block approach to multicomponent silicates. *Chemistry of materials* **1994**, *6*, 7.
(33) Clark, J. C.; Barnes, C. E. Reaction of the Si8O20 (SnMe3) 8 building block with silyl chlorides: a new synthetic methodology for preparing nanostructured building block solids. *Chemistry of materials* **2007**, *19*, 3212.
(34) Rouquerol, F.; Rouquerol, J.; Sing, K. In *Adsorption by Powders and Porous Solids*; Academic Press: London, 1999, p 93.
(35) Wakefield, B.; Goudy, A.; Orefuwa, S.; Lott, L. Q.; Alexander, D.; Kerr, A. In *242nd ACS National Meeting & Exposition*; American Chemical Society: 2011, p ORGN 425.
(36) Sing, K. S. Reporting physisorption data for gas/solid systems with special reference to the determination of surface area and porosity (Recommendations 1984). *Pure and applied chemistry* **1985**, *57*, 603.
(37) Brunner, E. Characterization of solid acids by spectroscopy. *Catalysis today* **1997**, *38*, 361.
(38) Lercher, J. A.; Gründling, C.; Eder-Mirth, G. Infrared studies of the surface acidity of oxides and zeolites using adsorbed probe molecules. *Catalysis Today* **1996**, *27*, 353.
(39) Corma, A.; Fornes, V.; Forni, L.; Marquez, F.; Martınez-Triguero, J.; Moscotti, D. 2, 6-di-tert-butyl-pyridine as a probe molecule to measure external acidity of zeolites. *Journal of Catalysis* **1998**, *179*, 451.
(40) Vlaic, G.; Andreatta, D.; Colavita, P. Characterisation of heterogeneous catalysts by EXAFS. *Catalysis today* **1998**, *41*, 261.
(41) Bare, S. R.; Kelly, S. D.; Sinkler, W.; Low, J. J.; Modica, F. S.; Valencia, S.; Corma, A.; Nemeth, L. T. Uniform catalytic site in Sn-β-Zeolite determined using x-ray absorption fine structure. *Journal of the American Chemical Society* **2005**, *127*, 12924.
(42) Calvin, S. *XAFS for Everyone*; CRC Press, 2013.
(43) Bordiga, S.; Coluccia, S.; Lamberti, C.; Marchese, L.; Zecchina, A.; Boscherini, F.; Buffa, F.; Genoni, F.; Leofanti, G. XAFS Study of Ti-Silicalite: structure of framework Ti (IV) in the presence and absence of reactive molecules (H2O, NH3) and comparison with Ultraviolet-Visible and IR results. *The Journal of Physical Chemistry* **1994**, *98*, 4125.
(44) Farges, F.; Brown, G. E.; Rehr, J. Ti K-edge XANES studies of Ti coordination and disorder in oxide compounds: Comparison between theory and experiment. *Physical Review B* **1997**, *56*, 1809.

(45) Wong, J.; Lytle, F.; Messmer, R.; Maylotte, D. K-edge absorption spectra of selected vanadium compounds. *Physical Review B* **1984**, *30*, 5596.
(46) Lee, M.-Y.; Jiao, J.; Mayes, R.; Hagaman, E.; Barnes, C. E. The targeted synthesis of single site vanadyl species on the surface and in the framework of silicate building block materials. *Catalysis today* **2011**, *160*, 153.
(47) Cramer, S. P.; Eccles, T.; Kutzler, F.; Hodgson, K. O.; Mortenson, L. Molybdenum x-ray absorption edge spectra. The chemical state of molybdenum in nitrogenase. *Journal of the American Chemical Society* **1976**, *98*, 1287.
(48) Meitzner, G.; Via, G.; Lytle, F.; Sinfelt, J. Analysis of X-ray absorption edge data on metal catalysts. *The Journal of Physical Chemistry* **1992**, *96*, 4960.
(49) Hubbert, M. K. Energy from Fossil Fuels. *Science* **1949**, *109*, 103.
(50) Callendar, G. S. The amount of carbon dioxide in the atmosphere. *Tellus* **1958**, *10*, 243.
(51) Deague, T. K. Global atmospheric consequences of the combustion of fossil fuels. *J. Inst. Fuel* **1975**, *48*, 153.
(52) Burdge, J. *Chemistry*; McGraw-Hill, 2009.
(53) Srivastava, S. K. Hydrogen, an alternative source of energy: feasibility of hydrogen production by plasma pyrolysis of water. *Fuel Sci. Technol.* **1995**, *14*, 39.
(54) Meissner, D.; Meier, A. In *The World Hydrogen Energy Conference, From Hydrogen Energy Progress XI*; International Association for Hydrogen Energy: 1996; Vol. 3, p 2389.
(55) Andreassen, K. In *the HYPOTHESIS Symposium,From Hydrogen Power: Theoretical and Engineering Solutions*; Kluwer: 1998, p 91.
(56) Khaselev, O.; Bansal, A.; Turner, J. A. High-efficiency integrated multijunction photovoltaic/electrolysis systems for hydrogen production. *Int. J. Hydrogen Energy* **2000**, *26*, 127.
(57) Ohmori, T.; Go, H.; Yamada, Y.; Matsuki, N.; Yamaguchi, N.; Nakayama, A.; Mametsuka, H.; Suzuki, E. Hydrogen production from solar light energy by photovoltaic water electrolysis. *Hem. Ind.* **2001**, *55*, 535.
(58) Esswein, A. J.; Nocera, D. G. Hydrogen Production by Molecular Photocatalysis. *Chemical Reviews* **2007**, *107*, 4022.
(59) Sakai, K.; Kizaki, Y.; Tsubomura, T.; Matsumoto, K. Homogeneous catalyses of mixed-valent octanuclear platinum complexes in photochemical hydrogen production from water. *Journal of Molecular Catalysis* **1993**, *79*, 141.
(60) Ni, M.; Leung, D. Y. C.; Leung, M. K. H.; Sumathy, K. An overview of hydrogen production from biomass. *Fuel Processing Technology* **2006**, *87*, 461.
(61) Al-Alawi, M. t.; Barbir, F., Ulgiati, S., Eds.; Springer Netherlands: 2008, p 273.
(62) Florin, N.; Harris, A. Hydrogen production from biomass. *The Environmentalist* **2007**, *27*, 207.
(63) Dillich, S. *FY 2009 Annual Progress Report* DOE Hydrogen Program 2009.
(64) Veenstra, M. J.; Hobein, B. On-board physical based 70 MPa hydrogen storage systems. *Soc. Automot. Eng., [Spec. Publ.] SP* **2011**, *SP-2309*, 99.
(65) Brunner, T.; Kircher, O.; Schnagl, J.; Bayerische Motoren Werke Aktiengesellschaft, Germany . 2009.
(66) Reese, W.-H.; Linde Aktiengesellschaft, Germany . 2006.
(67) Garrison, S. L.; Corgnale, C.; Hardy, B. J.; Tamburello, D. A.; Motyka, T.; Anton, D. L. In *International Chemical Congress of Pacific Basin Societies, From Pacifichem 2010*; American Chemical Society: 2010, p AETECH 208.
(68) Semelsberger, T. A.; Brosha, E.; Purdy, G.; Nakagawa, T.; Davis, B.; Rockward, T.; Burrell, T.; Borup, R.; Tafoya, J.; American Chemical Society: 2010, p AETECH 209.

(69) Stetson, N. T.; Read, C.; Ordaz, G.; Gardiner, M.; American Chemical Society: 2010, p AETECH 158.
(70) Elie, M.; Chaise, A.; Gillia, O.; Planque, M.; Commissariat a l'Energie Atomique et aux Energies Alternatives, Fr. . 2011.
(71) Saldan, I. A prospect for $LiBH_4$ as on-board hydrogen storage. *Cent. Eur. J. Chem.* **2011**, *9*, 761.
(72) Souahlia, A.; Dhaou, H.; Askri, F.; Sofiene, M.; Jemni, A.; Ben, N. S. Experimental and comparative study of metal hydride hydrogen tanks. *Int. J. Hydrogen Energy* **2011**, *36*, 12918.
(73) Wang, X.; Liu, H.; Li, H. A 70 MPa hydrogen-compression system using metal hydrides. *Int. J. Hydrogen Energy* **2011**, *36*, 9079.
(74) Huegle, T.; Hartl, M.; Lentz, D. The Route to a Feasible Hydrogen-Storage Material: MOFs versus Ammonia Borane. *Chem.--Eur. J.* **2011**, *17*, 10184.
(75) Jiang, H.-L.; Liu, B.; Lan, Y.-Q.; Kuratani, K.; Akita, T.; Shioyama, H.; Zong, F.; Xu, Q. From Metal-Organic Framework to Nanoporous Carbon: Toward a Very High Surface Area and Hydrogen Uptake. *J. Am. Chem. Soc.* **2011**, *133*, 11854.
(76) Sculley, J.; Yuan, D.; Zhou, H.-C. The current status of hydrogen storage in metal-organic frameworks-updated. *Energy Environ. Sci.* **2011**, *4*, 2721.
(77) Thomas, K. M. In *Energy Materials*; Bruce, D. W., O'Hare, D., Walton, R. I., Eds.; John Wiley & Sons Ltd.: 2011, p 245.
(78) Wang, L.; Stuckert, N. R.; Yang, R. T. Unique hydrogen adsorption properties of graphene. *AIChE J.* **2011**, *57*, 2902.
(79) Wenzel, S. E.; Frahm, D.; Fischer, M.; Hoffmann, F.; Froeba, M. Tuning metal-organic frameworks for hydrogen storage applications. *Prepr. Symp. - Am. Chem. Soc., Div. Fuel Chem.* **2011**, *56*, 171.
(80) Armandi, M.; Bonelli, B.; Cho, K.; Ryoo, R.; Garrone, E. Study of hydrogen physisorption on nanoporous carbon materials of different origin. *Int. J. Hydrogen Energy* **2011**, *36*, 7937.
(81) Cabria, I.; Lopez, M. J.; Alonso, J. A. Hydrogen storage in nanoporous carbon. *Handbook of Nanophysics* **2011**, *5*, 41/1.
(82) Shen, J.; Liu, N.; Ouyang, L.; Zhou, B.; Wu, G.; Ni, X.; Zhang, Z. Hydrogen storage property of nanoporous carbon aerogels. *Qiangjiguang Yu Lizishu* **2011**, *23*, 1517.
(83) Orimo, S.-i.; Nakamori, Y. In *From Yuki Chozo Zairyo to Nano Gijutsu*; Ichikawa, M., Ed.; Shi Emu Shi Shuppan: 2007, p 30.
(84) Hauback, B. C. In *the Risoe International Symposium on Materials Science, From Energy Materials: Advances in Characterization*; Risoe National Laboratory: 2008, p 83.
(85) Eigen, N.; Boesenberg, U.; Bellosta, v. C. J.; Jensen, T. R.; Cerenius, Y.; Dornheim, M.; Klassen, T.; Bormann, R. Reversible hydrogen storage in NaF-Al composites. *J. Alloys Compd.* **2009**, *477*, 76.
(86) Mendoza-Zelis, L.; Meyer, M.; Baum, L. Complex quaternary hydrides $Mg_2(Fe,Co)Hy$ for hydrogen storage. *Int. J. Hydrogen Energy* **2011**, *36*, 600.
(87) Zidan, R.; Mohtadi, R. F.; Fewox, C.; Sivasubramanian, P.; USA . 2011.
(88) http://www.bmw.com/com/en/insights/technology/cleanenergy/phase_2/cleanenergy.html.
(89) Rowsell, J. L. C.; Millward, A. R.; Park, K. S.; Yaghi, O. M. Hydrogen Sorption in Functionalized Metal-Organic Frameworks. *J. Am. Chem. Soc.* **2004**, *126*, 5666.
(90) Dinca, M.; Long, J. R. Hydrogen storage in microporous metal-organic frameworks with exposed metal sites. *Angew. Chem., Int. Ed.* **2008**, *47*, 6766.
(91) Rosi, N. L.; Eckert, J.; Eddaoudi, M.; Vodak, D. T.; Kim, J.; O'Keeffe, M.; Yaghi, O. M. Hydrogen Storage in Microporous Metal-Organic Frameworks. *Science* **2003**, *300*, 1127.
(92) Schlapbach, L.; Zuettel, A. Hydrogen-storage materials for mobile applications. *Nature (London, U. K.)* **2001**, *414*, 353.
(93) Hirscher, M. *Special Issue: Hydrogen Storage in Nanoscale Carbon and Metals. [In: Appl. Phys. A: Mater. Sci. process.; 72(2)]*; Springer, 2001.

(94) Hirscher, M.; Becher, M.; Haluska, M.; Dettlaff-Weglikowska, U.; Quintel, A.; Duesberg, G. S.; Choi, Y. M.; Downes, P.; Hulman, M.; Roth, S.; Stepanek, I.; Bernier, P. Hydrogen storage in sonicated carbon materials. *Appl. Phys. A: Mater. Sci. Process.* **2001**, *72*, 129.
(95) Bhatia, S. K.; Myers, A. L. Optimum Conditions for Adsorptive Storage. *Langmuir* **2006**, *22*, 1688.
(96) Zhao, Y.; Kim, Y.-H.; Dillon, A. C.; Heben, M. J.; Zhang, S. B. Hydrogen Storage in Novel Organometallic Buckyballs. *Phys. Rev. Lett.* **2005**, *94*, 155504.
(97) Kubas, G. J.; Ryan, R. R.; Swanson, B. I.; Vergamini, P. J.; Wasserman, H. J. Characterization of the first examples of isolable molecular hydrogen complexes, $M(CO)_3(PR_3)_2(H_2)$ (M = molybdenum or tungsten; R = Cy or isopropyl). Evidence for a side-on bonded dihydrogen ligand. *J. Am. Chem. Soc.* **1984**, *106*, 451.
(98) Kubas, G. J. Fundamentals of H_2 binding and reactivity on transition metals underlying hydrogenase function and H_2 production and storage. *Chem. Rev.* **2007**, *107*, 4152.
(99) Yildirim, T.; Ciraci, S. Titanium-decorated carbon nanotubes as a potential high-capacity hydrogen storage medium. *Phys. Rev. Lett.* **2005**, *94*, 175501.
(100) Hamaed, A.; Trudeau, M.; Antonelli, D. M. H_2 Storage Materials (22 kJ/mol) Using Organometallic Ti Fragments as σ-H_2 Binding Sites. *J. Am. Chem. Soc.* **2008**, *130*, 6992.
(101) Chertihin, G. V.; Andrews, L. Reactions of laser ablated Ti atoms with hydrogen during condensation in excess argon. Infrared spectra of the TiH, TiH2, TiH3, and TiH4 molecules. *Journal of the American Chemical Society* **1994**, *116*, 8322.
(102) Jena, P. Materials for Hydrogen Storage: Past, Present, and Future. *The Journal of Physical Chemistry Letters* **2011**, *2*, 206.
(103) Shao, H.; Felderhoff, M.; Schüth, F.; Weidenthaler, C. Nanostructured Ti-catalyzed MgH2 for hydrogen storage. *Nanotechnology* **2011**, *22*, 235401.
(104) Alba, M. D.; Luan, Z.; Klinowski, J. Titanosilicate mesoporous molecular sieve MCM-41: synthesis and characterization. *The Journal of Physical Chemistry* **1996**, *100*, 2178.
(105) Nakatsuji, H.; Ehara, M.; Palmer, M. H.; Guest, M. F. Theoretical study on the excited and ionized states of titanium tetrachloride. *The Journal of chemical physics* **1992**, *97*, 2561.
(106) Bal, R.; Chaudhari, K.; Srinivas, D.; Sivasanker, S.; Ratnasamy, P. Redox and catalytic chemistry of Ti in titanosilicate molecular sieves: an EPR investigation. *Journal of Molecular Catalysis A: Chemical* **2000**, *162*, 199.
(107) Fürstner, A.; Bogdanović, B. New Developments in the Chemistry of Low-Valent Titanium. *Angewandte Chemie International Edition in English* **1996**, *35*, 2442.
(108) Taylor, G. B.; Starkweather, H. W. REDUCTION OF METAL OXIDES BY HYDROGEN. *Journal of the American Chemical Society* **1930**, *52*, 2314.
(109) Harrison, B.; Diwell, A.; Hallett, C. Promoting platinum metals by ceria. *Platinum Metals Review* **1988**, *32*, 73.
(110) Brown, M.; Peierls, R.; Stern, E. White lines in x-ray absorption. *Physical Review B* **1977**, *15*, 738.
(111) Geiger Jr, W. E. Electroreduction of cobaltocene. Evidence for a metallocene anion. *Journal of the American Chemical Society* **1974**, *96*, 2632.
(112) Benrath, A.; Obladen, A. The photochemical reduction of titanium salts. *Z. Wiss. Photogr., Photophys. Photochem.* **1922**, *22*, 65.
(113) Durfee, L. D.; Latesky, S. L.; Rothwell, I. P.; Huffman, J. C.; Folting, K. Chemical and electrochemical reduction of titanium (IV) aryloxides. *Inorganic Chemistry* **1985**, *24*, 4569.
(114) Kolthoff, I.; Thomas, F. Polarography in acetonitrile of titanium tetrachloride and tetraiodide in various supporting electrolytes. *Journal of The Electrochemical Society* **1964**, *111*, 1065.
(115) Smith, M. B. In *Organic Synthesis (Third Edition)*; Academic Press: Oxford, 2010, p 347.
(116) Gilbert T., K. R., Foster N., Davoes g., *Chemistry Third Edition*; W. W. Norton & Company, Inc: New York, NY, 2012.

(117) Connelly, N. G.; Geiger, W. E. Chemical redox agents for organometallic chemistry. *Chemical Reviews* **1996**, *96*, 877.
(118) Drago, R. S. *Physical methods in chemistry Chapter 13 EPR sprecta of transition metal ion complexes*, 1977.
(119) Suraweera, N. S.; Barnes, C. E.; Keffer, D. J. The Adsorption Properties of Amorphous, Metal-Decorated Microporous Silsesquioxanes for Mixtures of Carbon Dioxide, Methane and Hydrogen. *The Journal of Physical Chemistry C* **2014**, *118*, 13008.
(120) Suraweera, N. S.; Albert, A. A.; Peretich, M. E.; Abbott, J.; Humble, J. R.; Barnes, C. E.; Keffer, D. J. Methane and carbon dioxide adsorption and diffusion in amorphous, metal-decorated nanoporous silica. *Molecular Simulation* **2014**, *40*, 618.
(121) Suraweera, N. S.; Albert, A. A.; Humble, J. R.; Barnes, C. E.; Keffer, D. J. Hydrogen adsorption and diffusion in amorphous, metal-decorated nanoporous silica. *International Journal of Hydrogen Energy* **2014**, *39*, 9241.
(122) Hagen, J. *Industrial catalysis: a practical approach*; John Wiley & Sons, 2015.
(123) Schlögl, R. Catalytic Synthesis of Ammonia—A "Never-Ending Story"? *Angewandte Chemie International Edition* **2003**, *42*, 2004.
(124) Coperet, C.; Comas-Vives, A.; Conley, M. P.; Estes, D. P.; Fedorov, A.; Mougel, V.; Nagae, H.; Nunez-Zarur, F.; Zhizhko, P. A. Surface Organometallic and Coordination Chemistry toward Single-Site Heterogeneous Catalysts: Strategies, Methods, Structures, and Activities. *Chem. Rev. (Washington, DC, U. S.)* **2016**, *116*, 323.
(125) Shylesh, S.; Jia, M.; Thiel, W. R. Recent progress in the heterogenization of complexes for single-site epoxidation catalysis. *Eur. J. Inorg. Chem.* **2010**, 4395.
(126) Lane, B. S.; Burgess, K. Metal-Catalyzed Epoxidations of Alkenes with Hydrogen Peroxide. *Chemical Reviews* **2003**, *103*, 2457.
(127) Tang, Q.; Zhang, Q.; Wu, H.; Wang, Y. Epoxidation of styrene with molecular oxygen catalyzed by cobalt (II)-containing molecular sieves. *Journal of catalysis* **2005**, *230*, 384.
(128) Kamigaito, M.; Sawamoto, M.; Higashimura, T. Alkoxy-Substituted Titanium (IV) Chlorides as Lewis Acid Activators for Living Cationic Polymerization of Isobutyl Vinyl Ether: Control of Lewis Acidity in the Design of Initiating Systems. *Macromolecules* **1995**, *28*, 5671.
(129) Jarupatrakorn, J.; Tilley, T. D. Silica-supported, single-site titanium catalysts for olefin epoxidation. A molecular precursor strategy for control of catalyst structure. *Journal of the American Chemical Society* **2002**, *124*, 8380.
(130) Guidotti, M.; Pirovano, C.; Ravasio, N.; Lázaro, B.; Fraile, J. M.; Mayoral, J. A.; Coq, B.; Galarneau, A. The use of H 2 O 2 over titanium-grafted mesoporous silica catalysts: a step further towards sustainable epoxidation. *Green Chemistry* **2009**, *11*, 1421.
(131) Liu, C.; Huang, J.; Sun, D.; Zhou, Y.; Jing, X.; Du, M.; Wang, H.; Li, Q. Anatase type extra-framework titanium in TS-1: A vital factor influencing the catalytic activity toward styrene epoxidation. *Applied Catalysis A: General* **2013**, *459*, 1.
(132) Ramachandran, C. E.; Du, H.; Kim, Y. J.; Kung, M. C.; Snurr, R. Q.; Broadbelt, L. J. Solvent effects in the epoxidation reaction of 1-hexene with titanium silicalite-1 catalyst. *Journal of Catalysis* **2008**, *253*, 148.
(133) Guidotti, M.; Pirovano, C.; Ravasio, N.; Lazaro, B.; Fraile, J. M.; Mayoral, J. A.; Coq, B.; Galarneau, A. The use of H2O2 over titanium-grafted mesoporous silica catalysts: a step further towards sustainable epoxidation. *Green Chemistry* **2009**, *11*, 1421.
(134) Lluch, A.-M.; Sánchez-Baeza, F.; Messeguer, A.; Fusco, C.; Curci, R. Regio- and chemoselective epoxidation of fluorinated monoterpenes and sesquiterpenes by dioxiranes. *Tetrahedron* **1993**, *49*, 6299.

VITA

Austin A. Albert grew up in Fort Morgan, CO and graduated from Fort Morgan High School in May of 2005. He then enrolled at University of Northern Colorado and completed his B.S. in chemistry (with ACS certified) May 2010. Over the summer of 2008, he completed a research internship at Array Biopharma, where he conducted research on the applications of total organic carbon analysis within the quality control and quality assurance of a pharmaceutical company. During the summer of 2009, Austin accepted a summer research internship at Los Alamos National Laboratory (LANL) within the emergency operation and emergency responses(EO-ER) division. There he helped integrate chemistry knowledge into the EO-ER division for more effective knowledge base and response capabilities. In the summer of 2010, Austin returned to LANL for an additional summer research internship. Here he focused his efforts into synthesizing fluoroalkanes poly(ethylene glycol) thin films for artificial retina stability.

In August 2010, he joined the Chemistry Department at the University of Tennessee – Knoxville where he began work on a doctoral degree in chemistry under the guidance of Prof. Craig E. Barnes. His research was part of an ongoing research program to develop new synthetic methodologies for the targeted preparation of heterogeneous catalysts. He completed the requirements for the Doctor of Philosophy in chemistry in December 2016.